

NASA/CR—2003-212724



Initial Feasibility Assessment of a High Altitude Long Endurance Airship

Anthony Colozza
Analex Corporation, Brook Park, Ohio

The NASA STI Program Office . . . in Profile

Since its founding, NASA has been dedicated to the advancement of aeronautics and space science. The NASA Scientific and Technical Information (STI) Program Office plays a key part in helping NASA maintain this important role.

The NASA STI Program Office is operated by Langley Research Center, the Lead Center for NASA's scientific and technical information. The NASA STI Program Office provides access to the NASA STI Database, the largest collection of aeronautical and space science STI in the world. The Program Office is also NASA's institutional mechanism for disseminating the results of its research and development activities. These results are published by NASA in the NASA STI Report Series, which includes the following report types:

- **TECHNICAL PUBLICATION.** Reports of completed research or a major significant phase of research that present the results of NASA programs and include extensive data or theoretical analysis. Includes compilations of significant scientific and technical data and information deemed to be of continuing reference value. NASA's counterpart of peer-reviewed formal professional papers but has less stringent limitations on manuscript length and extent of graphic presentations.
- **TECHNICAL MEMORANDUM.** Scientific and technical findings that are preliminary or of specialized interest, e.g., quick release reports, working papers, and bibliographies that contain minimal annotation. Does not contain extensive analysis.
- **CONTRACTOR REPORT.** Scientific and technical findings by NASA-sponsored contractors and grantees.

- **CONFERENCE PUBLICATION.** Collected papers from scientific and technical conferences, symposia, seminars, or other meetings sponsored or cosponsored by NASA.
- **SPECIAL PUBLICATION.** Scientific, technical, or historical information from NASA programs, projects, and missions, often concerned with subjects having substantial public interest.
- **TECHNICAL TRANSLATION.** English-language translations of foreign scientific and technical material pertinent to NASA's mission.

Specialized services that complement the STI Program Office's diverse offerings include creating custom thesauri, building customized databases, organizing and publishing research results . . . even providing videos.

For more information about the NASA STI Program Office, see the following:

- Access the NASA STI Program Home Page at <http://www.sti.nasa.gov>
- E-mail your question via the Internet to help@sti.nasa.gov
- Fax your question to the NASA Access Help Desk at 301-621-0134
- Telephone the NASA Access Help Desk at 301-621-0390
- Write to:
NASA Access Help Desk
NASA Center for Aerospace Information
7121 Standard Drive
Hanover, MD 21076

NASA/CR—2003-212724



Initial Feasibility Assessment of a High Altitude Long Endurance Airship

Anthony Colozza
Analex Corporation, Brook Park, Ohio

Prepared under Contract NAS3-00145

National Aeronautics and
Space Administration

Glenn Research Center

December 2003

Trade names or manufacturers' names are used in this report for identification only. This usage does not constitute an official endorsement, either expressed or implied, by the National Aeronautics and Space Administration.

Available from

NASA Center for Aerospace Information
7121 Standard Drive
Hanover, MD 21076

National Technical Information Service
5285 Port Royal Road
Springfield, VA 22100

Available electronically at <http://gltrs.grc.nasa.gov>

Table of Contents

TABLE OF CONTENTS	iii
LIST OF TABLES	iv
LIST OF FIGURES	iv
INTRODUCTION	1
BACKGROUND	2
MISSION	6
AIRSHIP CONFIGURATION	9
ENVIRONMENT	12
WINDS	17
<i>East Coast Wind Profiles</i>	20
<i>West Coast Wind Profiles</i>	21
INCIDENT SOLAR RADIATION	25
POWER AND PROPULSION SYSTEM	33
SOLAR ARRAY	35
FUEL CELL SYSTEM.....	44
<i>Reactant Storage Tanks</i>	49
<i>Air Compressor System</i>	50
ELECTROLYZER	52
ELECTRIC MOTOR	54
PROPELLER	55
ANALYSIS	65
RESULTS	72
REFERENCE	94

List of Tables

Table 1.	Earth’s Physical Properties	19
Table 2.	Major Gas Components of Earth’s Atmosphere.....	21
Table 3.	Standard Atmosphere	23
Table 4.	Raw Wind Data Sites.....	25
Table 5.	Input Parameter Ranges for Wind Equations.....	29
Table 6.	Fuel Cell System Component Scaling Factors	54
Table 7.	Scaling Factors for Compressor Components.....	56
Table 8.	Compressor System Component Inlet and Outlet Temperatures And Pressures.....	58
Table 9.	Electrolyzer System Component Scaling Factors.....	60
Table 10.	Power Levels to which the Power/Propulsion System Components Scale	77
Table 11.	Single Point Airship Design.....	93
Table 12.	Advancements Needed for Baseline Airship to Operate at 42° N Latitude Year-Long	99

List of Figures

Figure 1a.	U2 High Altitude Aircraft	9
Figure 1b.	SR71 High Altitude Aircraft.....	9
Figure 2a.	Condor High Altitude UA.....	9
Figure 2b.	Global Hawk High Altitude UAV	9
Figure 3.	Helios High Altitude Long Endurance Solar Powered UAV	10
Figure 4a.	Air Force High Altitude Balloon (HABE).....	11
Figure 4b.	Lockheed Martin Tethered Aerostat.....	11
Figure 5.	Horizon as Seen from the Airship (not to scale).....	13
Figure 6.	Horizon Distance as a Function of Altitude.....	14
Figure 7.	Relative Drag on an Airship Sized to Carry a Fixed Payload at a Given Altitude.....	15
Figure 8.	Lockheed Martin’s High Altitude Airship Concept	16
Figure 9a.	ESA High Altitude Airship Concept	17
Figure 9b.	Skycat Heavy Lift Airship Concept.....	17
Figure 10a.	Techsphere System’s Spherical Airship Concept.....	17
Figure 10b.	LTAS/Cabot’s Saucer Airship Concept	17
Figure 11.	Analysis Baseline Airship Configuration.....	18
Figure 12.	Earth From Space	19
Figure 13.	Profile of Earth’s Atmosphere	20
Figure 14.	Troposphere Region of the Atmosphere	21
Figure 15.	Mean Winds for Cape Kennedy, FL Throughout The Year	24
Figure 16.	Mean Winds for Albuquerque, NM Throughout the Year.....	24
Figure 17.	Winter Mean Wind Speed Profile for the East Coast.....	28
Figure 18.	99 th Percentile East Coast Wind Speed for an Altitude of 21.5 km.....	29

Figure 19.	99 th Percentile West Coast Wind Speed for an Altitude of 21.5 km.....	30
Figure 20.	Mean East Coast Wind Speed for an Altitude of 21.5 km.....	30
Figure 21.	Mean West Coast Wind Speed for an Altitude of 21.5 km.....	31
Figure 22.	Environmental Factors that Affects the Airship’s Power Production Capabilities	32
Figure 23.	Solar Array Incident Flux Geometry.....	35
Figure 24.	Incident Power on the Array at Various Times During the Day for June 21 st , 38° N Latitude and Airship Orientation of 0° E to W	36
Figure 25.	Incident Power on the Array at Various Times During the Day for June 21 st , 38° N Latitude and Airship Orientation of 45° SE	37
Figure 26.	Incident Power on the Array at Various Times During the Day for June 21 st , 38° N Latitude and Airship Orientation of 90° N to S.....	37
Figure 27.	Incident Power on the Array at Various Times During the Day for December 21 st , 38° N Latitude and Airship Orientation of 0° E to W	38
Figure 28.	Incident Power on the Array at Various Times During the Day for December 21 st , 38° N Latitude and Airship Orientation of 45° SE	38
Figure 29.	Incident Power on the Array at Various Times During the Day for December 21 st , 38° N Latitude and Airship Orientation of 90° N to S.....	39
Figure 30.	Component Breakdown for a Power/Propulsion System Module (drawing not to scale).....	40
Figure 31.	Thin Film Solar Array Operation	43
Figure 32.	Thin Film Solar Array Efficiency Over the Last 20 Years	44
Figure 33.	Amorphous Silicon Commercially Available Thin Film Solar Arrays	44
Figure 34.	Solar Array Available Power on June 21 st for Various Latitudes and Airship Orientations	45
Figure 35.	Solar Array Available Power on December 21 st for Various Latitudes and Airship Orientations.....	46
Figure 36.	1 st Quadrant Solar Array Available Power on June 21 st for Various Latitudes and Airship Orientations.....	47
Figure 37.	1 st Quadrant Solar Array Available Power on December 21 st for Various Latitudes and Airship Orientations.....	47
Figure 38.	2 nd Quadrant Solar Array Available Power on June 21 st for Various Latitudes and Airship Orientations.....	48
Figure 39.	2 nd Quadrant Solar Array Available Power on December 21 st for Various Latitudes and Airship Orientations.....	48
Figure 40.	Principle of Operation of a PEM Fuel Cell.....	50
Figure 41.	Voltage and Output Power Versus Current Density for a Typical PEM Cell	52
Figure 42a.	Ballard Automotive Fuel Cell.....	53
Figure 42b.	IFC Automotive Fuel Cell.....	53
Figure 43.	Fuel Cell System Layout.....	54

Figure 44.	Hydrogen/Air High Altitude Fuel Cell System	57
Figure 45.	Electrolyzer System Layout	59
Figure 46.	Propeller Reynolds Number as a Function of Airship Altitude.....	63
Figure 47.	Blade Twist and Chord Length as a Function of Radial Station	64
Figure 48.	Lift Coefficient to Drag Coefficient for SD8000-PT airfoil at A Reynolds Number of 300,000.....	65
Figure 49.	Lift Coefficient to Angle of Attack for SD8000-PT airfoil at A Reynolds Number of 300,000.....	65
Figure 50.	SD8000-PT Airfoil Cross Section: To Scale and with Y Axis Exaggerated by 5 Times X Axis	66
Figure 51.	Thrust Coefficient vs Advance Ratio for a 4 Bladed Propeller At Various Pitch Angles.....	67
Figure 52.	Power Coefficient vs Advance Ratio for a 4 Bladed Propeller At Various Pitch Angles.....	67
Figure 53.	Thrust Coefficient vs Advance Ratio for a 5 Bladed Propeller At Various Pitch Angles.....	68
Figure 54.	Power Coefficient vs Advance Ratio for a 5 Bladed Propeller At Various Pitch Angles.....	68
Figure 55.	Thrust Coefficient vs Advance Ratio for a 6 Bladed Propeller At Various Pitch Angles.....	69
Figure 56.	Power Coefficient vs Advance Ratio for a 6 Bladed Propeller At Various Pitch Angles.....	69
Figure 57.	Mission and Environmental Factors that Influence the Airship Feasibility	71
Figure 58.	Main Components of the Analysis and Their Dependence.....	72
Figure 59.	Energy Balance Diagram	73
Figure 60.	Airship Sizing Process.....	74
Figure 61.	East Coast, Spring, Payload vs Latitude for Various Airship Lengths	79
Figure 62.	East Coast, Summer, Payload vs Latitude for Various Airship Lengths	80
Figure 63.	East Coast, Autumn, Payload vs Latitude for Various Airship Lengths	80
Figure 64.	East Coast, Winter, Payload vs Latitude for Various Airship Lengths	81
Figure 65.	West Coast, Spring, Payload vs Latitude for Various Airship Lengths	81
Figure 66.	West Coast, Summer, Payload vs Latitude for Various Airship Lengths	82
Figure 67.	West Coast, Autumn, Payload vs Latitude for Various Airship Lengths	82
Figure 68.	West Coast, Winter, Payload vs Latitude for Various Airship Lengths	83
Figure 69.	Airship Length vs Volume for a Fineness Ratio of 4.....	83
Figure 70.	East coast, Spring Mean Power Level for Various Airship Lengths.....	84
Figure 71.	East coast, Summer Mean Power Level for Various Airship Lengths.....	85

Figure 72.	East coast, Autumn Mean Power Level for Various Airship Lengths.....	85
Figure 73.	East coast, Winter Mean Power Level for Various Airship Lengths.....	86
Figure 74.	West coast, Spring Mean Power Level for Various Airship Lengths.....	86
Figure 75.	West coast, Summer Mean Power Level for Various Airship Lengths.....	87
Figure 76.	West coast, Autumn Mean Power Level for Various Airship Lengths.....	87
Figure 77.	West coast, Winter Mean Power Level for Various Airship Lengths.....	88
Figure 78.	East coast, Spring Maximum Power Level for Various Airship Lengths.....	89
Figure 79.	East coast, Summer Maximum Power Level for Various Airship Lengths.....	89
Figure 80.	East coast, Autumn Maximum Power Level for Various Airship Lengths.....	90
Figure 81.	East coast, Winter Maximum Power Level for Various Airship Lengths.....	90
Figure 82.	West coast, Spring Maximum Power Level for Various Airship Lengths.....	91
Figure 83.	West coast, Summer Maximum Power Level for Various Airship Lengths.....	91
Figure 84.	West coast, Autumn Maximum Power Level for Various Airship Lengths.....	92
Figure 85.	West coast, Winter Maximum Power Level for Various Airship Lengths.....	92
Figure 86.	Mass Breakdown for East Coast Airship	94
Figure 87.	Mass Breakdown for West Coast Airship.....	95
Figure 88.	Airship Length and Maximum Power Needed for Continuous Operation Along the East Coast with a Payload of 2000 kg.....	96
Figure 89.	Large Airship Solution for Observing Within High Wind Areas....	97
Figure 90.	Observation Solution for Observing Within High Wind Areas.....	97
Figure 91.	Rotate Airship Solution for Observing Within High Wind Areas.....	98
Figure 92.	Altitude Change Solution for Observing Within High Wind Areas.....	98

Introduction

The ability to fly for an extended duration of time (months to years) at high altitudes (18km and higher) has been an elusive goal. However, in recent years renewable energy technology has progressed to the point where ultra long duration air vehicles can be considered. The airship is one type of long endurance air vehicle that has significant potential. Airships, unlike aircraft, generate lift through the buoyancy effect instead of through aerodynamics. This means that the airship does not need to stay in motion to remain aloft. An airship also has the ability to carry heavy payloads with minimal volume constraints. These characteristics, compared to that of a conventional aircraft are what make airships a unique candidate for a long endurance high altitude flight vehicle. The purpose of the analysis presented within this paper is to evaluate the potential capabilities and limitations of using an airship for a high altitude long endurance mission.

For any type of long endurance vehicle, technologies such as thin film solar arrays, fuel cells, electrolyzers and power management are the key elements in the feasibility of achieving long duration high altitude flight. To enable a vehicle to operate solely off of the incoming energy of the sun is a fine balance between energy collection and energy consumption. This energy balance is influenced by a number of factors such as the operational environment and the capabilities and efficiencies of the power system components. Items such as where and when the vehicle is to fly will greatly influence the available power. And payload capacity and power requirements, size (drag), component efficiencies and power management will determine power consumption. Since the basic power source, the sun, is not available throughout the whole day, managing the collection, storage and consumption of energy will determine the feasibility of the vehicle.

Utilizing the sun as the main power source for the airship presents some unique design challenges compared to a more conventionally powered vehicle. Available power is now directly coupled to the size and layout of the airship. Therefore changing its size not only changes its power requirements but also its power availability. This coupling of available power to a vehicle's size and layout adds an additional layer of complexity to the design process. It also intertwines the power and propulsion system design to the vehicle design essentially making them one. In essence the vehicle is nothing more than a flying power system that is used mainly to run motors and drive the propellers. Because of this close connection between the airship design and the power and propulsion system capabilities, any analysis that is done to examine the requirements of these systems must also include the requirements, capabilities and limitations of the airship itself.

In addition to the airship characteristics, the environment and mission have a significant influence on the airship's capabilities. Factors such as the time of the year and latitude will affect the available solar power. As the airship is used at higher latitudes the variation in day length and solar elevation angle (at a given time during the day) will become more severe. Collecting enough power during the winter months at northern latitudes will be a significant challenge to the airship design. The wind speed that the airship must overcome to maintain its location is also dependent on the time of year, latitude and altitude. Although the wind doesn't affect the power generation capability

of the airship, it has a significant effect on its drag and therefore power consumption. So flying in locations that have high winds could pose a significant challenge to the power system design.

The following analysis takes an initial look at combining these environmental conditions and state of the art power and propulsion technologies to determine what the capabilities and limitations of a high altitude airship are. The analysis is intended as a beginning step in the evaluation of the viability of a high altitude airship. It is meant to provide some insight into the effect of the power and propulsion system technologies on the airship sizing and capabilities and to determine what level of technology is needed to perform a given mission. Also, in a general sense the viability and limitations of an airship as a high altitude long endurance platform will be addressed.

Background

High altitude flight provides a unique vantage point for scientific exploration as well as for observation and surveillance. For this report we will define “high altitude” as being greater than 18 km (~60,000 ft), which is much higher than most conventional aircraft can fly. The main issue in high altitude flight is generating lift within this low atmospheric density environment. The majority of vehicles that can operate at high altitudes do so by flying very fast. High-speed vehicles compensate for the low-density air in this manner. The majority of these types of vehicles have been military and the most notable of these are the military’s U2 and SR71, shown in figures 1a and 1b respectively. The U2 is capable of flight to altitudes up to 21 km (~70,000 ft) at a cruising speed of 692 km/hr (430 mph) and an endurance of approximately 7 hours [1]. The SR71 is capable of flight to altitudes of 27 km (~90,000 ft) with a cruising speed of 3,380 km/hr (2,100 MPH, Mach 3.2) and a flight endurance of approximately 1.5 hours [2].

Although capable of high altitude flight, the endurance of these types of aircraft is limited. Recently there has been an increase in high altitude endurance with the introduction of unmanned air vehicles (UAV). Examples of these are the Condor from the late 1980’s and the present day Global Hawk. These aircraft are UAVs that are designed for surveillance and to loiter over a particular site. They are shown in figures 2a and 2b respectively. The Condor had limited use and was mostly a prototype aircraft. It was propeller driven and capable of flights up to 21 km (~67,000 ft) [3]. The global hawk is the latest in high altitude UAV development. It is capable of flight at 20 km (65,000 ft) with a cruise speed of 643 km/hr (400 mph) and endurance of 35 hours [4].



Figure 1a U2 High Altitude Aircraft Figure 1b SR71 High Altitude Aircraft

The Global Hawk pushes the limits of flight duration that can be achieved using a fuel driven aircraft at high altitudes. To extend the duration beyond this, a renewable power system has to be considered. The only presently constructed aircraft that is trying to employ this strategy is Aerovironment's Helios.



Figure 2 a Condor High Altitude UAV

Figure 2b Global Hawk High Altitude UAV

The Helios, shown in figure 3, is a solar powered aircraft with a regenerative fuel cell system as the means for energy storage. It is estimated that the aircraft would be capable of flight at altitudes up to 21 km (~70,000 ft) for durations on the order of months [5]. The Helios would be capable of station keeping over a desired site for extended periods of time. However, its main drawback is in its limited payload capacity, estimated to be on

the order of 250 kg, and the requirement to have the payload somewhat distributed along the wing plan form. This payload capacity should be sufficient for certain types of science and observational missions. However, if a centralized, more massive payload were required, such as a radar system, this type of air vehicle would not be applicable.



Figure 3 Helios High Altitude Long Endurance Solar Powered UAV

None of the types of aircraft discussed previously can carry a large payload (on the order of 2000 kg or more) at high altitudes and remain aloft for months to years. To achieve this, a different type of air vehicle needs to be considered. An airship has the ability to meet these needs. Since an airship does not need to be in motion to generate lift, it is not nearly as power intensive as an aircraft (that is while carrying the same payload). This is a big advantage for a vehicle based on a renewable power system. In addition, the limitations of an airship, such as slow speed and weather sensitivity, are not factors for a station-keeping mission at altitudes well above the active weather.

Lighter than air vehicles, in the form of weather balloons, routinely operate at high altitudes. Balloons can carry heavy payloads to altitudes upwards of 36 km (120,000 ft). These balloons, which are used mainly for scientific research and weather data collection, are uncontrolled and typically operate for short durations. An example of a high altitude balloon is the Air Force's High Altitude Balloon Experiment (HABE), shown in figure 4a [6]. To overcome the problem of control, a balloon can be tethered (aerostat) and thereby held in a fixed location. Aerostats are common devices and have been used for both military and civilian applications. An example of an aerostat is shown in figure 4b. This aerostat is Lockheed Martin's Tethered Aerostat Radar System [7]. It is capable of flights up to 5 km for durations of up to a week. Like balloons, aerostats can be used for science data gathering, weather data, communications and surveillance. However, significant

materials development is needed to produce a tether that is light enough and strong enough to maintain an aerostat within the desired high altitude range being considered in this study [8,9]. In the future, with the development of breakthrough materials such as carbon nanotube wires, aerostats may be a viable alternative for a high altitude long endurance vehicle.



Figure 4a Air Force High Altitude Balloon (HABE)



Figure 4b Lockheed Martin Tethered Aerostat

The next class of vehicles capable of achieving high altitude flight is the airship. Although they generate lift in the same manner, an airship is a much more complicated and versatile vehicle than a balloon or aerostat. To operate at high altitudes for extended durations requires a renewable based power system. The leading choice for this type of power system is a photovoltaic array coupled to an electrochemical energy storage system such as a fuel cell or battery. Other types of power production systems can be considered such as beaming power from the surface to the airship. This would effectively eliminate the need for energy storage. However, significant development would be needed to perfect a safe and effective beamed power system. Also the airship locations would be limited to the range of the power beam. This would significantly limit the versatility and mission capability of the airship. Because of these concerns this analysis will focus on a photovoltaic powered airship with a fuel cell /electrolyzer as the energy storage system.

To date airships have not been constructed that can reach the desired high altitude range of 18 km or higher. Some of the highest altitudes ever achieved by airships were accomplished by the German Zeppelins in the early 1900's. These ships reached altitudes near 7.5 km (25,000 ft) [10]. This was quite an accomplishment considering these ships were equipped with little environmental control for the personnel on board. The concept of a high altitude airship began with the United States Navy in the late 1970's. This initial Navy sponsored program was titled "High Altitude Super-Pressure Powered Aerostat

(HASPA). This program was then followed in the 1980s by the “High Surveillance Platform for Over-the-Horizon Targeting” (HI-SPOT) program. These efforts were the first serious look at the possibility of a high altitude airship. The programs were classified so there is little information available on their status or outcome. Since then there have been a number of studies performed over the last 20 years from a variety of organizations in various countries that investigated the design issues of high altitude airship flight, construction and operation. Although none of these have yet progressed into an actual airship, the analysis and design efforts have been instrumental in identifying and in some cases offering potential solutions to many of the issues related to flying a high altitude long endurance airship.

Mission

To fly at high altitudes for extended durations provides a vantage point and capability that is presently not available with conventional air vehicles or satellites. There are a number of potential applications both civilian and military that can take advantage of this type of vehicle.

The main interest in high altitude airships has been for communications or wide area surveillance. For civilian applications, high altitude airships represent a low cost alternative to a geostationary satellite. For the military it represents a versatile platform that can be positioned over key areas of interest quickly and provide continuous wide area coverage for extended periods of time.

An airship with its heavy lifting capacity provides the potential for carrying certain types of payloads that would not be practical for other types of high altitude long endurance vehicles. An example of this type of payload would be a radar system. Radar systems provide a unique and unmatched observational capability. Radar can penetrate clouds and rain and allows for continuous observation of a selected area. It works equally well during the day or night. Radar systems as well as visible imagery are examples of line of site devices, which benefit from the high altitude operation. The range these devices can see will depend on the altitude of the airship. Therefore the higher up in the atmosphere you can position the airship the greater the view or coverage area. The coverage area of the airship is determined by calculating the distance to the horizon from the airship. This radial distance (S) is calculated based on the height of the airship (h) and the Earth’s radius (r). It is given by equation 1 and is shown in figure 5. The coverage radius as a function of altitude is shown in figure 6.

$$S = \cos^{-1}\left(\frac{r}{r+h}\right)r \quad [1]$$

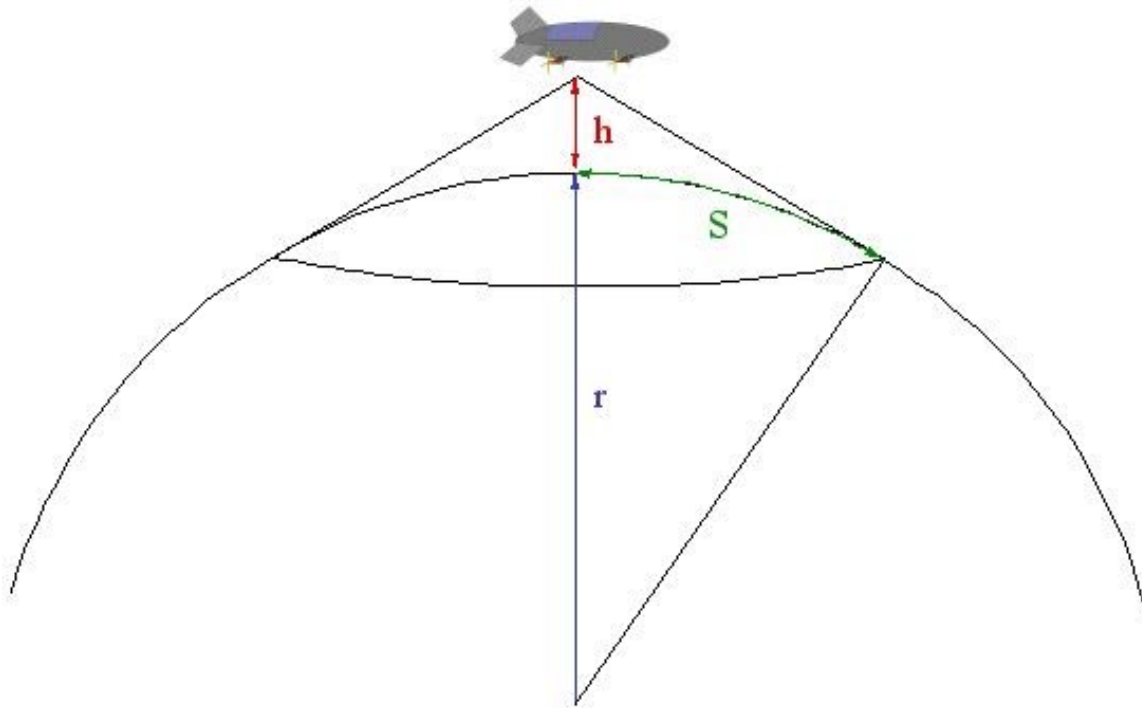


Figure 5 Horizon as seen from the Airship (not to scale)

From figure 6 it can be seen that at an altitude of 20 km the horizon distance is approximately 500 km (310 miles). This enables a single airship to provide coverage over a significant amount of surface area. This compares to a 100 m ground tower that would have a horizon distance of 36 km (22 miles). These distances assume sea level horizon conditions. From this comparison, the benefit of a high altitude platform for line of sight observations can be seen. To completely observe the East coast of the United States, with an overlap area of 1/4, it would take approximately 6 airships operating at an altitude of 20 km. In contrast, it would take approximately 60 ships or land-based towers to observe the same territory. It should also be noted that the land-based towers could not observe more than 36 km out into the ocean, whereas the airship can observe 500 km out into the ocean. This 500 km view out into the ocean provides additional security by enabling sufficient reaction time to intercept any unknown vehicle before it gets near the coast.

In addition to affecting the viewing range, the altitude at which the airship will operate at can significantly affect its design and performance capabilities. The key to minimizing the airship's required size or maximizing the performance of a given size airship is to operate it under minimum drag conditions. For an observational mission where the airship is station- keeping the majority of the time, minimum drag will be a combination of the mean wind velocity, airship size necessary to lift the desired payload, and the air density at the operational altitude.

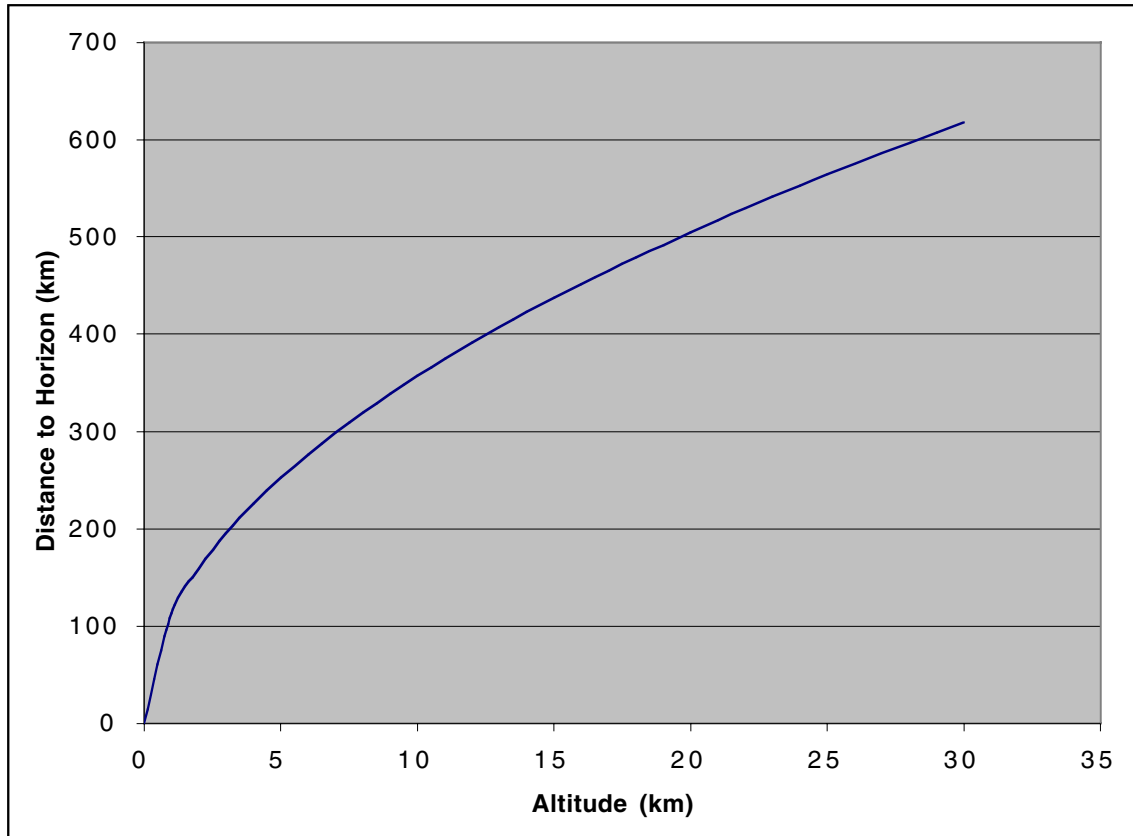


Figure 6 Horizon Distance as a Function of Altitude

The drag (D) on the airship is proportional to the wind velocity (V) and air density (ρ). This proportionality is given in equation 2. It is based on an estimate of the scaling of the airship mass with volume. The inverse relationship between drag and air density may seem counter intuitive. However this is based on the fact that as the air density decreases the air ship volume must increase to lift the given payload and ship mass. It is this increase in air ship volume and therefore mass with decreasing air density that produces the inverse relationship between drag and air density.

$$D \propto \frac{V^2}{\rho^{(2/3)}} \quad [2]$$

The relationship given in equation 2 is plotted in figure 7. This figure shows the airship's relative drag for an altitude range from the surface to 30 km. The figure is based on the mean wind speed profile for the winter months at 38° N latitude along the East coast.

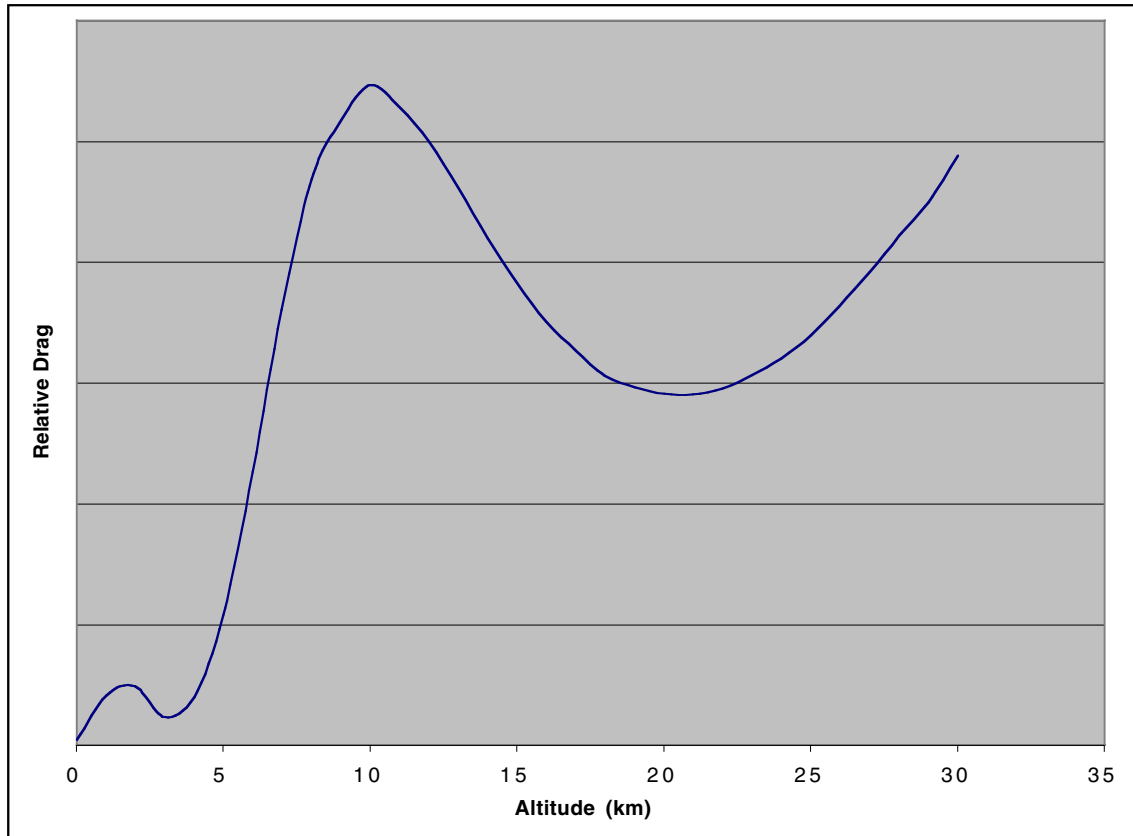


Figure 7 Relative Drag on an Airship Sized to Carry a Fixed Payload at a given Altitude at 38° N Latitude along the East coast

This figure represents how the drag and therefore power requirements of the airship would scale to carry a fixed payload at a specific altitude. From the figure it can be seen that for high altitude operation there is a minimum in drag at around 22 km in altitude.

To evaluate the capabilities and requirements for a high altitude airship a baseline mission was chosen. The mission selected was to evaluate the potential of positioning a high altitude airships along the east and west coasts of the United States as observational platforms for coastal security. The operational altitude was selected to be 21.5 km (~70,000 ft). This mission design point provides an observational radius of approximately 500 km (310 miles) and minimizes the operational power requirements.

Airship Configuration

A number of airship configurations capable of achieving high-altitude long-endurance flight have previously been proposed by the various analyses and design efforts that have been performed by various organizations both public and private. These designs range from conventional cylindrical shapes to the non-conventional spherical or saucer shaped vehicles. An example of a conventional airship layout is Lockheed’s high altitude airship concept [11]. This concept is shown in figure 8. This airship is an elliptical shaped

vehicle with three conventional tail fins for stability and four side mounted engine pods for propulsion and control.



Figure 8 Lockheed Martin's High Altitude Airship Concept

This type of layout is the most common proposed for a high altitude airship. Other organizations, such as Japan's National Aerospace Laboratory [12], have also proposed similar configurations. This type of layout has good drag characteristics and has heritage with low altitude airship designs. There are some variations on the elliptical airship layout that have also been proposed. These include the designs from the European Space Agency (ESA) performed through their contractor Lindstrand Balloons Ltd. (LBL) for a high altitude long endurance (HALE) aerostatic platform [13], and the design for a heavy lift airship for the Air Force by Skycat Technologies [14]. The ESA design, shown in figure 9a, is a half elliptical body with a modified tail section. The Skycat 1000, shown in figure 9b, is an airfoil shaped airship. Although this airship was design for carrying heavy loads at low altitudes it could also be considered as a high altitude airship due to its size. This design presents an interesting configuration for a long endurance airship. Because of the airfoil shape, the airship has a relatively flat top section. This flat area would provide a location for the solar array allowing the entire array to be illuminated throughout the day. For the standard cylindrical configuration a portion of the solar array is almost always shaded, depending on the orientation of the airship and the time of day. This means that the full potential of the array is never utilized. It also presents some power management problems due to the partial shadowing of the array. The flat topped Skycat type vehicle has the potential to eliminate these issues. To determine whether there is a benefit would require a detailed power analysis of the Skycat configuration compared to the more traditional cylindrical airship configuration. Since the array on the Skycat will be mostly horizontal, the output profiles will be significantly different than that of the cylindrical airship's arrays. Time of year and latitude of operation would also need to be considered to determine if, where and when there is a benefit to this design. The evaluation of this type of airship configuration was beyond the scope of this initial analysis but would be worthwhile considering in future analysis.



Figure 9a ESA High Altitude Airship Concept



Figure 9b Skycat Heavy Lift Airship Concept

Other more non-conventional configurations have also been proposed for a high altitude airship. These are mostly symmetrical designs either spherical or saucer shaped. Examples of these are Techsphere Systems International's spherical high altitude airship concept [15] and LTAS/Cambot's saucer shaped high altitude airship concept [16]. These concepts are shown in figures 10a and 10b. The designs present an interesting deviation from the conventional approach. These designs will produce a much better volume to surface area ratio than the cylindrical designs, thereby minimizing envelope mass. However, their main drawback is the higher drag coefficient they will produce due to their shape. The low Reynolds number environment at altitude will tend to make the air flow over their surface separate at the mid point of the vehicle. This will cause a significant increase in drag coefficient over a more streamlined airship design. This problem may be able to be overcome through active boundary layer control but this will consume power. A tradeoff would need to be performed to determine whether the increased power and equipment needed for the boundary layer control is offset by the reduced envelope mass.

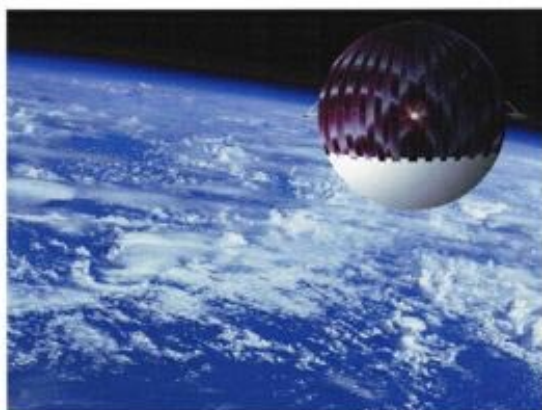


Figure 10a Techsphere System's Spherical Airship Concept



Figure 10b LTAS/Cabot's Saucer Airship Concept

Although some of the non-conventional airship configurations are interesting and may hold potential as viable high altitude airship designs, for this analysis a conventional cylindrical airship shape was used. To simplify the analysis a cylindrical shaped airship

with hemispherical ends was chosen as the baseline configuration. The airship had a three tail fin arrangement and four engine pod systems. The engine pods and the support structure were arranged in groupings of two (one on the left and one on the right side) evenly spaced along the bottom of the airship. The solar array was positioned on the upper half of the cylindrical section. The full upper half of the cylinder was not completely covered with the solar array. The amount of array coverage depended on the airship sizing and mission details. A diagram of the airship configuration used throughout the analysis is shown in figure 11.

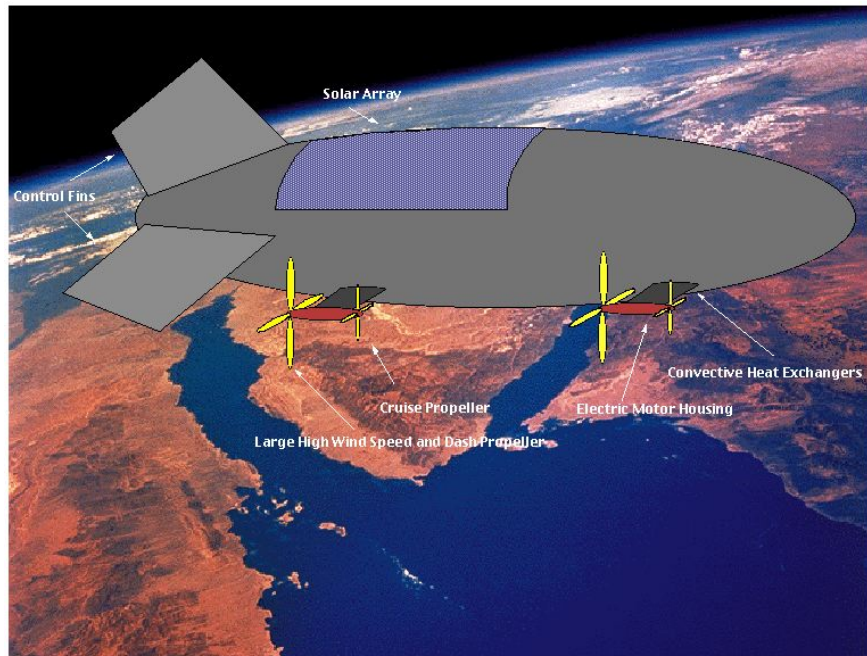


Figure 11 Analysis Baseline Airship Configuration

Environment

The atmosphere of our planet is a very dynamic environment (figure 12) with great fluctuations in temperature, density, pressure, wind speeds and solar intensity. This environment in which the airship will operate has a large influence on its performance, design and capabilities. The main physical properties of the Earth's environment are given in table 1 and the structure of the atmosphere is shown in figure 13. The influence of the environment is greater for a long endurance airship than it is for most conventional aircraft flying under the same conditions. This is due mainly to the large size of the airship (which is necessary to fly at the desired altitudes) and the fact that the airship receives all of its operating power from the sun. Because of these characteristics the airship design is very sensitive to atmospheric winds and the available incident solar radiation. The airship can potentially operate at any location that has sufficient solar intensity to generate the required power and atmospheric density to maintain the required lift for the vehicle. Daily solar intensity profiles will vary only with the time of year and latitude whereas the statistical mean and 99th percentile wind speeds will vary with the time of year, latitude, longitude and altitude.

Aside from these two main environmental factors, other issues unique to high altitude flight will also influence the airship design. These factors include UV radiation, cosmic rays, temperature and electrical discharges from lower altitude storm clouds.

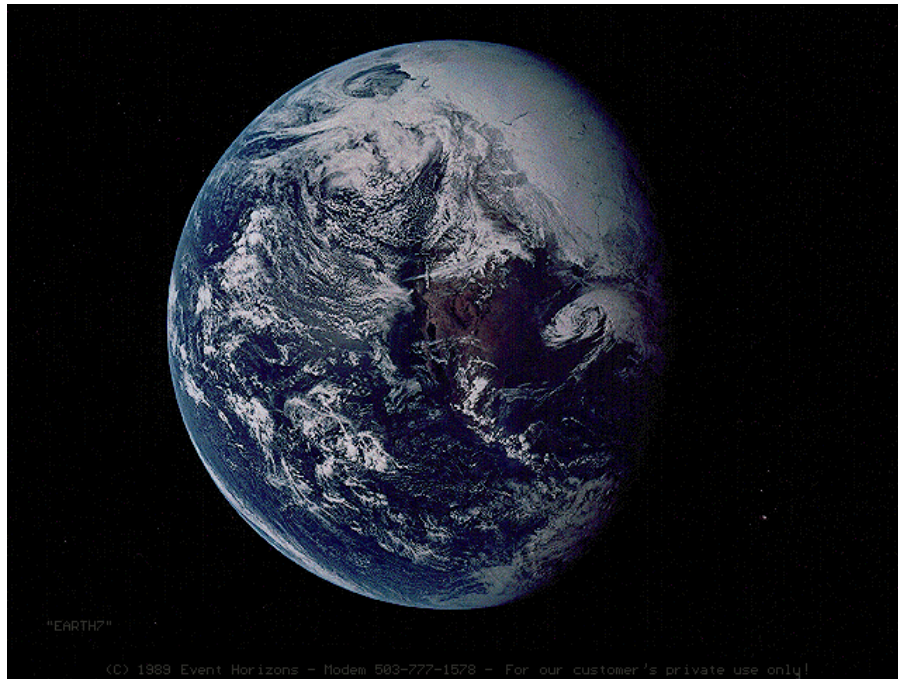


Figure 12 Earth from Space

Table 1 Earth's Physical Properties [17]

Inclination of Equator to Orbit	23.45°
Orbital Eccentricity	0.01673
Day Period	23h 57.8 m
Solar Radiation Intensity	Mean: 1352 W/m ² Perihelion: 1399 W/m ² Aphelion: 1307 W/m ²
Albedo	0.37
Gravitational Constant	9.81 m/s ²
Sidereal Year	365.26 (Earth Days)
Surface Temperature Extremes	130 K to 300 K
Diameter	12,756 km

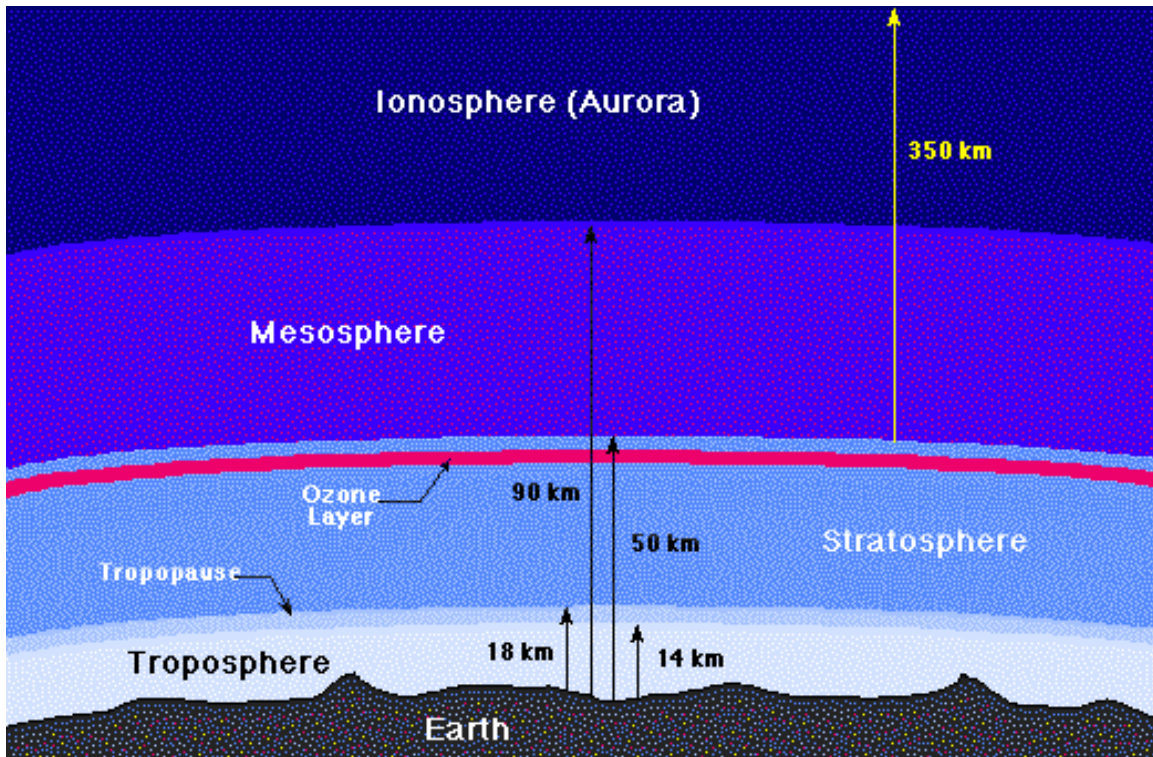


Figure 13 Profile of Earth's Atmosphere [18]

Earth's atmosphere is broken down into layers, as shown in figure 13. The layers of interest for the airship are the troposphere (from the surface to approximately 14 km), the tropopause (from ~14 km to ~18 km) and the lower 1/3 portion of the stratosphere (~18 km to ~30 km). The *troposphere* is the region in the atmosphere where all the active weather occurs. Air rises and falls due to heating and ground effects causing winds and weather patterns. The majority of cloud formations and the atmosphere as we see it occurs in the troposphere, figure 14. There is a gradual change from troposphere to the stratosphere that begins at approximately 14 km in altitude. This is called the Tropopause. The temperature in the lower stratosphere is extremely stable and cold at -57°C . Here, strong winds occur as part of defined circulation patterns and are mostly horizontal with little mixing. Above the tropopause is the stratosphere, high cirrus clouds sometimes form in the stratosphere, but for the most part there are no significant weather patterns in the stratosphere [19].

The Earth standard atmosphere table was used as the source of atmospheric properties for this analysis. It is based on idealized year round conditions at 45°N latitude. From this table the ideal gas constant for the Earth's atmosphere is 8.31432 J/mol K . The viscosity (μ) and thermal conductivity (k) of the atmosphere are based on temperature (T) and can be approximated by the following equations [20].

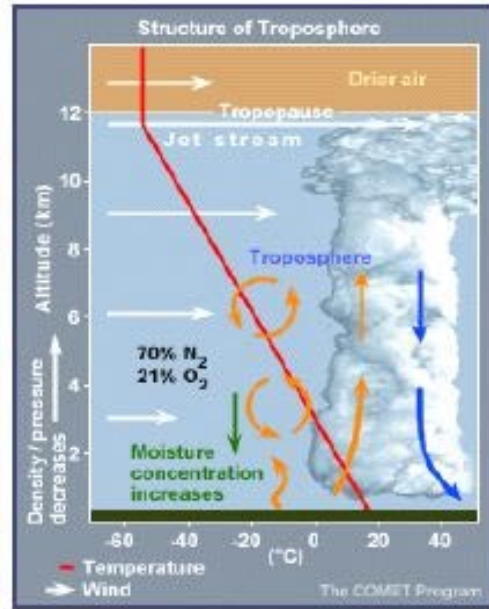


Figure 14 Troposphere Region of the Atmosphere

Viscosity in (kg/m s)
$$\mu = \frac{(1.458E - 6)T^{1.5}}{T + 110.4} \quad [3]$$

Thermal conductivity in (kcal m s K)
$$k = \frac{(6.325E - 7)T^{1.5}}{T + 245.4 \times 10^{\left(-\frac{12}{T}\right)}} \quad [4]$$

The atmospheric composition is given in table 2 and the standard atmospheric profile is given in table 3.

Table 2 Major Gas Components of Earth's Atmosphere [20]

Gas	Percent Volume
N ₂	78.084
O ₂	20.947
Ar	0.934
CO ₂	0.0314
Ne	0.00181
He	0.000524

Table 3 Standard Atmosphere [20]

Altitude (m)	Temp. °K	Pressure mBar	Density (kg/m ³)	Speed of Sound (m/s)	Viscosity (Kg/m s)	Conductivity (kcal m s °K)
0	288.15	1013.3	1.225	340.3	1.789E-5	0.6053E-5
200	286.85	989.5	1.202	339.5	1.783E-5	0.6029E-5
400	285.55	966.1	1.179	338.8	1.777E-5	0.6004E-5
600	284.25	943.2	1.156	338.0	1.771E-5	0.5980E-5
800	282.95	920.8	1.134	337.2	1.764E-5	0.5955E-5
1000	281.65	898.8	1.112	336.4	1.758E-5	0.5931E-5
1200	280.35	877.2	1.090	335.7	1.752E-5	0.5906E-5
1400	279.05	856.0	1.069	334.9	1.745E-5	0.5881E-5
1600	277.75	835.3	1.048	334.1	1.739E-5	0.5857E-5
1800	276.45	814.9	1.027	333.3	1.732E-5	0.5832E-5
2000	275.15	795.0	1.007	332.5	1.726E-5	0.5807E-5
2200	273.86	775.5	0.987	331.7	1.720E-5	0.5784E-5
2400	272.56	756.3	0.967	331.0	1.713E-5	0.5759E-5
2600	271.26	737.6	0.947	330.2	1.707E-5	0.5733E-5
2800	269.96	719.2	0.928	329.4	1.700E-5	0.5708E-5
3000	268.66	701.2	0.909	328.6	1.694E-5	0.5683E-5
3200	267.36	683.6	0.891	327.8	1.687E-5	0.5658E-5
3400	266.06	666.3	0.872	327.0	1.681E-5	0.5634E-5
3600	264.76	649.4	0.854	326.2	1.674E-5	0.5609E-5
3800	263.47	632.8	0.837	325.4	1.668E-5	0.5584E-5
4000	262.17	616.6	0.819	324.6	1.661E-5	0.5559E-5
4200	260.87	600.7	0.802	323.8	1.655E-5	0.5534E-5
4400	259.57	585.2	0.785	323.0	1.648E-5	0.5508E-5
4600	258.27	570.0	0.769	322.2	1.642E-5	0.5483E-5
4800	256.97	555.1	0.752	321.4	1.635E-5	0.5458E-5
5000	255.68	540.5	0.736	320.5	1.628E-5	0.5433E-5
5200	254.38	526.2	0.721	319.7	1.622E-5	0.5408E-5
5400	253.08	512.3	0.705	318.9	1.615E-5	0.5383E-5
5600	251.78	498.6	0.690	318.1	1.608E-5	0.5357E-5
5800	250.48	485.2	0.675	317.3	1.602E-5	0.5332E-5
6000	249.191	472.2	0.660	316.5	1.595E-5	0.5307E-5
6200	247.89	459.4	0.646	315.6	1.588E-5	0.5282E-5
6400	246.59	446.9	0.631	314.8	1.582E-5	0.5256E-5
6600	245.29	434.7	0.617	314.0	1.575E-5	0.5231E-5
6800	244.00	422.7	0.604	313.1	1.568E-5	0.5205E-5
7000	242.70	411.1	0.590	312.3	1.561E-5	0.5180E-5
7500	239.46	383.0	0.572	310.2	1.544E-5	0.5116E-5
8000	236.22	356.5	0.526	308.1	1.527E-5	0.5052E-5
8500	232.97	331.6	0.496	306.0	1.510E-5	0.4988E-5
9000	229.73	308.0	0.467	303.8	1.493E-5	0.4924E-5
9500	226.49	285.8	0.440	301.7	1.475E-5	0.4859E-5
10000	223.25	265.0	0.414	299.5	1.458E-5	0.4794E-5

Table 3 Standard Atmosphere (Concluded)

11000	216.77	227.0	0.365	295.2	1.422E-5	0.4664E-5
2000	216.65	194.0	0.312	295.1	1.422E-5	0.4664E-5
13000	216.65	165.8	0.267	295.1	1.422E-5	0.4664E-5
14000	216.65	141.7	0.228	295.1	1.422E-5	0.4664E-5
15000	216.65	121.1	0.195	295.1	1.422E-5	0.4664E-5
16000	216.65	103.5	0.166	295.1	1.422E-5	0.4664E-5
17000	216.65	88.5	0.142	295.1	1.422E-5	0.4664E-5
18000	216.65	75.7	0.122	295.1	1.422E-5	0.4664E-5
19000	216.65	64.7	0.104	295.1	1.422E-5	0.4664E-5
20000	216.65	55.3	0.0889	295.1	1.422E-5	0.4664E-5
22000	218.57	40.5	0.0645	296.4	1.433E-5	0.4702E-5
24000	220.56	29.7	0.0469	297.8	1.444E-5	0.4742E-5
26000	222.54	21.9	0.0343	299.1	1.454E-5	0.4782E-5
28000	224.53	16.2	0.0251	300.4	1.465E-5	0.4820E-5
30000	226.51	12.0	0.0184	301.7	1.475E-5	0.4859E-5
35000	236.51	5.75	0.0085	308.3	1.529E-5	0.5058E-5
40000	250.35	2.87	0.0040	317.2	1.601E-5	0.5330E-5
50000	270.65	.798	0.0010	329.8	1.704E-5	0.5721E-5
100000	210.02	3e-4	5e-7	---	---	---

Winds

The wind speed on Earth is highly variable. It is dependent on the location, time of year and altitude. Examples of mean wind profiles are shown, in figures 15 and 16, for two locations (Cape Kennedy, Fl and Spokane, WA) throughout the year. Although the absolute value of the wind speed will vary with altitude, the trends (shown in these figures) are similar for most locations.

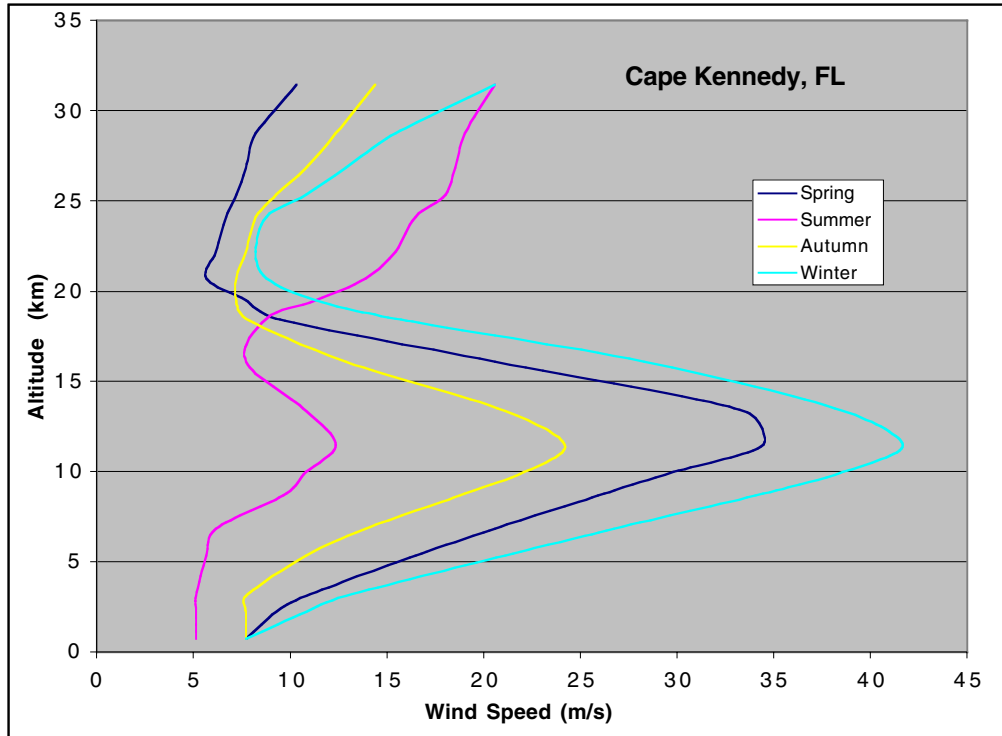


Figure 15 Mean Winds for Cape Kennedy, FL, Throughout the Year [21]

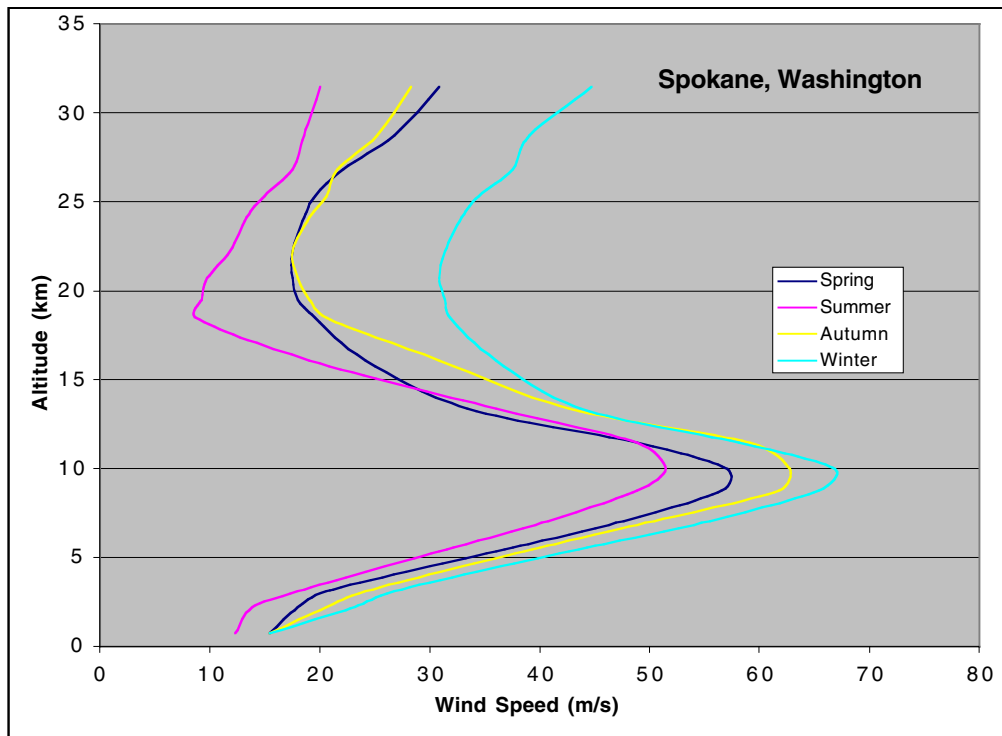


Figure 16 Mean Winds for Albuquerque, NM Throughout the Year [21]

Because of the size of the airship, drag and therefore wind speed at altitude and throughout the desired period of operation are critical factors in the airship's design and capabilities. To accurately determine the feasibility of the high altitude airship concept a detailed model of the wind environment is needed. This wind model would provide mean and 99th percentile winds along the area of interest for the analysis. The model would need to be variable with time of year, latitude and altitude to be consistent with the modeling scheme. To bound the problem as well as being consistent with the initial analysis objective, only the wind environment along the East and West coast of the US was considered.

The wind data for the derivation of the modeling equations was based on the data provided in reference 21. This data originated from the National Climatic Center and represented all available wind data at the specified locations from the surface up to 10 mb (~31km) in altitude. The data was presented seasonally and included mean, mean +5%, mean -5%, 95th percentile and 99th percentile winds. Examples for mean winds are shown in figures 15 and 16. The locations along or near the coast where the wind data was available are listed in table 4.

Table 4 Raw Wind Data Sites [21]

<i>Location</i>	<i>City</i>	<i>Latitude</i>	<i>Longitude</i>	<i>Data Collection Period</i>	<i>Total Profiles Sampled</i>
East Coast	Portland, Maine	44°N	71°W	January 1948 to September 1972	10,483
	Washington DC	38°N	76°W	October 1960 to December 1971	13,439
	Charleston, S. Carolina	32°N	80°W	January 1948 to December 1971	11,795
	Cape Kennedy, Florida	28°N	81°W	February 1950 to May 1970	16,424
West Coast	Spokane, Washington	48°N	118°W	January 1950 to December 1970	11,144
	Oakland, California	37°N	122°W	January 1950 to December 1970	10,771
	Vandenberg, California	34°N	121°W	July 1958 to May 1970	11,933

The wind profile data from the sites listed in table 4 was used to generate equations that would provide mean and 99th percentile wind speeds for a specified altitude and latitude along the East and West coasts of the United State. The equations generated represent mathematical surfaces of wind speed versus altitude versus latitude. Since the wind data for each of these locations was separated into seasons, there were eight wind speed equations generated for each coast (mean and 99th percentile wind speed). These equations were used in the subsequent analysis to provide the wind speed information and greatly simplified the analysis process. An example of the output of one of the wind surface equations is given in figure 17. This figure was generated using the equation for mean wind speed along the East coast in the winter. The sixteen wind speed profiles, which encompass mean and 99th percentile winds for both coasts and each season, are

given in equations 5 through 20. For these equations latitude (ϕ) is in degrees, Altitude (h) is given by atmospheric pressure (P, in millibars) and the wind velocity (V) is in m/s. The conversion of atmospheric pressure (P) in millibars to kilometers is given in equation 21.

East Coast Wind Profiles

Mean wind velocity for spring:

$$V = (-6266.7606 + 639.33071\phi - 21.334456\phi^2 + 0.17361051\phi^3 + 3.59335E-3\phi^4 - 5.341E-5\phi^5 + 0.18089073P + 0.1.10336E-3P^2 - 5.966E-6P^3 + 8.329E-9P^4 - 3.644E-12P^5) 0.5144 \quad [5]$$

Mean wind velocity for summer:

$$V = (-9156.146 + 909.857053\phi - 28.318281\phi^2 + 0.13604351\phi^3 + 7.33643E-3\phi^4 - 9.155E-5\phi^5 - 0.3459049P + 3.2912E-3P^2 - 1.003E-5P^3 + 1.1961E-8P^4 - 4.893E-12P^5) 0.5144 \quad [6]$$

Mean wind velocity for autumn :

$$V = (-8905.7603 + 865.059882\phi - 25.524994\phi^2 + 0.05131931\phi^3 + 8.60907E-3\phi^4 - 9.918E-5\phi^5 - 0.0759347P + 2.39655E-3P^2 - 8.876E-6P^3 + 1.1346E-8P^4 - 4.794E-12P^5) 0.5144 \quad [7]$$

Mean wind velocity for winter :

$$V = (-10056.977 + 985.214629\phi - 30.129253\phi^2 + 0.12888569\phi^3 + 8.12247E-3\phi^4 - 9.918E-5\phi^5 + 0.05001086P + 2.31194E-3P^2 - 9.575E-6P^3 + 1.2515E-8P^4 - 5.313E-12P^5) 0.5144 \quad [8]$$

99th Percentile wind velocity for spring:

$$V = (-17118.752 + 1755.24355\phi - 59.402868\phi^2 + 0.52861784\phi^3 + 8.68393E-3\phi^4 - 1.373E-4\phi^5 + 0.08836463P + 4.26753E-3P^2 - 1.763E-5P^3 + 2.3174E-8P^4 - 9.898E-12P^5) 0.5144 \quad [9]$$

99th Percentile wind velocity for summer :

$$V = (-18380.633 + 1777.9568\phi - 51.4944\phi^2 + 0.04697891\phi^3 + 0.01897739\phi^4 - 2.136E-4\phi^5 - 0.5056217P + 5.84477E-3P^2 - 1.885E-5P^3 + 2.3031E-8P^4 - 9.547E-12P^5) 0.5144 \quad [10]$$

99th Percentile wind velocity for autumn:

$$V = (-23322.236 + 2294.30671\phi - 69.992832\phi^2 + 0.26353416\phi^3 + 0.02021216\phi^4 - 2.441E-4\phi^5 - 0.490624P + 7.25683E-3P^2 - 2.438E-5P^3 + 3.0116E-8P^4 - 1.252E-11P^5)0.5144 \quad [11]$$

99th Percentile wind velocity for winter:

$$V = (-23684.526 + 2333.24941\phi - 71.458827\phi^2 + 0.28778566\phi^3 + 0.02006288\phi^4 - 2.441E-4\phi^5 - 0.3989153P + 7.1656E-3P^2 - 2.462E-5P^3 + 3.0389E-8P^4 - 1.258E-11P^5)0.5144 \quad [12]$$

West Coast Wind Profiles

Mean wind velocity for spring:

$$V = (504339.36 - 61362.878\phi + 2976.05397\phi^2 - 71.916641\phi^3 + 0.8659332\phi^4 - 4.1564E-3\phi^5 - 0.1008834P + 2.47988E-3P^2 - 8.736E-6P^3 + 1.0845E-8P^4 - 4.493E-12P^5) 0.5144 \quad [13]$$

Mean wind velocity for summer:

$$V = (611887.222 - 74493.194\phi + 3614.89414\phi^2 - 87.400052\phi^3 + 1.05288402\phi^4 - 5.0561E-3\phi^5 - 0.2639922P + 3.1923E-3P^2 - 1.03E-5P^3 + 1.2493E-8P^4 - 5.137E-12P^5) 0.5144 \quad [14]$$

Mean wind velocity for autumn:

$$V = (437807.731 - 53265.846\phi + 2583.24068\phi^2 - 62.42262\phi^3 + 0.75161779\phi^4 - 3.6078E-3\phi^5 - 0.0208545P + 1.94285E-3P^2 - 7.45E-6P^3 + 9.5675E-9P^4 - 4.044E-12P^5)0.5144 \quad [15]$$

Mean wind velocity for winter:

$$V = (571292.993 - 69505.987\phi + 3370.79711\phi^2 - 81.449701\phi^3 + 0.98064803\phi^4 - 4.7067E-3\phi^5 - 0.1381809P + 2.82793E-3P^2 - 9.826E-6P^3 + 1.2162E-8P^4 - 5.039E-12P^5) 0.5144 \quad [16]$$

99th percentile wind velocity for Spring:

$$V = (1292870.35 - 157368.62\phi + 7635.13356\phi^2 - 184.56614\phi^3 + 2.22299925\phi^4 - 0.0106731\phi^5 - 0.4615459P + 6.81239E-3h^2 - 2.222E-5P^3 + 2.6712E-8P^4 - 1.087E-11P^5) 0.5144 \quad [17]$$

99th percentile wind velocity for Summer:

$$V = (1363536.73 - 165908.55 \phi + 8046.81928 \phi^2 - 194.46117 \phi^3 + 2.3415885 \phi^4 - 0.01124 \phi^5 - 0.5727243P + 7.47318E-3P^2 - 2.41E-5P^3 + 2.9016E-8P^4 - 1.185E-11P^5)0.5144 \quad [18]$$

99th percentile wind velocity for Autumn:

$$V = (1164188.38 - 141669.35 \phi + 6871.71399 \phi^2 - 166.07304 \phi^3 + 1.99984056 \phi^4 - 9.5998E-3 \phi^5 - 0.25701950P + 5.61218E-3P^2 - 1.964E-5P^3 + 2.4381E-8P^4 - 1.012E-11P^5)0.5144 \quad [19]$$

99th percentile wind velocity for Winter:

$$V = (1200555.53 - 146114.69 \phi + 7088.33208 \phi^2 - 171.33159 \phi^3 + 2.063429 \phi^4 - 9.9063E-3 \phi^5 - 0.4553727P + 6.30509E-3P^2 - 2.074E-5P^3 + 2.5273E-8P^4 - 1.04E-11P^5)0.5144 \quad [20]$$

$$h = \frac{\ln \frac{P}{1118.3}}{-0.15} \quad [21]$$

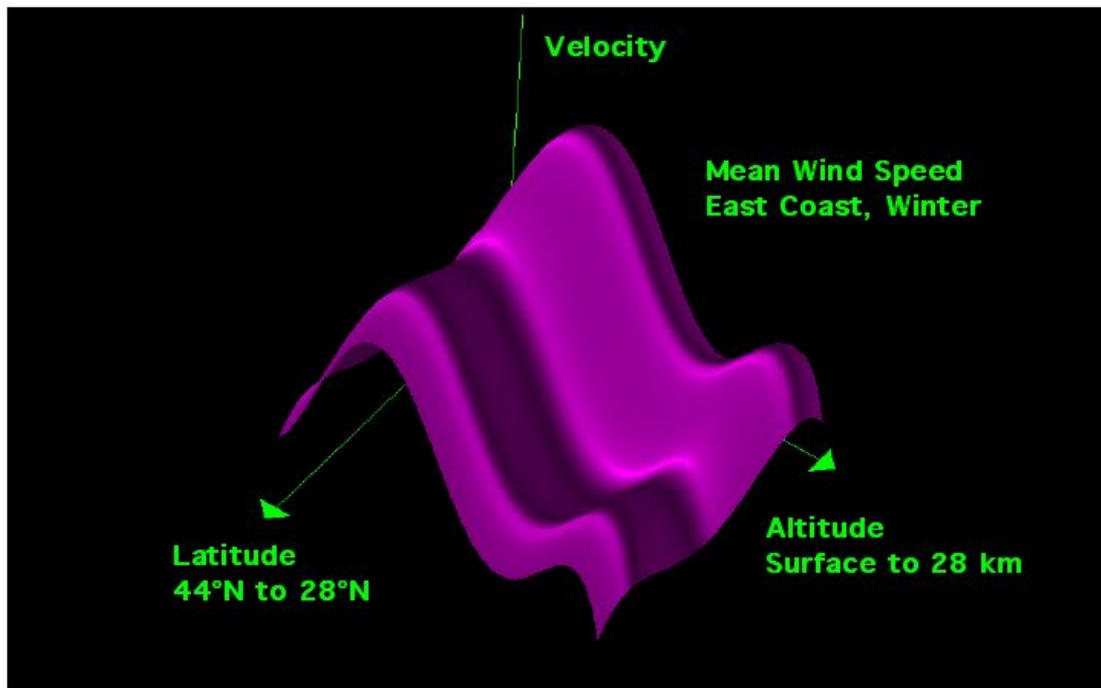


Figure 17 Winter Mean Wind Speed Profile for the East Coast

The curve fits given in equations 5 through 20 are very useful for providing wind speed information quickly and in a format that is easily integrated into an analysis tool. There are however limitations to the equations based on the range of the data from which they were derived. The equations should not be used to predict wind speed outside of limits of the original data. The range limits for these equations are given in table 5.

Table 5 Input Parameter Ranges for Wind Equations

<i>Location</i>	<i>Latitude Range</i>	<i>Altitude Range</i>
East Coast	28°N to 44°N	Surface to 28 km
West Coast	35°N to 48°N	Surface to 28 km

Using the equations given above, plots were generated to show the variation in wind speed throughout the year over the latitude range of interest along both the east and west coasts. The plots represent wind speeds at the operational altitude of 21.5 km that was selected for this analysis.

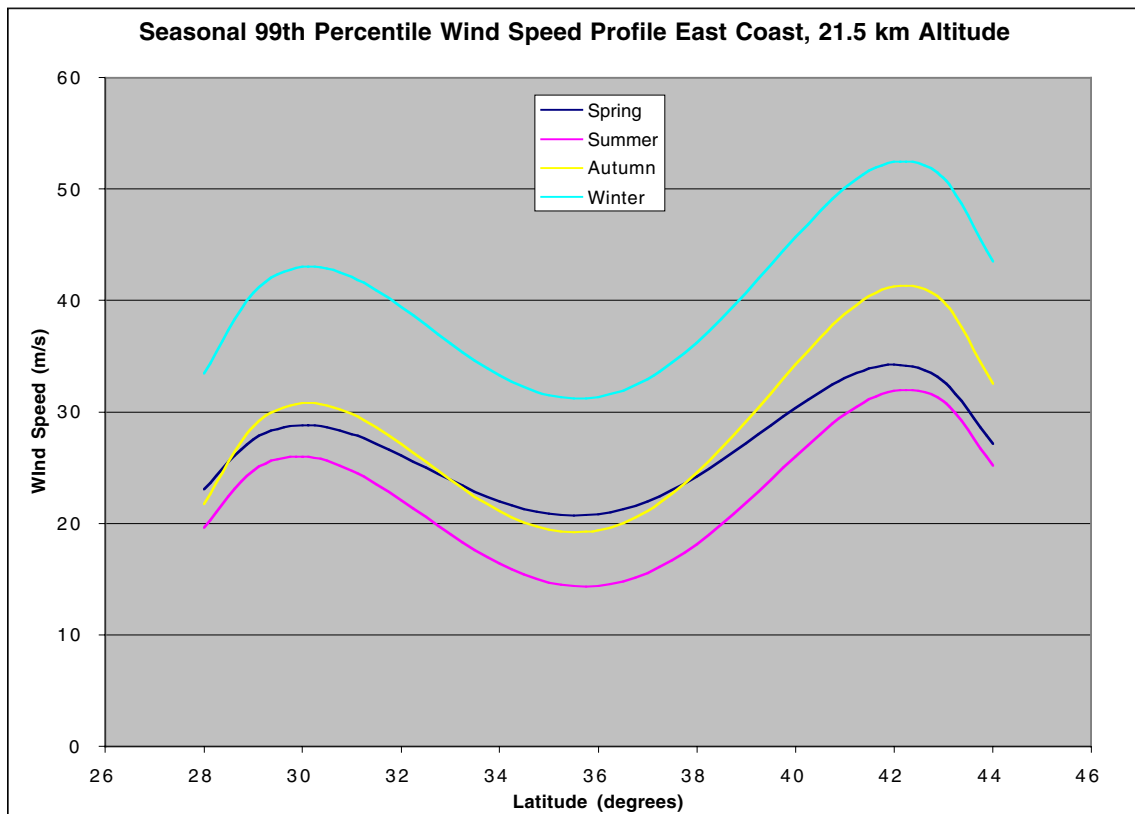


Figure 18 99th Percentile East Coast Wind Speed for an Altitude of 21.5 km

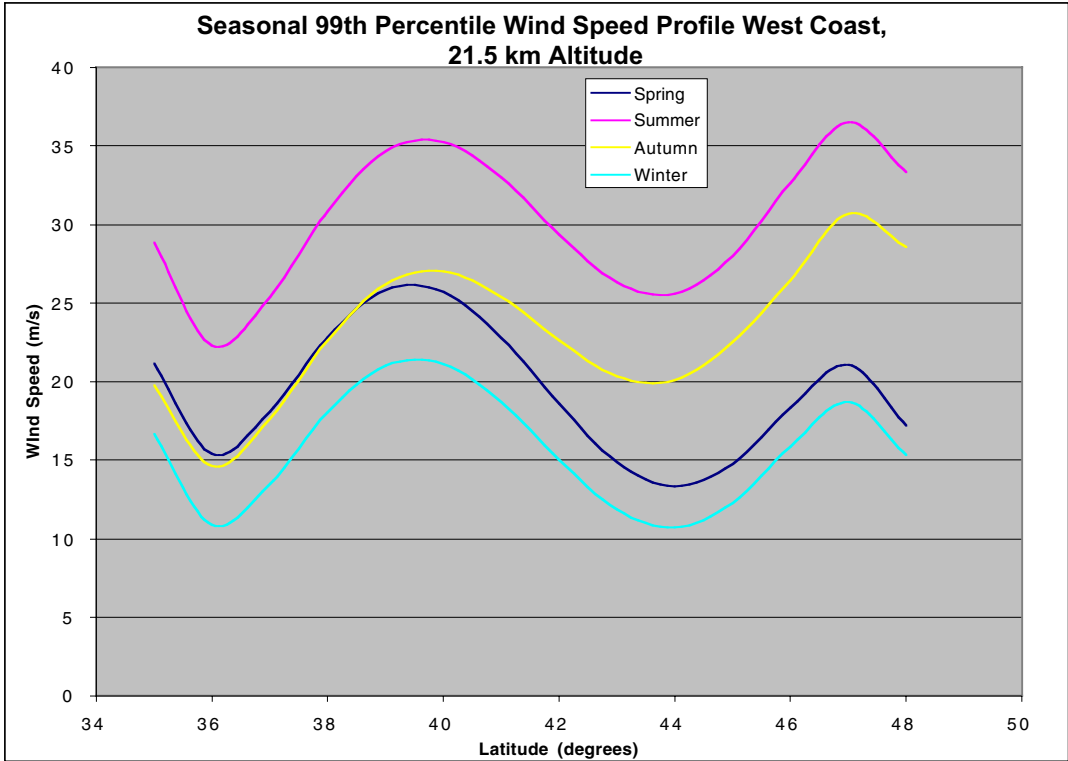


Figure 19 99th Percentile West Coast Wind Speed for an Altitude of 21.5 km

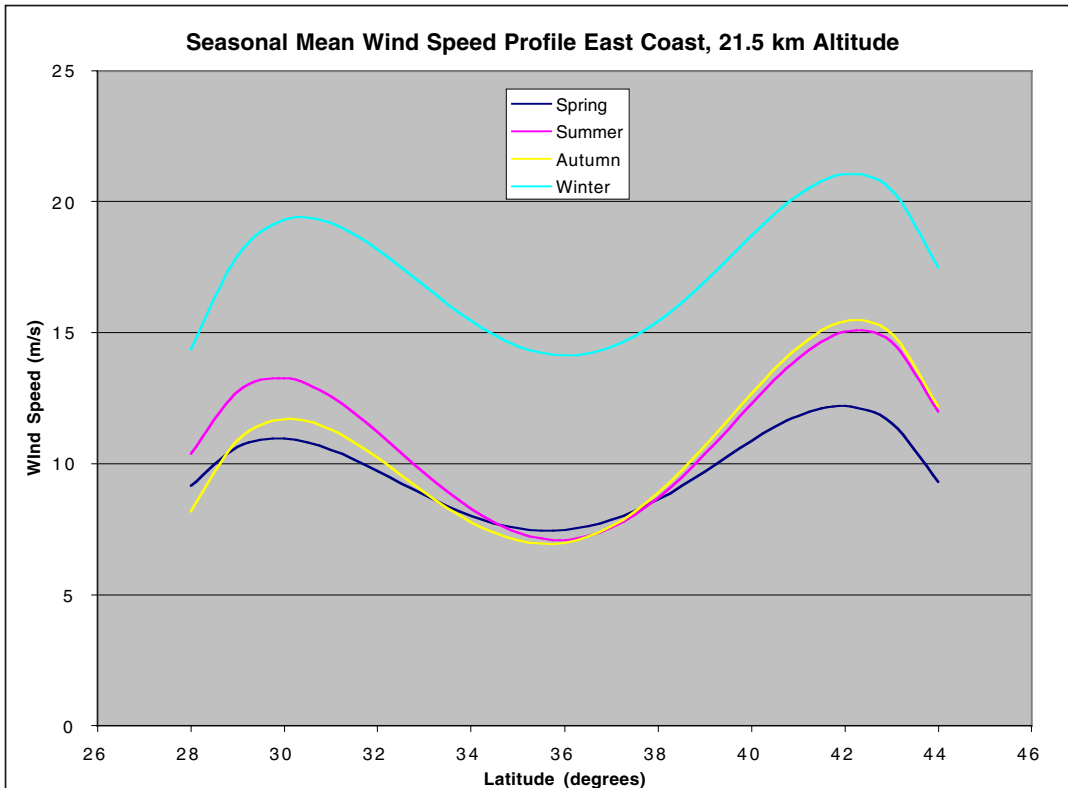


Figure 20 Mean East Coast Wind Speed for an Altitude of 21.5 km

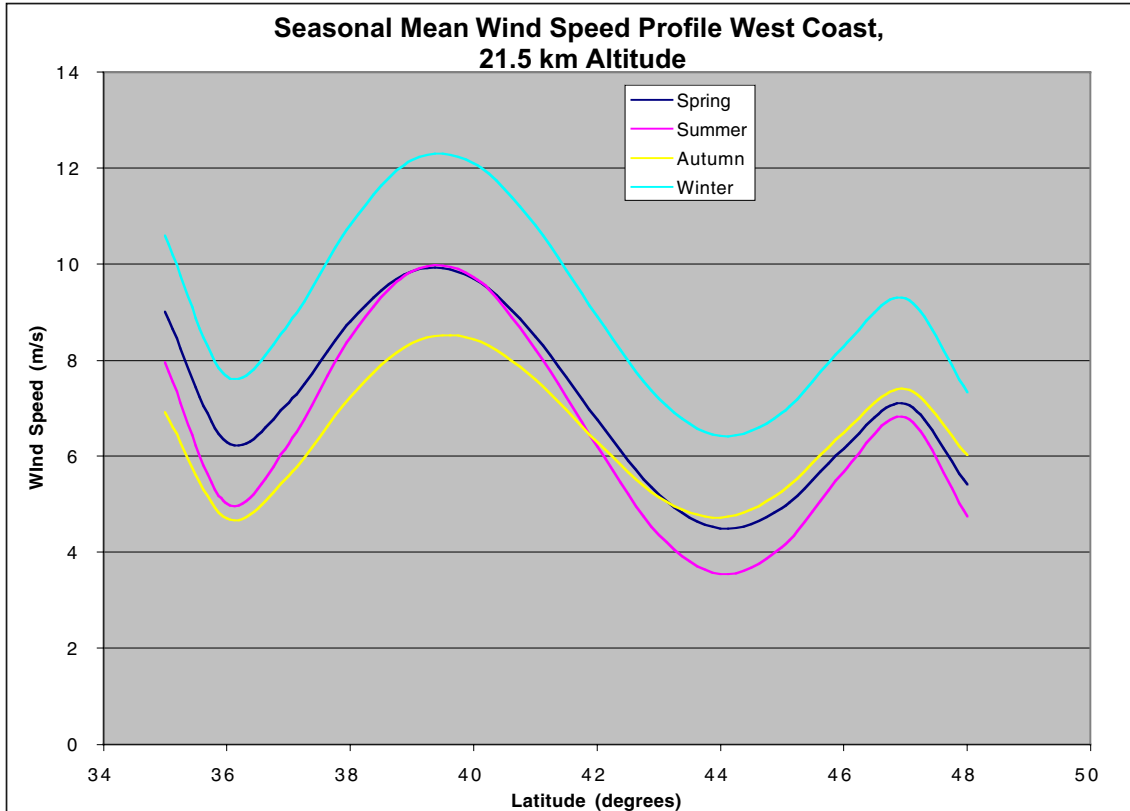


Figure 21 Mean West Coast Wind Speed for an Altitude of 21.5 km

Incident Solar Radiation

In addition to the winds, the solar radiation environment is the second significant environmental factor that drives the design and capabilities of the airship. However, unlike the winds, the incident solar radiation is very predictable and can be modeled with significant accuracy. The solar radiation environment is constantly changing. As the solar elevation angle changes throughout the day the available output power from the solar array will vary. This change in elevation angle is also dependent on the time of year as well as the latitude. The solar intensity also changes throughout the year due to slight variations in the distance of the Earth from the Sun.

To determine the amount of power produced by the solar array the incident flux on the array must be known. Due to the shape of the airship this flux will vary depending on the specific location of a given photovoltaic cell on the airship. Other variables that determine the array output include time of day, time of year, latitude and orientation of the airship. All of these factors must be considered when determining the incident solar radiation on a given photovoltaic cell. The environmental factors that influence the output of the solar array are shown in figure 22.

The solar flux at earth's orbital location is on average $1352 \text{ W/m}^2 (SI_m)$. The actual flux will vary throughout the year as the Earth orbits the Sun. This variation is caused by the Earth's orbit not being completely circular. The variation in Earth's orbital radius (r_{orb})

from the mean orbital radius (r_{orbm}) is represented by the eccentricity (ϵ) of Earth's orbit which has a value of 0.017. The actual solar flux (or intensity, SI) in W/m^2 for a specific day of the year is determined by equations 22 and 23.

$$SI = SI_m (r_{orbm}^2 / r_{orb}^2) \quad [22]$$

Power Production

The amount of power available to the airship is based on the Environmental conditions it is flying within

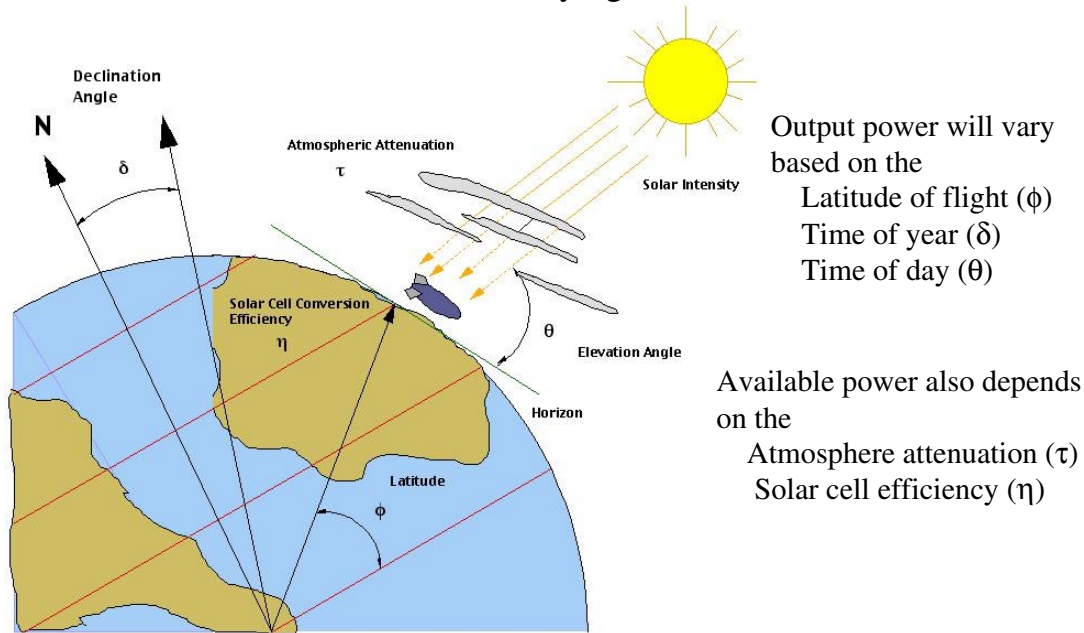


Figure 22 Environmental Factors that Affect the Airship's Power Production Capabilities

The mean orbital radius of the Earth is 1.496E8 km. The actual orbital radius is given by the following equation.

$$r_{orb} = (1 - \epsilon^2) / (1 + \epsilon \cos(\alpha)) \quad [23]$$

The day angle (α) is defined as 0° on January 4th (perihelion of Earth's orbit) and increases by 0.98° per day.

The power incident on the array is given by the normal component of the incident flux given in equation 22. Due to the shape of the airship and the variation in the sun elevation angle and position throughout the day this incident angle will be different along the array (from the side of the airship to the top) and will vary throughout the day. Determining this incident angle is a critical factor in modeling the output power for the array.

It is assumed that the airship is a cylinder capped with a hemispherical surface on the front and rear. The solar array is assumed to be on the upper surface of the cylinder portion starting from the midpoint of the cylinder. There is no solar array on the hemispherical portions of the airship. If needed, additional solar array can be placed on the tail fin surfaces. It is assumed that the airship has 3 tail fins, one vertical and two at angles of 45° below the horizontal. The incident angle for these tail fins will also need to be determined. The airship is assumed to be orientated horizontal (parallel to the surface) with no pitching of the nose upward or downward. The array configuration can be seen in figures 11 and 23.

To calculate the power from the array the incident flux (component normal to the array) must be determined. Due to the variation in angle of the array because of the curved shape of the airship the normal component of the solar flux will need to be calculated incrementally and then summed over the surface of the airship. The geometry of an incremental section of the solar array is given in figure 23. It was assumed that on the cylindrical portion along the central axis of the airship there was no curvature or variation in array angle. Therefore a strip of array from the nose to the tail would all be at the same angle to the sun at any given moment. For this analysis these strips were broken down into 1° increments over the surface of the airship.

The incident power (P_n) on the array in W/m^2 for a specific time during the day is given by equation 24 where τ is the attenuation of the solar flux due to the atmosphere, θ_l is the local sun elevation angle as seen from a specific segment of array which has an inclination angle of β and an orientation angle of α . The orientation angle is represented by the position of the airship. For this analysis the atmospheric attenuation was assumed to be 15% ($\tau = 0.15$). The angle range for β of $\pi/2$ to 0 represents the southern facing side of the airship and from 0 to $-\pi/2$ the northern facing side. If the airship is facing north to south the east side is in the 0 to $\pi/2$ region. Also it should be noted that for the side of the airship in shadow, if the solar elevation angle is less than the array inclination angle ($\theta_l < \beta$), that portion of the array is shadowed and will not produce any power.

$$P_n = \sum_{\beta=-\frac{\pi}{2}}^{\frac{\pi}{2}} SI(1 - \tau) \sin(\theta_l) \quad [24]$$

The local solar elevation angle (θ_l) is the elevation to the sun as seen from a specific segment of the solar array. This angle will depend on the inclination of the solar array segment (β), this is the angle of the specific solar array cells to the horizontal. For $\beta = 0^\circ$ the array segment is horizontal and for $\beta = 90^\circ$ the array segment is vertical. The local solar elevation angle is also based on the solar elevation angle (θ) relative to the surface (or horizontal), the latitude (ϕ) of the airship location, the declination angle (δ) of the Earth (which is based on the time of year) and the geometry and orientation of the airship. Using figure 23 the local solar elevation angle can be derived based on the

position of the sun and the inclination angle (β) of a given array segment on the airship. From this figure the following relationships can be derived.

$$\sin(\theta_i) = \frac{x}{a} \quad [25]$$

$$x = b(\tan(\theta)\cos(\beta) - \sin(\omega_i)\sin(\beta)) \quad [26]$$

$$a = \frac{b}{\cos(\theta)} \quad [27]$$

Substituting equations 26 and 27 into equation 25 yields a relation for the local solar elevation angle given in equation 28.

$$\theta_i = \sin^{-1}[\sin(\theta)\cos(\beta_i) - \sin(\omega_i)\sin(\beta_i)\cos(\theta)] \quad [28]$$

$$\theta = \frac{\pi}{2} - \cos^{-1}(C - D\cos(\omega)) \quad [29]$$

$$C = \sin(\phi)\sin(\delta) \quad [30]$$

$$D = \cos(\phi)\cos(\delta) \quad [31]$$

The solar hour angle (ω) is a function of the time of day and is given by equation 32, where the time of day in hours (t) is based on a 24-hour clock. The solar hour angle is defined as being zero at noon, positive before noon, and negative after noon with each hour representing 15° of rotation.

$$\omega = -\frac{2\pi t}{24} + \pi \quad [32]$$

The local hour angle (ω_i) is based on the position of the sun as well as the orientation angle (α) of the airship. The local hour angle is given by equation 33 where the airship orientation angle is defined as being 0 when the airship is positioned West to East and $\pi/2$ when the airship is positioned North to South.

$$\omega_i = \alpha + \frac{\pi}{2} - \frac{2\pi t}{24} \quad [33]$$

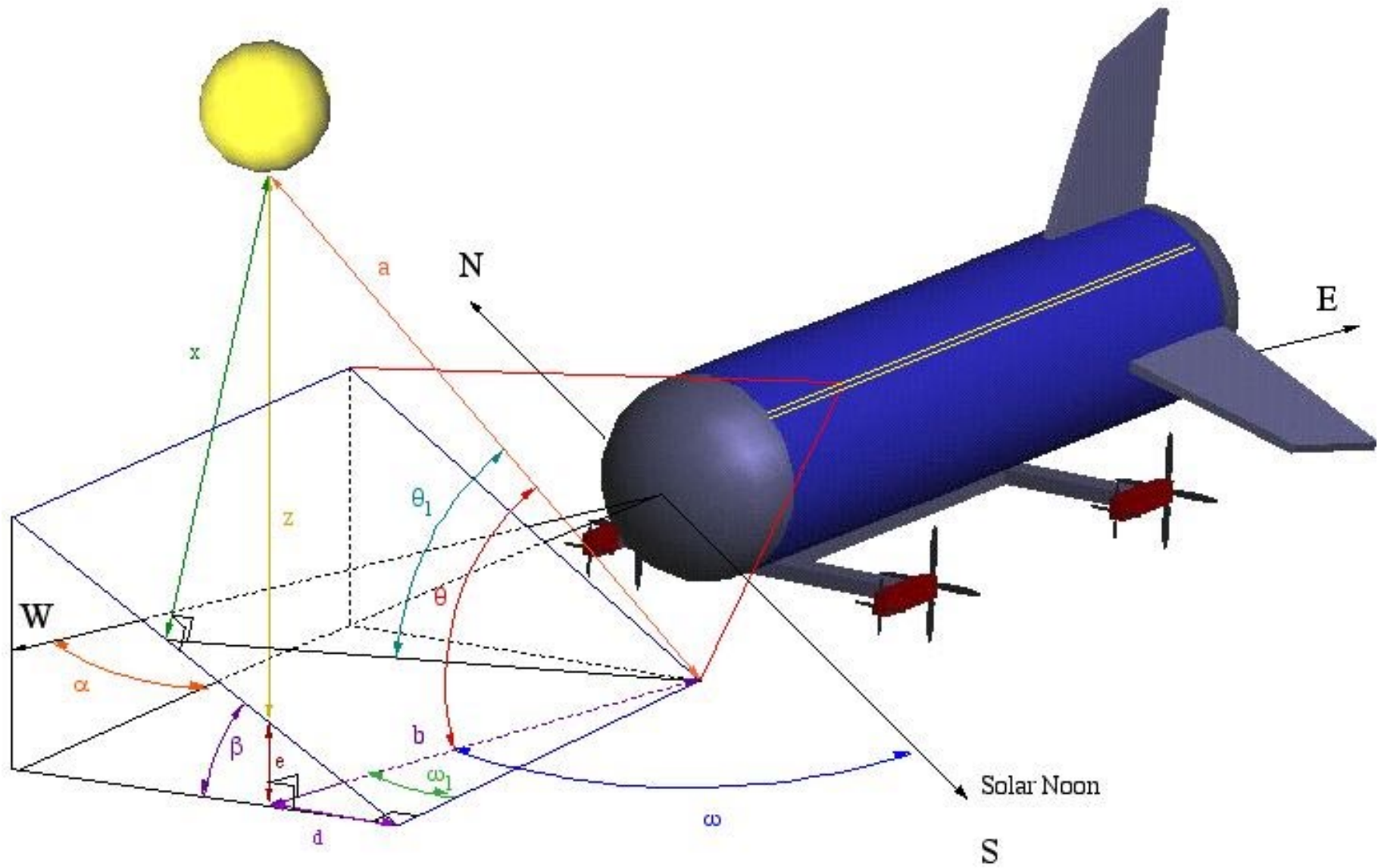


Figure 23 Solar Array Incident Flux Geometry

Examples of incident power profiles for the array are shown in figures 24 to 29. These figures show the incident power (normal to the array) for various times of the day for array angles of 0° (horizontal) to 90° (vertical). This encompasses the full range of array angles present on the airship over the upper surface. Figures 24 through 26 are for June 21st (summer solstice, maximum solar output) and figures 27 through 29 are for December 21st (winter solstice, minimum solar output). All of the curves were produced for a single latitude, 38° N. Variations in latitude will effect the magnitude of these curves dependent on the time of year.

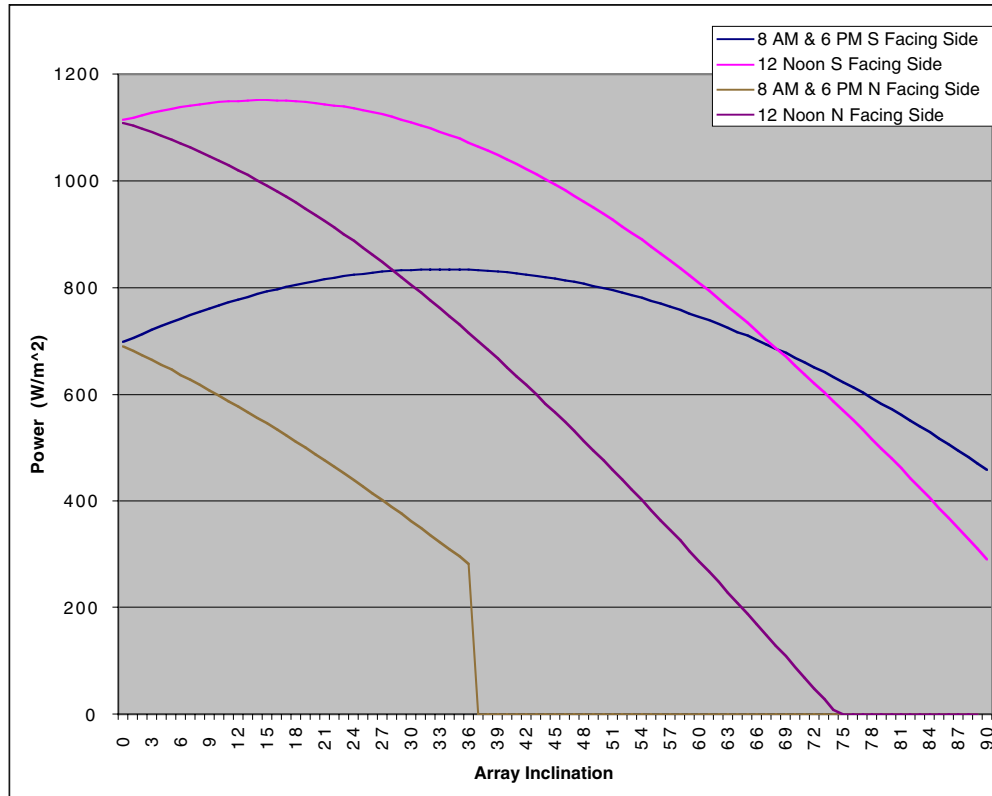


Figure 24 Incident Power on the Array at Various Times During the Day for June 21st, 38° N Latitude, Airship Orientation of 0° (E to W)

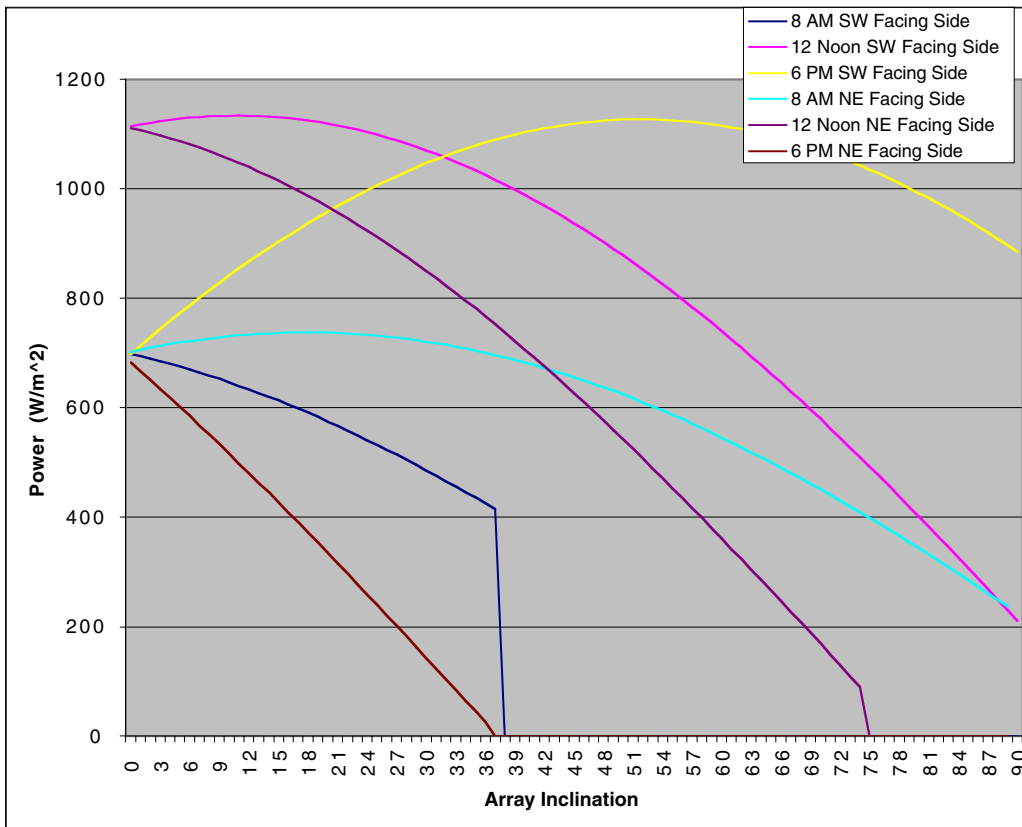


Figure 25 Incident Power on the Array at Various Times During the Day for June 21st, 38° N Latitude, Airship Orientation of 45° (SE)

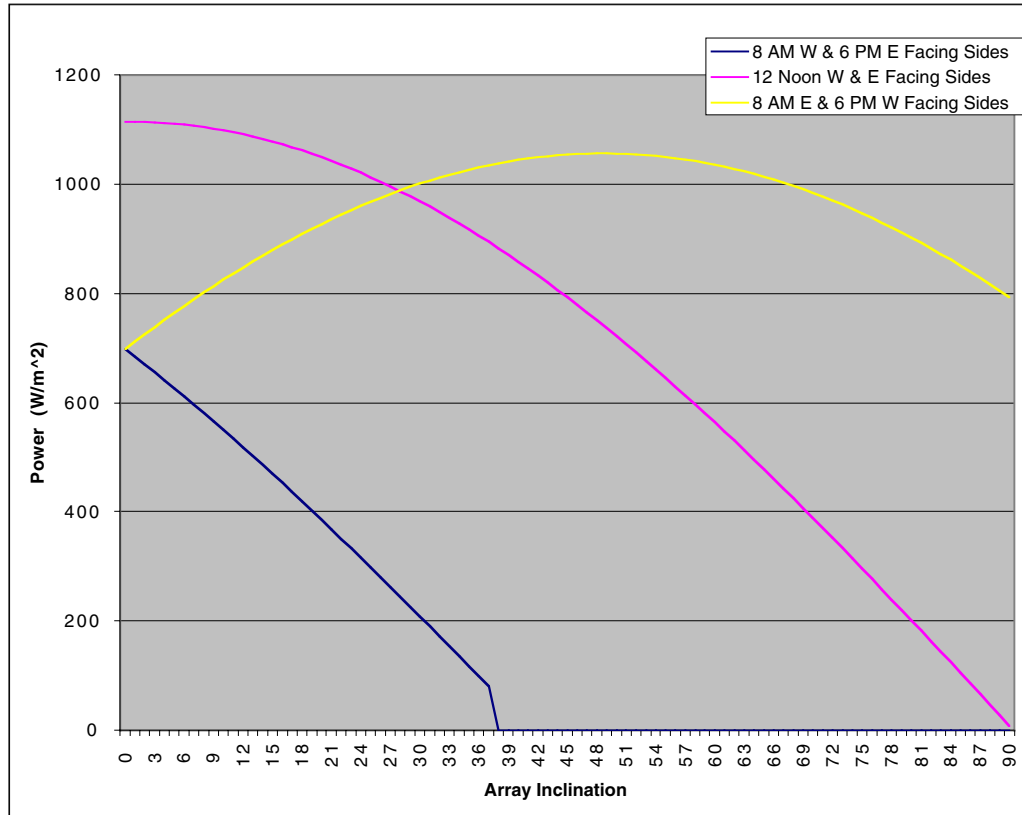


Figure 26 Incident Power on the Array at Various Times During the Day for June 21st, 38° N Latitude, Airship Orientation of 90° (N to S)

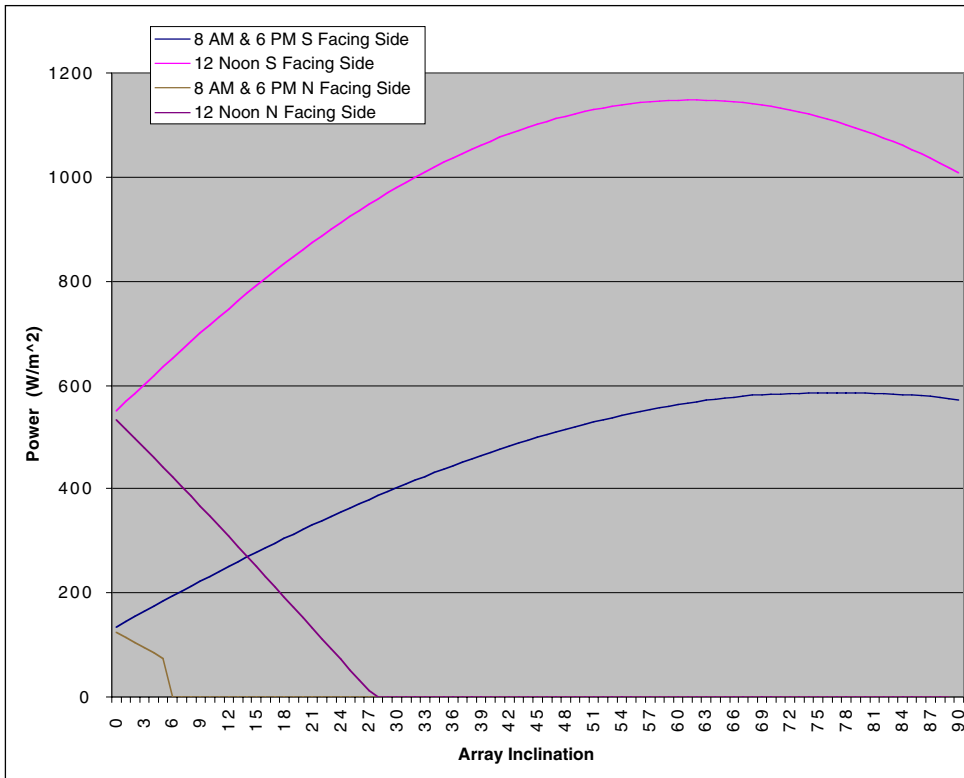


Figure 27 Incident Power on the Array at Various Times During the Day for December 21st, 38° N Latitude, Airship Orientation of 0° (E to W)

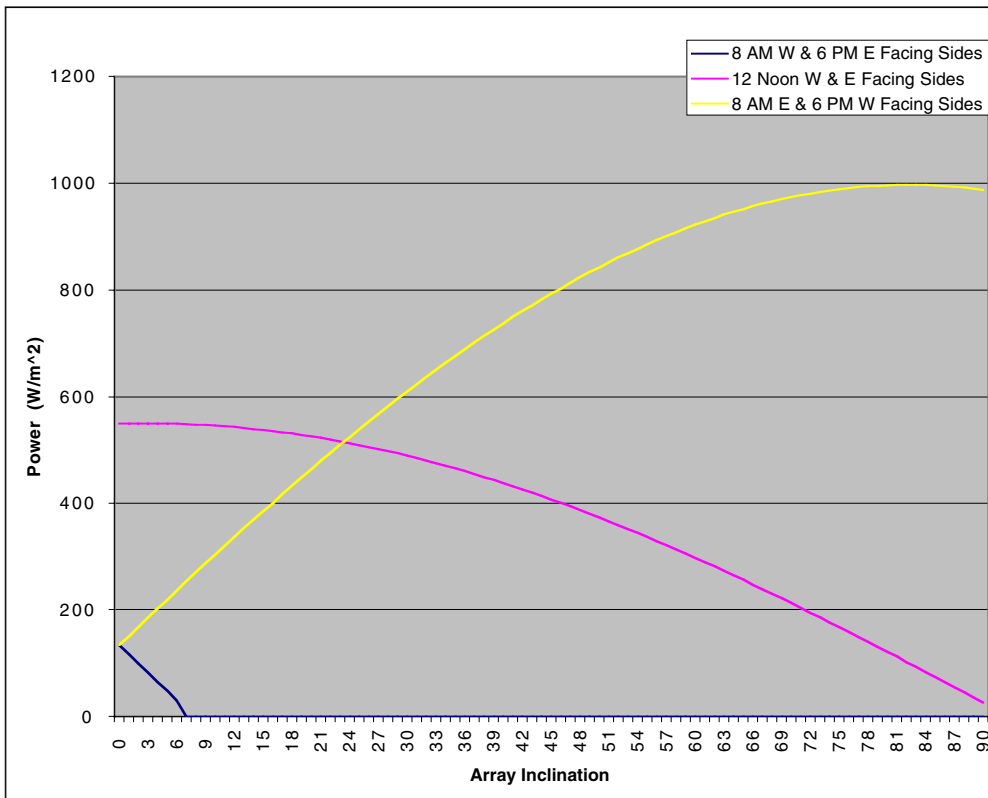


Figure 28 Incident Power on the Array at Various Times During the Day for December 21st, 38° N Latitude, Airship Orientation of 45° (SE)

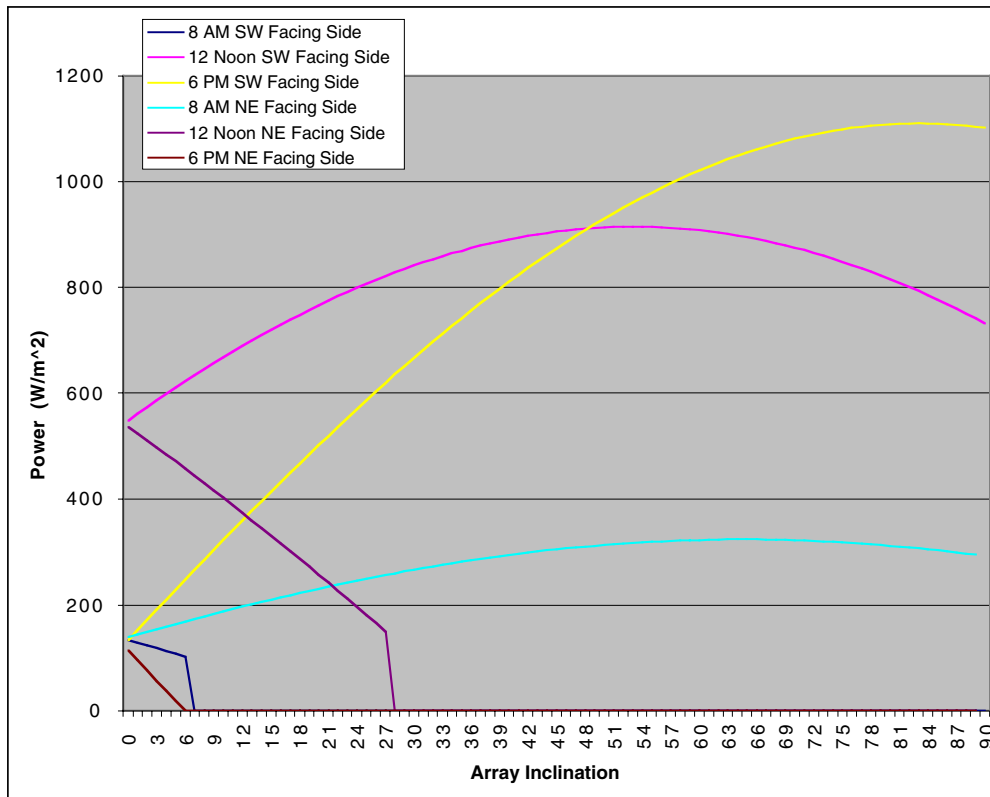


Figure 29 Incident Power on the Array at Various Times During the Day for December 21st, 38° N Latitude, Airship Orientation of 90° (N to S)

Power and Propulsion System

The power and propulsion systems consist of all of the components that collect, generate, and store energy and convert that energy into useable power and thrust. The propulsion system is the main power consuming function on the airship. Because of this the power and propulsion systems are intimately dependant and need to be designed and operated as a single system to maximize efficiency and optimize the airship design. Therefore they will be referred to as a single system throughout the text.

The power and propulsion system can be broken down into individual components. The characteristics of each of these components must be known in order to size the system for various power and thrust requirements. Also, how the components scale to different power or thrust levels must be understood. A baseline power and propulsion system was chosen for setting up the initial analysis. This baseline system was a photovoltaic/fuel cell system powering electric motors to drive a propeller to generate thrust. A hydrogen/oxygen based fuel cell/electrolyzer system was identified as the baseline energy storage and production system.

The following list comprises the main components for these systems for the baseline airship configuration.

- Photovoltaic Array
- Fuel Cell (Hydrogen/Oxygen, PEM)
- Electrolyzer
- Power Management
- Electric Motors / Gearbox
- Propeller

Due to the inherent size of a high altitude airship, a modular approach to the power/propulsion system design was selected. The modular approach minimizes the need for long wire and piping runs within the airship and provides redundancy in the systems. Each modular system would utilize a segment of the photovoltaic array that would be dedicated to its operation. Each modular unit would also have its own fuel cell, electrolyzer, gas storage tanks, control electronics, thermal management system, electric motors and propellers. A diagram showing the components of the system is given in figure 30. Another advantage of this modular system is that it allows more versatility in the scaling of the airship.

The components in each module can be scaled to meet a specific thrust need. However the number of modules used on the airship can also be varied. Depending on the airship payload requirements and airship size, two, four, six or more system modules can be utilized. The ability to scale the system modules and to vary the number that are present on the airship enables significant flexibility in optimizing the propulsion and power system design.

Besides the flexibility benefits of the modular approach there are other practical benefits. The development of the power / propulsion system can be simplified and its production cost can be reduced by designing and producing a system module at a specified power level. These modules could then be added to the airship design as needed to meet its power and propulsion requirements. Determining the appropriate size for a system module was one of the goals of this analysis.

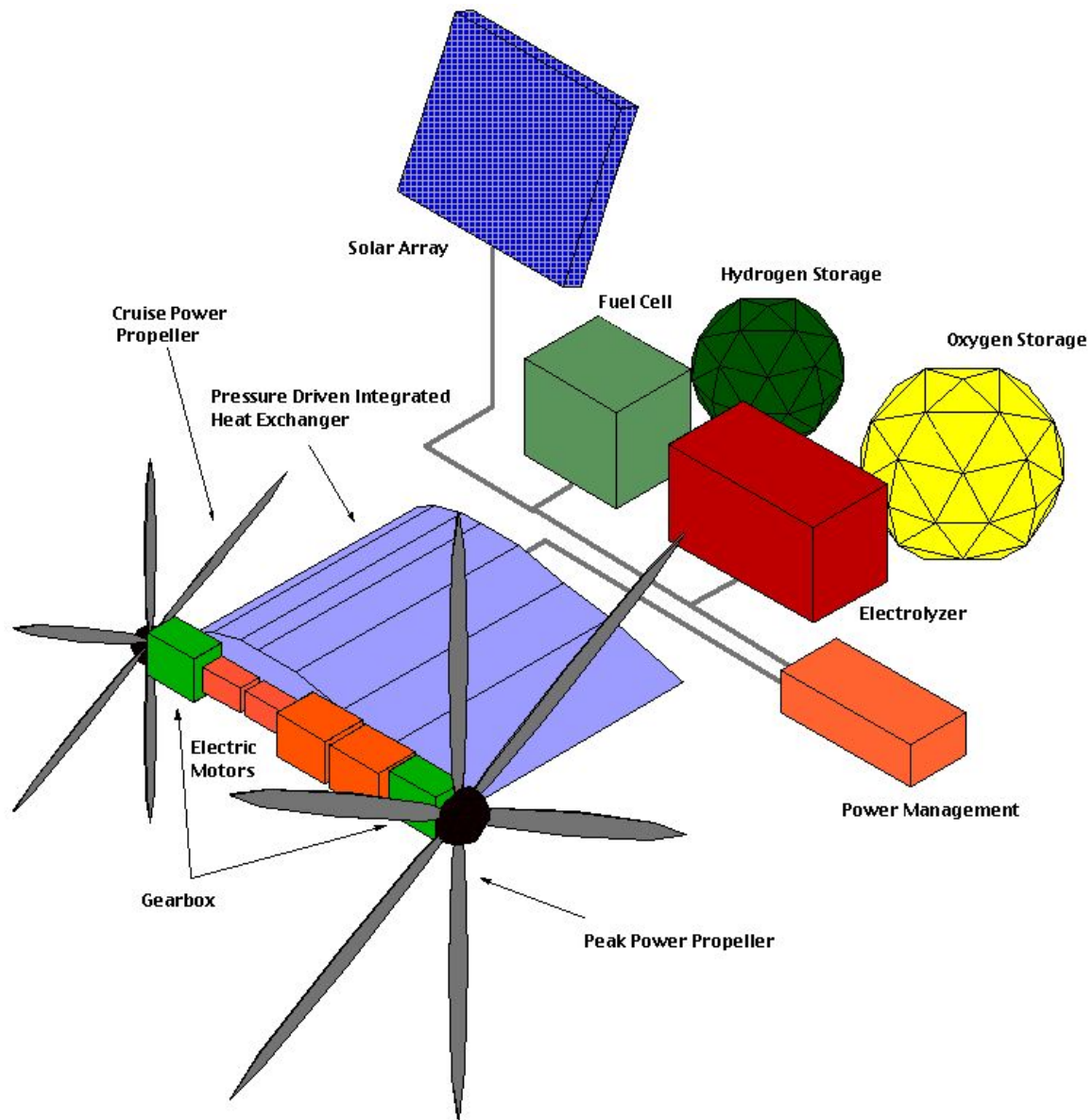


Figure 30 Component Breakdown for a Power / Propulsion System Module (drawing is not to scale)

Solar Array

The sun is the main power source for the airship and the solar arrays are the means of converting this incoming energy to a useable form. The arrays and their operation are one of the most critical aspects to the vehicle's design and capabilities. Because the airship needs to operate for extended periods of time and perform tasks throughout the day and night time periods, the power system must be capable of providing sufficient power to meet these needs. This means that enough energy must be collected during daylight hours to meet the power needs of the complete day / night period. To determine the amount of

solar array necessary to accomplish this, the output and physical characteristics of the solar array must be well understood.

A critical factor in the airship design is minimizing mass.. Because of this desire to minimize mass a thin film array was selected as the baseline type of array for the analysis. The typical mass of an amorphous silicon thin film array is approximately 0.12 kg/m^2 [22]. This compares to approximately 1.3 kg/m^2 for the space-station solar array without its mounting frame and hardware. The space-station solar array is constructed of rigid silicon solar cells mounted on a Kapton substrate and is representative of a modern lightweight rigid cell array design [23]. Thin film arrays have a number of characteristics that are desirable for an airship application. Mainly thin film arrays can be made very lightweight. The active material that makes up the array is only 1 to 2 microns thick, whereas the typical thickness of a rigid silicon solar cell is approximately 250 to 350 microns. The substrate that the active array material is deposited on can be made out of most materials. Presently the best candidate is Kapton (or potentially other polymers). In addition the potential exists to use the airship envelope material itself as the substrate material and deposit directly onto it during manufacturing. This is beyond the present day capabilities of both the envelope materials and manufacturing techniques but does provide a technology development path that can have a significant impact in reducing the airship's overall mass and therefore size. A diagram of the makeup of a thin film solar array is shown in figure 31 [24].

In addition to being lightweight, thin film arrays are also flexible. This is a major benefit due to the curved surface of the airship. By having an array that can conform to the surface curvature the amount of structure mass needed to support it can be greatly reduced. Also solar arrays constructed from rigid single crystal solar cells are significantly more fragile than the thin film arrays. This durability is also a feature that fits well with the airship application. The airship will be exposed to numerous stresses and flexing during its ascent and while operating at altitude. A solar array that can flex with the structure and bend without fracturing is great benefit to the airship. It increases the ships reliability and lifetime.

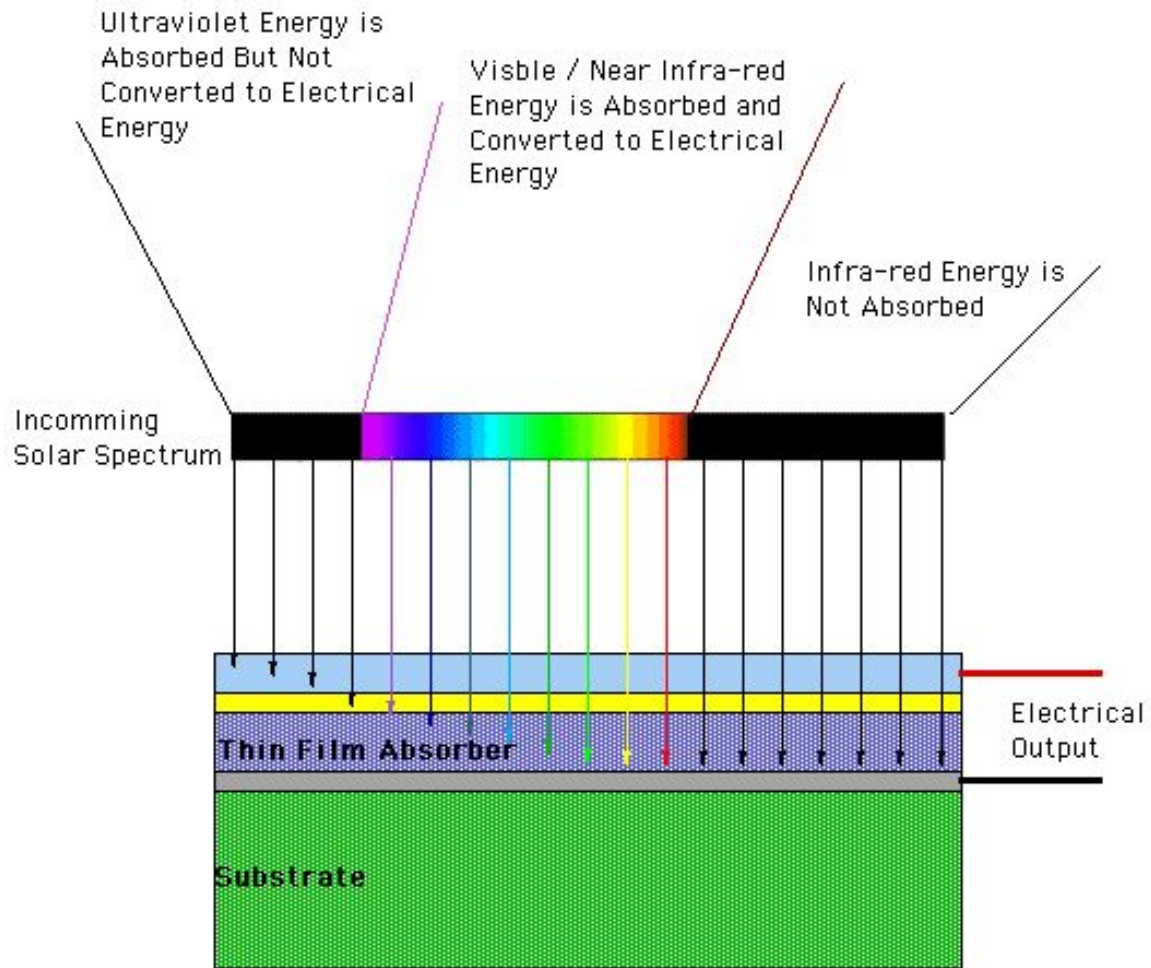


Figure 31 Thin Film Solar Array Operation

Thin film solar arrays can be made out of a variety of material. The various materials have differences in conversion efficiency and weight. The development history of some of the most common types of thin film arrays is shown in figure 32. From this figure it can be seen that there has been a steady increase in the efficiency of thin film arrays. However, one of the main drawbacks to this type of solar array is that their conversion efficiencies are significantly less than that of single crystal solar cells. In large-scale production thin film array efficiencies are less than 10% compared to upwards of 20% for some of the higher efficiency types of rigid solar cells. Examples of thin film arrays are shown in figure 33.

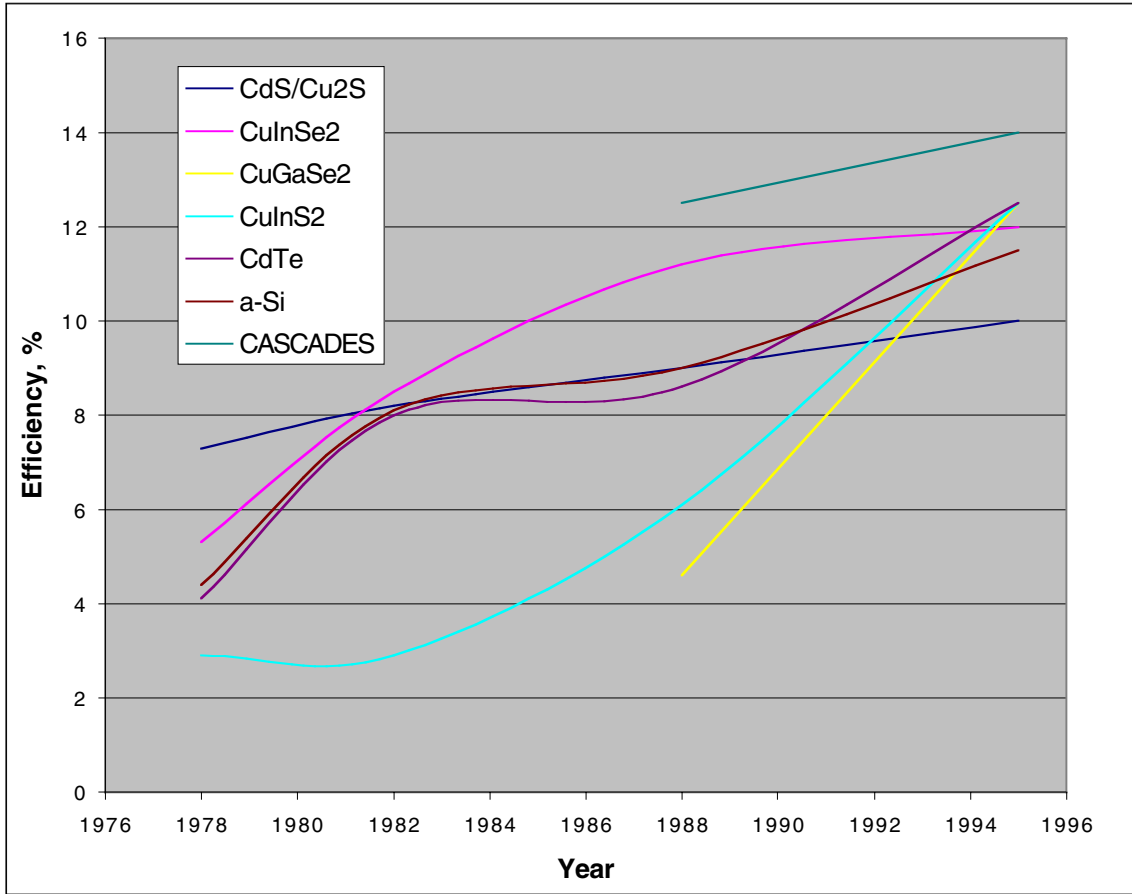


Figure 32 Thin Film Solar Array Efficiencies Over the Last 20 Years [25]



Figure 33 Amorphous Silicon Commercially Available Thin Film Solar Arrays [26]

The output of the solar array is determined by the incident solar radiation on the array, the geometry of the airship and the performance characteristics of the array. The incident solar radiation analysis, given in the environmental section, along with the efficiency of the solar array can be used to determine the output power profile for the array at various latitudes, times during the year and airship orientations. All of these factors as well as the airship size and geometry will influence the array performance. Examples of how the array output performance is influenced by these variables are shown in the following figures. These figures were generated for the single point airship geometry given in table 11 within the results section. The overall geometry is a cylindrical shaped airship with a solar array on the upper half of the cylinder. For the curves shown there was no array located on the tail surface.

Figures 34 and 35 show the output power curves for the full array for the summer and winter solstice (June 21st and December 21st) respectively. These two dates represent the maximum and minimum in solar output for the year. The figures show how the latitude and ship orientation affect the array output. Latitudes of 28° and 44° were used, which represent a latitude range that encompasses the majority of the continental United States. For each of these latitudes three airship orientations were used to calculate the power profiles. The orientations were defined as the cylindrical axis of the airship being pointed in the specified direction and included; North-South, East-West and SE (the nose of the airship is pointed East 45° from the East-West orientation).

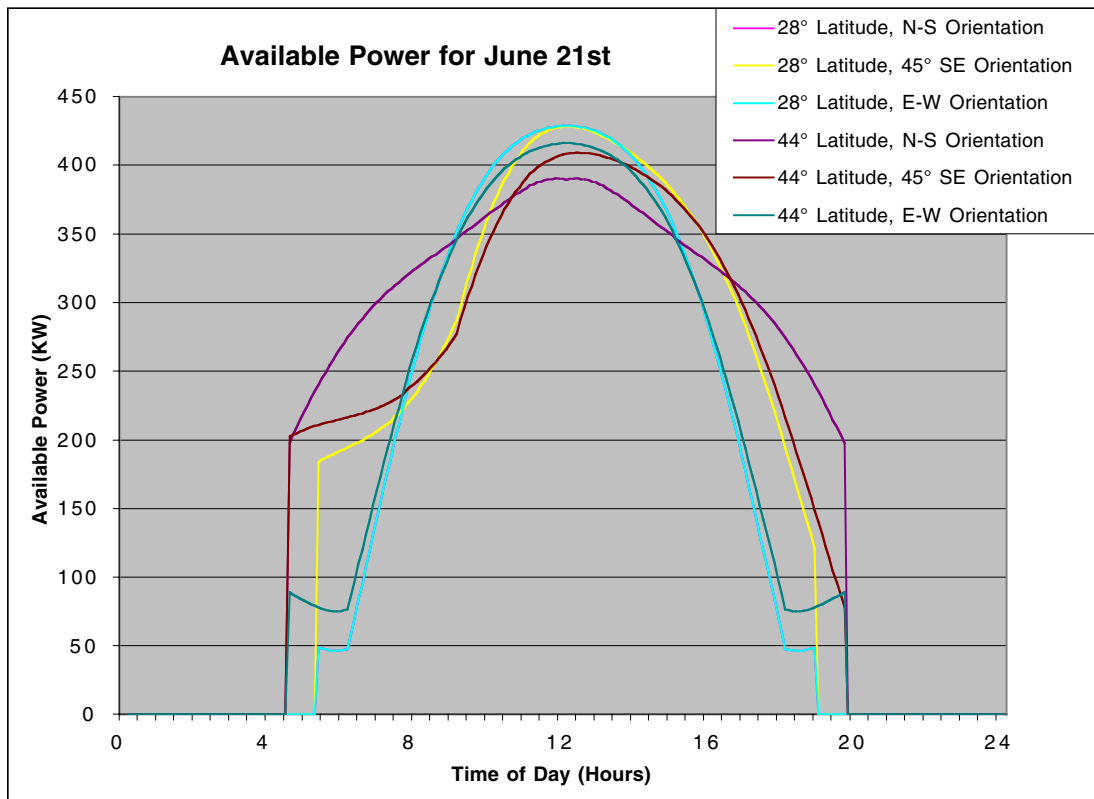


Figure 34 Solar Array Available Power on June 21st for Various Latitudes and Airship Orientations

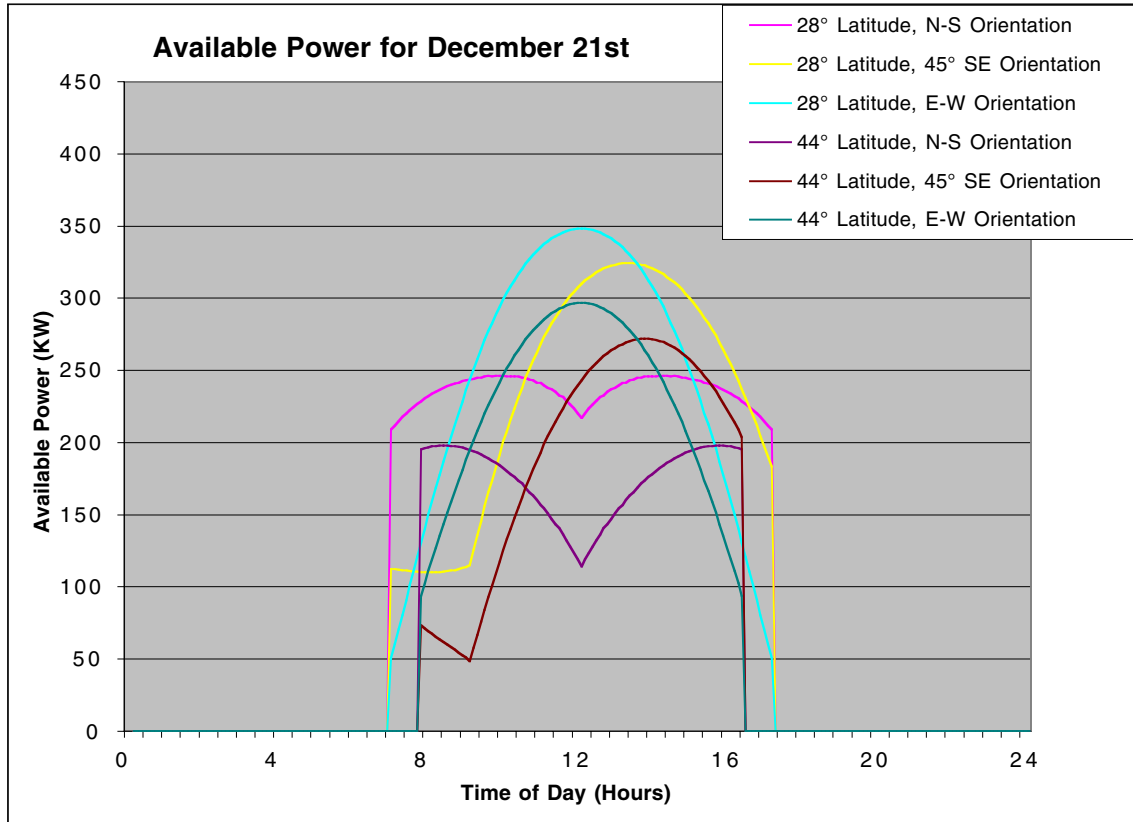


Figure 35 Solar Array Available Power on December 21st for Various Latitudes and Airship Orientations

For analysis purposes the array was separated into two quadrants. The first quadrant was on the south or west facing side of the airship and the second quadrant was on the north or east facing side (the actual direction depends on the orientation of the airship). The output power profile for each quadrant is very different. This is due to the variations in shadowing on the array throughout the day. The shadowing affects the array output but it is mostly a concern in how the arrays will actually be wired on the airship. The output current of a given string of solar arrays wired together in series will be equal to the lowest current producing cell in the string. If a string has 10 cells and one is shadowed then this has the same effect as shadowing all 10 cells. Therefore the wiring scheme for the solar array will need to take into account the shadowing of the array throughout the day. A wiring scheme will have to be devised that minimizes the effect of shadowing on the array. The results shown in these figures assume that only the portion of the solar array that is in shadow does not produce any power. It does not take into account any effects of the shadowing and the series wiring of the cells.

Figures 36 through 39 show the output power for the 1st and 2nd quadrant solar array for latitudes of 44° N and 28° N and airship orientations of 0° (N-S), 45° SE and 90° (E-W).

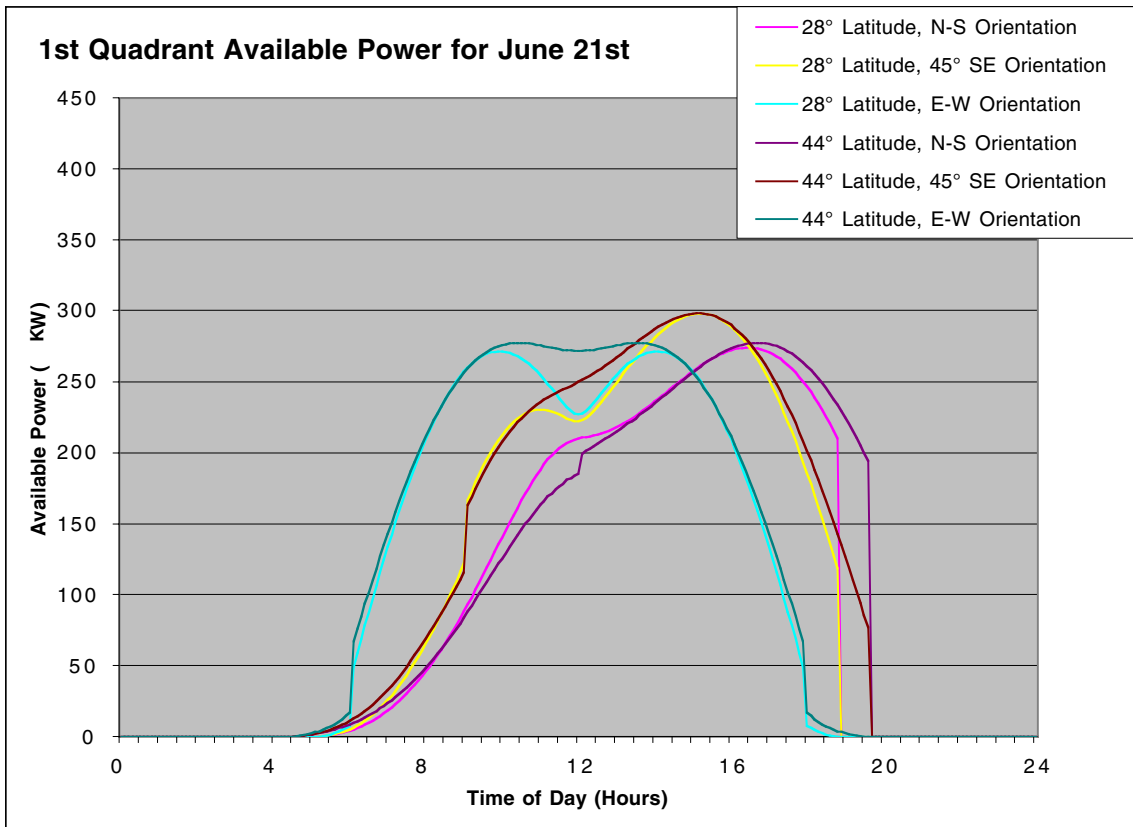


Figure 36 1st Quadrant Solar Array Available Power on June 21st for Various Latitudes and Airship Orientations

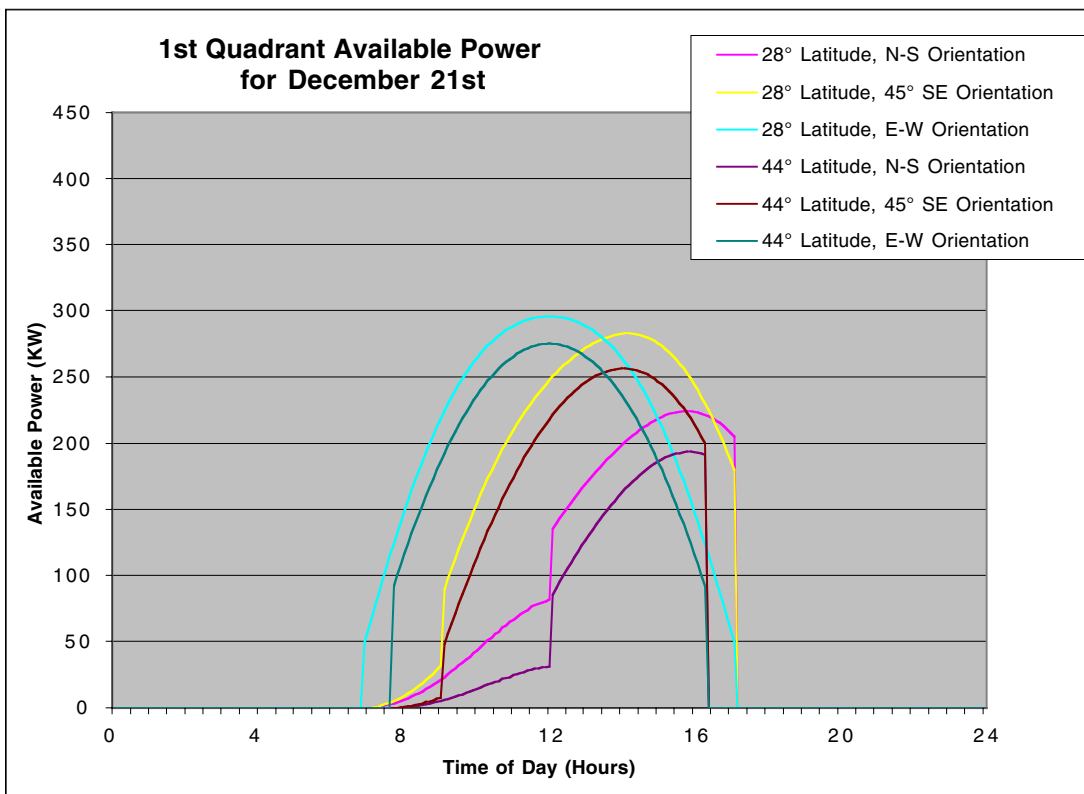


Figure 37 1st Quadrant Solar Array Available Power on December 21st for Various Latitudes and Airship Orientations

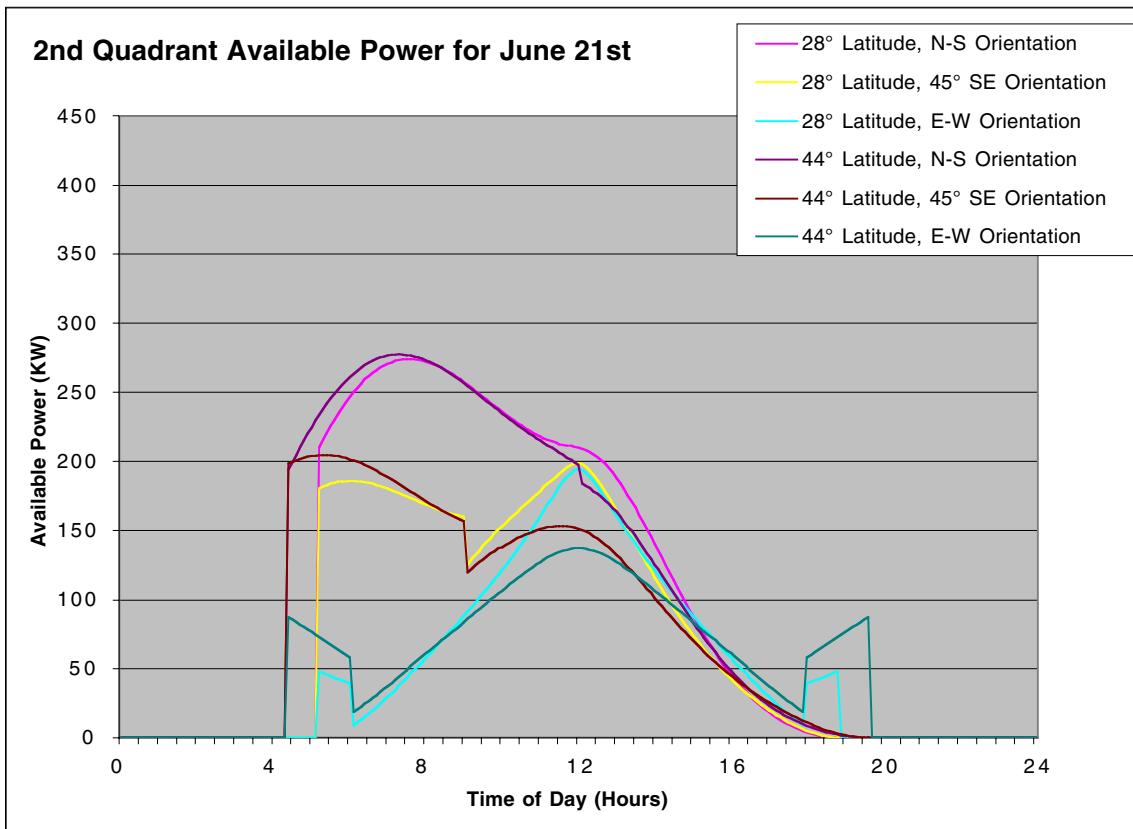


Figure 38 2nd Quadrant Solar Array Available Power on June 21st for Various Latitudes and Airship Orientations

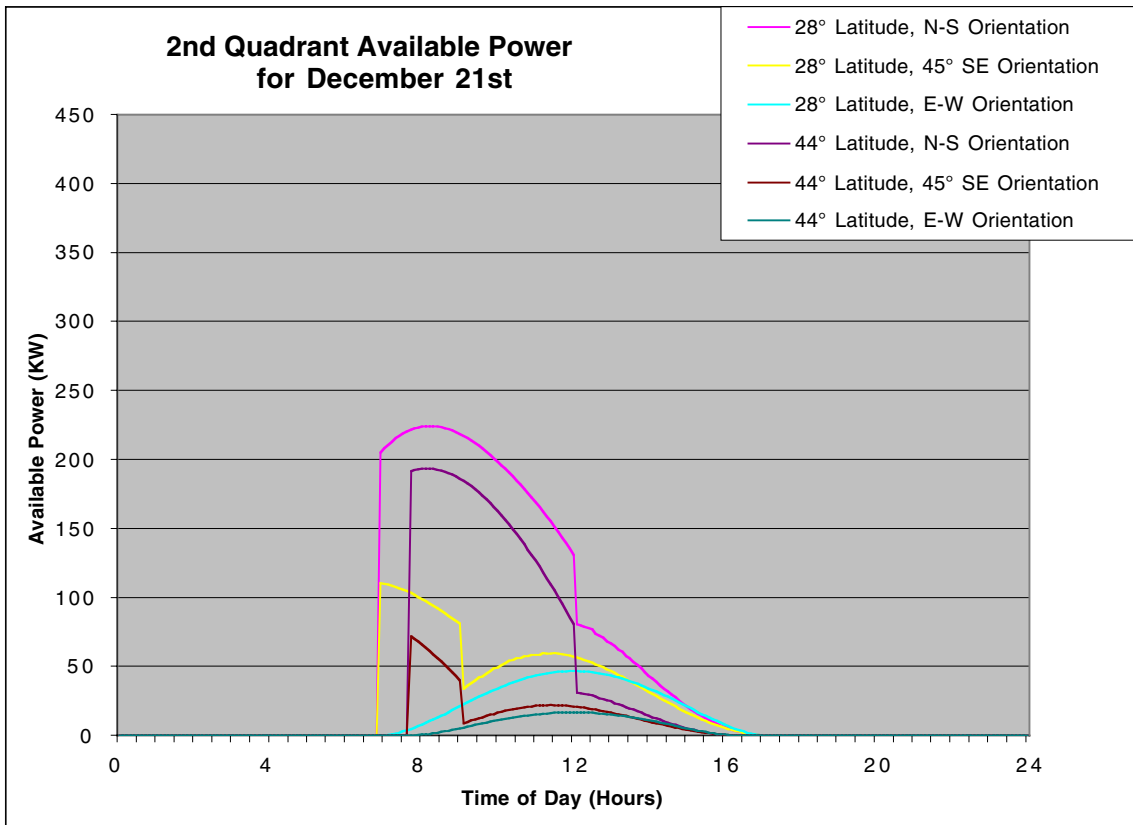


Figure 39 2nd Quadrant Solar Array Available Power on December 21st for Various Latitudes and Airship Orientations

The power profiles for the front and backside arrays (1st and 2nd quadrants) on the airship demonstrate how the shadowing of the array occurs as the sun moves throughout the day. For example in figure 37 the curve for 44° N latitude with an airship orientation of 90° (E-W) shows the output power of the backside (2nd quadrant) of the airship. The sun rises and illuminates the backside of the airship. This occurs because at a latitude of 44° during the summer the sun will rise in the NE shining on the backside of the airship. The elevation angle is low so the array output is not that great. As the sun moves toward the west it crosses the nose of the airship at around 6:30 AM and there is a significant drop off in the output of the backside array. This is because the backside array falls mostly into shadow. As the sun elevation angle increases throughout the day the output of the backside continues to increase until the peak output is reached at noon. For the remainder of the day the pattern is reversed, decreasing output followed by an increase in output as the sun illuminates the back side of the airship just before sunset to no output at sunset.

It should be noted that the output profiles do not take into account any land features such as mountains or atmospheric features such as clouds that could obscure the sun near sunrise or sunset. Since the altitude of the airship is fairly high, these effects would be minimal and occur at times of low sun elevation angles. Therefore they should not have a significant effect on the overall performance of the solar array.

Fuel Cell System

The baseline power system uses a hydrogen/oxygen fuel cell. In place of oxygen, air could be used as the oxidizer for the fuel cell. However, because of the high altitude operation, this type of system requires the use of compressors to increase the air pressure enabling the fuel cell to operate. As a variation from the baseline, a hydrogen / air system was considered and details are included in the following section.

The fuel cell is an electrochemical device that produces electricity through the combination of hydrogen and oxygen. It doesn't "burn" the hydrogen as a conventional engine would. Instead it combines it electrochemically to produce electricity and water. This reaction is shown by the following basic equation for the formation of water.



The advantages of this type of energy conversion is that it is clean (the only bi-product is water) and has a high energy conversion efficiency (upwards of 50%). The energy conversion of a fuel cell is much higher than if the hydrogen were burned in a combustion engine. This is mainly due to the fact that fuel cells are not limited by the Carnot efficiency that combustion power plants are.

The type of fuel cell that has seen the most commercial development and therefore would be a good candidate for the high altitude airship application is a polymer electrolyte membrane (PEM) fuel cell. In this type of fuel cell electricity is produced by flowing hydrogen over an anode. At the anode electrons are striped from the hydrogen atoms producing a hydrogen ion and an electron. This is know as the oxidation half reaction. The hydrogen ion passes through a membrane that separates the anode from the cathode. It then combines with oxygen and electrons on the cathode side producing water. This is

known as the reduction half-reaction. The electrons, which cannot pass through the membrane, are forced to flow to the cathode side through an external circuit thereby producing useful work. A diagram of this operation is shown in figure 40. To increase the rate of these reactions within a fuel cell, a catalyst (usually platinum) is used on both the anode and cathode.

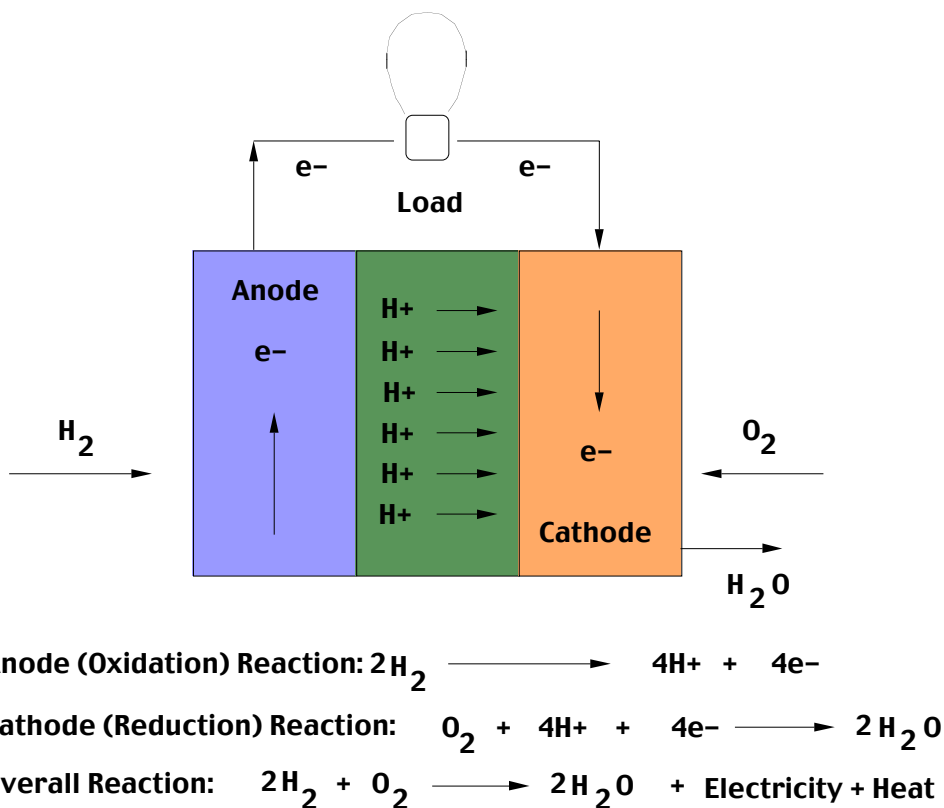


Figure 40 Principle of Operation of a PEM Fuel Cell [27]

A PEM fuel cell operates at relatively low temperature, compared to other types of fuel cells. It is limited in temperature by the requirement to keep the water, within the fuel cell, in a liquid state. This is necessary because the polymer electrolyte membrane (also known as a proton exchange membrane) must contain liquid water so that the hydrogen ions can carry their charge within the membrane. That is it becomes electrically conductive in the presence of water. This membrane is the key to the operation of a PEM fuel cell. The membrane is constructed of a polymer such as Nafion. Because of the need for the membrane to be saturated with water in order for the fuel cell to operate efficiently, some manufacturers require the hydrogen gas and oxygen (or air) to be humidified. For the baseline system it was assumed that the fuel cell does not require pre-humidified gasses. However, depending on the cost and fuel cell availability this may not be possible and a means for humidifying the gasses to the fuel cell will need

to be implemented. The main drawback to humidification of the reactant gases is that a supply of liquid water will be needed plus additional power to heat the water to enhance absorption by the reaction gasses and maintain it in a liquid state under high altitude conditions. This power load will effectively reduce the overall efficiency of the system as well as increase its complexity. With many modern fuel cell stack designs the internal water generated by the hydrogen/oxygen reaction is sufficient to maintain the correct humidity level within the stack. Excess water is removed from the stack by periodically purging the hydrogen and oxygen lines to remove the trapped water. If not removed, this water, which has not been absorbed by the membrane, would eventually flood the cathode and significantly reduce the fuel cell's performance.

To channel the reactant gasses and evenly distribute them onto the anode and cathode surfaces, a plate is used. These plates are constructed of a gas-impermeable, electron conducting material such as graphite or a metal. Micro-channels are etched into these plates. These channels provide the gas flow field to the anode or cathode. The pattern, depth and shape of these channels is unique to each fuel cell manufacturer and is usually a key element in their design process. Water supply to the membrane and removal from the cathode is also affected by this plate design. Because of the small size of the gas channels within these plates they are prone to blockage due to any impurities within the reactant gasses. The blockage of these gas channels can significantly impact the fuel cell performance. Therefore, the hydrogen, oxygen and any humidifying gasses will need to be filtered to minimize any impurities getting into the fuel cell stack.

Ideally the theoretical output voltage of a single fuel cell "cell" is 1.16 volts. This voltage represents the case in which all (100%) of the energy in the fuel is being turned into electricity. However, during real world operation this voltage will drop to some level below this ideal limit. The difference between this ideal voltage and the actual cell operating voltage translates into the efficiency of the fuel cell. For example if the individual cell is operating at 0.7 volts then it is operating at approximately 60% efficiency. That is 60% of the reaction goes into producing electricity and 40% turns into heat. High operating efficiencies can be achieved at low power levels. This can be seen in figure 41. This figure shows a representative curve of cell voltage versus current density for a typical PEM fuel cell. As can be seen by this graph, the greater the output power or current produced by the fuel cell the lower its operating voltage and hence efficiency. Therefore under operating conditions a means for removing this excess heat must be incorporated into the fuel cell system design. If the fuel cell is not cooled its temperature will rise significantly due to the inefficiencies of operation and damage to or complete failure of the fuel cell will occur.

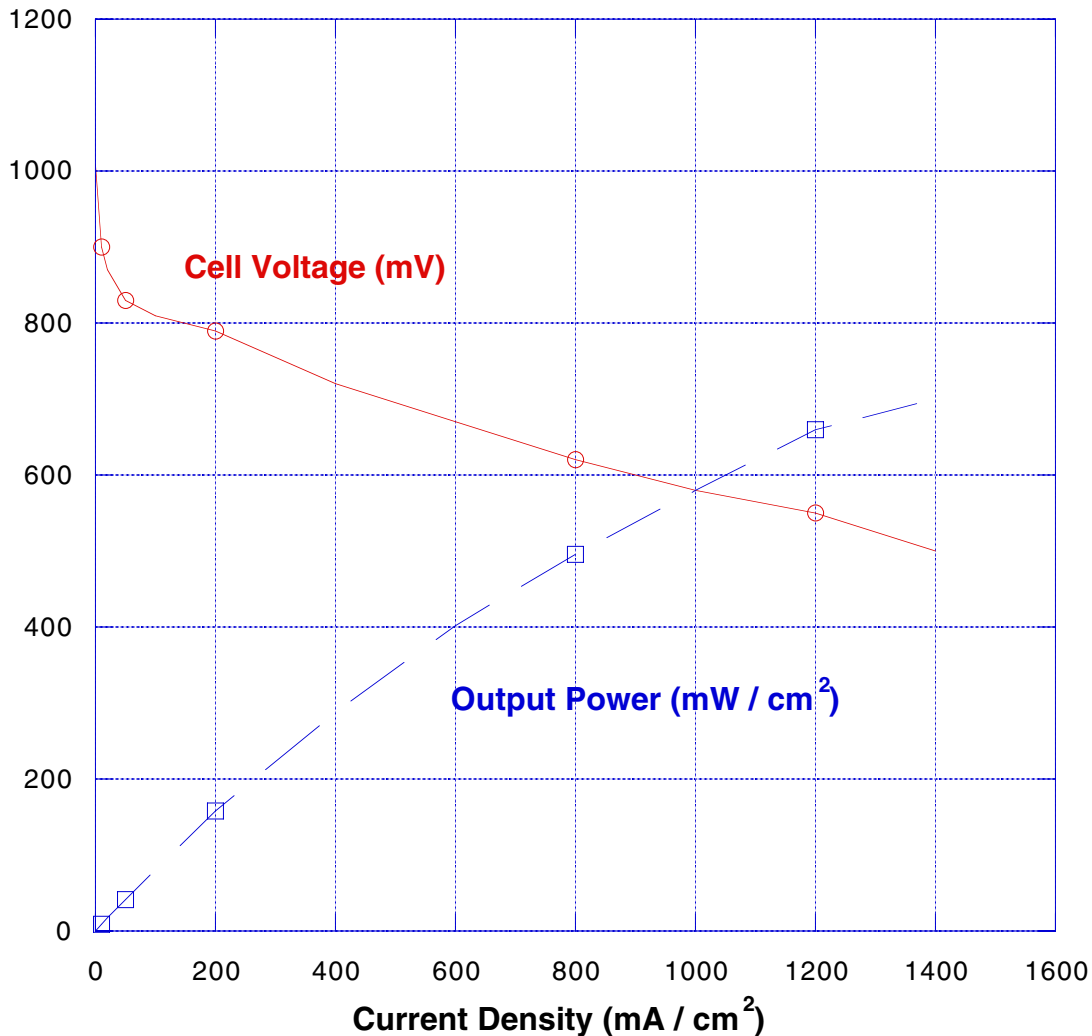


Figure 41 Voltage & Output Power versus Current Density for a Typical PEM Cell [28]

For high altitude operation where there is little air for convective cooling, a liquid heat exchanger would be the best choice for removing heat from the fuel cell stack. Depending on the fuel cell stack design, the cooling flow would either be internal or external. If the stack is designed for liquid cooling, internal passages would exist for the passage of cooling fluid. For external cooling, the liquid loop system would consist of a number of non-conducting tubes wrapped around the fuel cell. In either system, a cooling fluid would be passed through the passages or tubes and then sent to a radiator to reject the heat. The main issue with the cooling system is that it is another parasite load on the system and will tend to reduce the system's overall efficiency. In order to optimize the performance of the system, thermocouples will need to be installed on the fuel cell to monitor its temperature. If the temperature exceeds a predetermined level then the cooling system can be turned on to maintain the temperature of the fuel cell within specified limits. This temperature monitoring adds complexity to the system controls; however, it can effectively minimize the power consumption of the cooling system.

In recent years the greatest advance in PEM fuel cell technology has come through the automotive industry. The fuel cell stacks under development for use in automobiles are compact, high power and durable. Examples of these from Ballard [29] and International Fuel Cell (IFC) [30] are shown in figure 42a and 42b respectively. There are three main companies developing fuel cells for use in automobile applications, they are General Motors [31], Ballard and IFC.



Figure 42a Ballard Automotive Fuel Cell

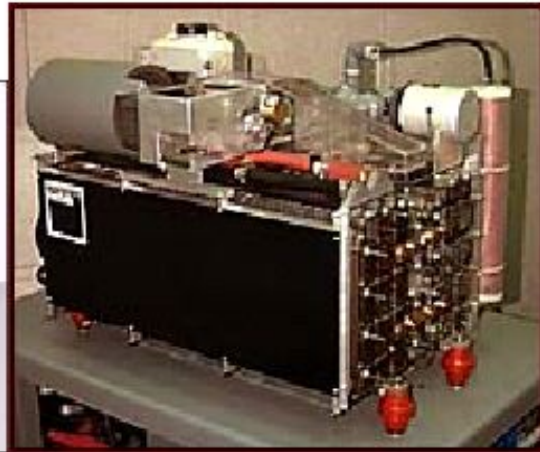


Figure 42b IFC Automotive Fuel Cell

For the airship application the automotive fuel cell stacks are probably the best available for near term use. The main issue with their use is whether they can operate directly on oxygen as the oxidizer or would a diluting gas such as nitrogen be necessary. If a diluting gas is necessary this entails adding a consumable into the system or a means of extracting nitrogen from the environment. Neither solution is preferable; therefore, developing a fuel cell that could operate directly on oxygen would be the logical choice. Evaluating the use of the automotive fuel cells with undiluted oxygen would be a worthwhile first step in the development of a fuel cell stack for high altitude airship use.

The fuel cell stack itself is only one of the components that make up the fuel cell system. The complete system consists of the fuel cell stack, reactant tanks, valves, regulators, filters, piping and control electronics. A diagram of the fuel cell system layout used for the airship analysis is shown in figure 43. Each of the components within the system has to be scaled as a function of the required output power of the fuel cell. The scaling was done to determine the mass of the individual components. For most of the components a linear relationship between mass and power was used. The scaling factors were based on present day “off-the-shelf” components that were selected based on a power range concurrent with that estimated for the airship operation. If components could not be found that operated within this power range then estimates were made as to how they would scale.

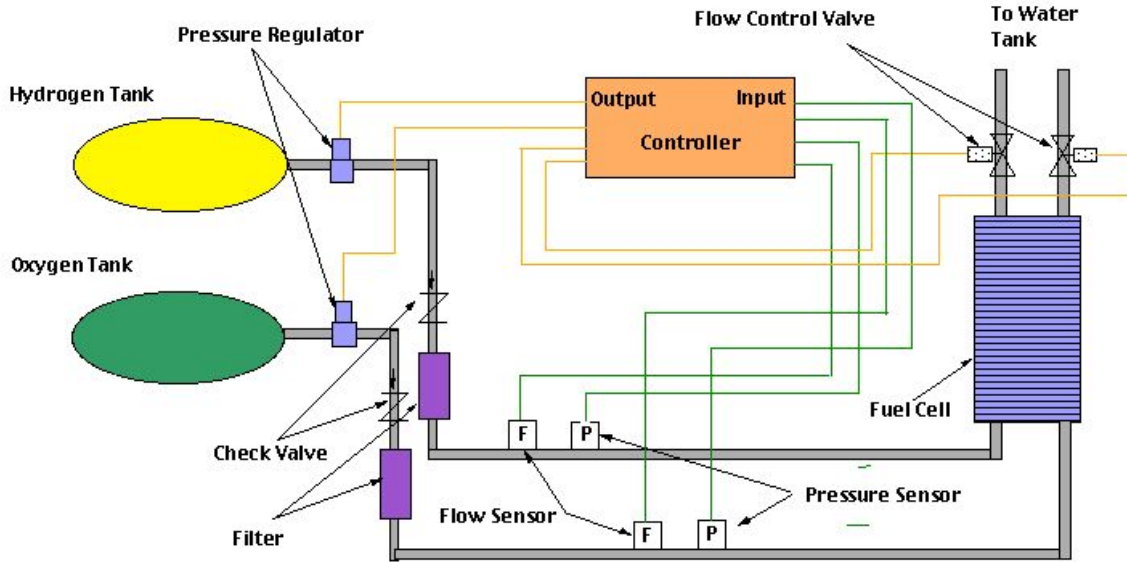


Figure 43 Fuel Cell System Layout

A list of the components and their linear scaling factors for the fuel cell system is given in table 6. The scaling factors for the fuel cell and its components are based on the maximum power the system will have to deliver (P_{max}). This is the engine power based on the 99th percentile wind speed plus the ship operations and payload power.

Table 6 Fuel Cell System Component Scaling Factors

Component	Scaling Factor
Fuel Cell Stack	1.0 kg/kw
Pressure Sensors	0.04 kg/kw
Temperature Sensors	0.01 kg/kw
Check Valves	0.04 kg/kw
Flow Sensors	0.04 kg/kw
Filters	0.06 kg/kw
Flow Control Valves	0.08 kg/kw
Controller	0.08 kg/kw
Power Converter	1.0 kg/kw
Lines and Fittings	0.26 kg/kw
Phase Separator	0.07 kg/kw
Hydrogen Regulators	0.05 kg/kw
Oxygen Regulators	0.09 kg/kw
Heat Exchanger	0.50 kg/kw
Wiring	0.30 kg/kw

Reactant Storage Tanks

The tank sizing and amount of hydrogen and oxygen reactants needed are dependent on the duration of operation and on the mean power level over that duration.

The conversion efficiency of fuel to electricity is assumed to be 50%. Therefore the flow rate of hydrogen (\dot{M}_h) needed can be determined by the following equation where P_{tot} is the mean power output of the fuel cell during operation in kilowatts, η_{fc} is the fuel cell efficiency estimated to be 50% and F is based on Faraday's constant, 96484 (A s / equivalent), which for hydrogen is 192968 (A s / g mole).

$$\dot{M}_h = \frac{2P_{tot}}{1.2\eta_{fc}F} \quad [35]$$

The total mass of hydrogen needed for a given day's operation (M_h) can be calculated by multiplying the mean flow rate of hydrogen by the amount of time the fuel cell is operating during the day. This operational time is determined through an energy balance between the output of the solar array, the efficiency of the energy storage and production system components and the mean power level of the airship for a day's operation (24 hours). The energy balance is discussed further in the analysis section of this report.

The mass of oxygen needed (M_o) to react with the hydrogen can be determined from the basic chemical reaction of combining hydrogen and oxygen to form water, given in equation 34. Based on this reaction 8 grams of oxygen are consumed for each gram of hydrogen. Therefore the reaction mass flow of oxygen (\dot{M}_o) is 8 times that of the hydrogen flow. It should be noted for this analysis that a residual of 20% hydrogen and oxygen by mass was added to the total amount required to account for reactants and water left in the lines and tanks of the system.

For this analysis it was assumed that the storage tanks for both the hydrogen and oxygen gasses were spherical and operating at a storage pressure (P_h and P_o respectively) of 20.7 Mpa (3000 psi) with a factor of safety (F_s) of 1.8 for the tanks. The gas volumes for both hydrogen (V_h) and oxygen (V_o) were calculated using the equation of state with a compressibility factor for the hydrogen gas (Z). The storage temperatures for the hydrogen (T_h) and oxygen (T_o) gas were assumed to be equal to the ambient air temperature at the operating altitude of the airship. The tank mass is based on a carbon composite tank (3500 Mpa, 507 kpsi yield (σ_t) and 1608 Kg/m³, 0.058 lb/in³ density (ρ)) with a thin metal liner that is resistant to the gas migration out of the tank [32].

$$V_h = \frac{4157.2ZM_hT_h}{P_h} \quad [36]$$

$$Z = 0.99704 + 6.4149E - 9P_h \quad [37]$$

$$V_o = \frac{259.83M_oT_o}{P_o} \quad [38]$$

Using the gas volume, storage pressure and tank material properties the mass for the hydrogen and oxygen tanks can be calculated. These are given by equations 39 and 40 respectively.

$$M_{th} = \rho_t V_h \left[\left(1 + \frac{P_h F_s}{2\sigma_t} \right)^3 - 1 \right] \quad [39]$$

$$M_{to} = \rho_t V_o \left[\left(1 + \frac{P_o F_s}{2\sigma_t} \right)^3 - 1 \right] \quad [40]$$

Air Compressor System

As an alternative to using stored oxygen as the oxidizer for the fuel cell reaction, oxygen from the air can also be considered. Utilizing atmospheric oxygen eliminates the need for collecting and storing the oxygen from the electrolyzer. The main issue with utilizing atmospheric oxygen is that the air pressure at the operational altitude of 21.5 km is very low, 40.5 mbar. Most present day PEM fuel cells require at least 1000 mbar (1 atmosphere) of air pressure to operate correctly. Therefore the air at altitude would need to be compressed in order for it to be utilized by the fuel cell. This will require compressors, heat exchangers and electric motors to drive the compressors. All these components will add mass to the fuel cell system and the motors that are needed to drive the compressors will add an additional parasitic power load to the airship's operation. This additional power load will need to be considered in the overall power system sizing. A diagram of this system is shown in figure 44. Table 7 lists the scaling numbers for the air compressor system. The efficiency of the compressor drive motors was assumed to be 85%.

Table 7 Scaling Factors for Compressor Components [33]

Component	Scaling Factor
Low Pressure Compressor and Drive Motor	0.79 kg/kw
Intercooler	83.33 kg/ \dot{M}_{air}
High Pressure Compressor and Drive Motor	0.113 kg/kw
Aftercooler	118.2 kg/ \dot{M}_{air}

To size the intercooler and aftercooler the mass flow of air is needed. This can be calculated based on the oxygen mass flow requirement given previously and that the atmospheric composition of gasses is approximately 21% oxygen. The mass flow of air required is given in equation 41. The total output power from the fuel cell (P_{tot} , in kilowatts) also must include the power to run the motors that drive the compressors.

$$\dot{M}_{air} = (6.91E - 4)P_{tot} \quad [41]$$

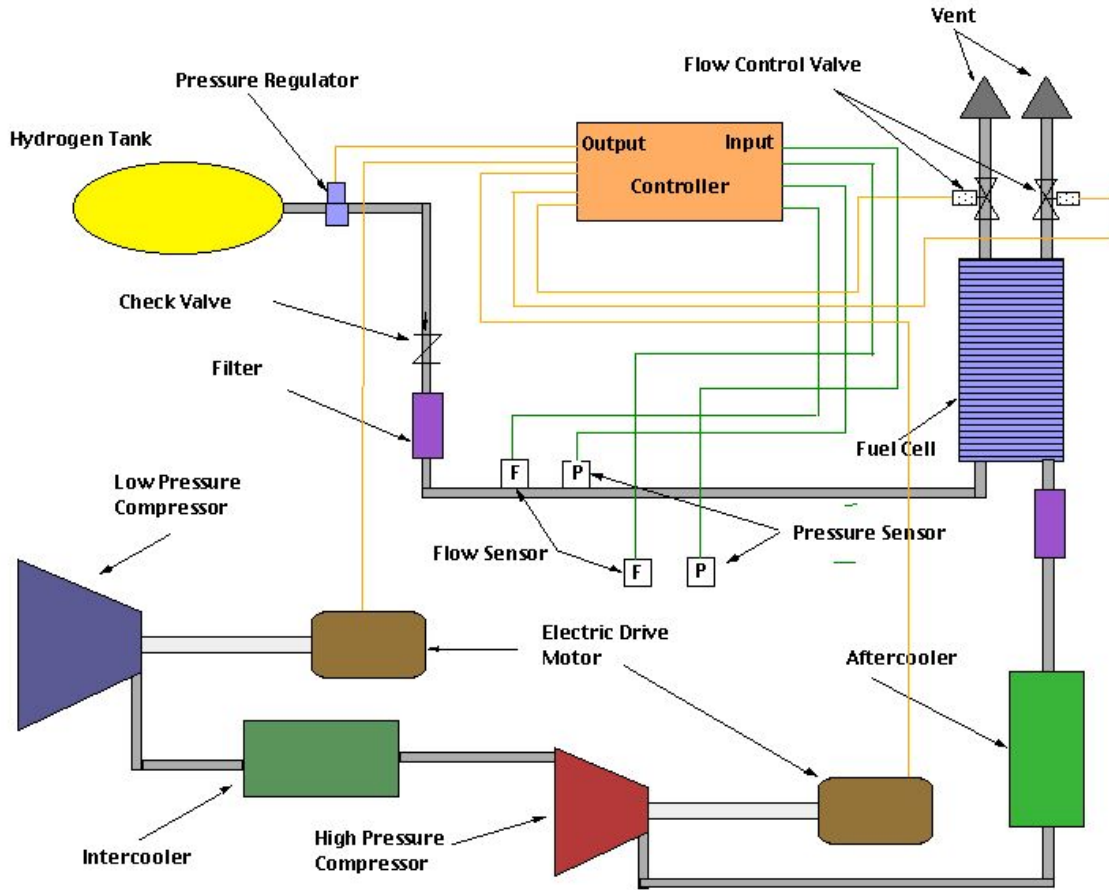


Figure 44 Hydrogen / Air High Altitude Airship Fuel Cell System

To determine the total power output from the fuel cell requires information on the compressors and intercoolers in order to estimate the power consumption needed to drive the compressors. It is assumed that the compression ratio of each of the compressors is 4.7 [33]. With an ambient pressure of 4445 Pa this will provide an inlet air pressure to the fuel cell of 1 atmosphere (101352 Pa) via the two compressors. The temperature ratio across the inter-cooler and after-cooler were assumed to be 1.62 [33]. Based on these ratios the temperature and pressure before and after each component of the compressor system can be estimated. These temperatures and pressures are listed in table 8. Assuming adiabatic flow through each compressor, the power required to operate a compressor (P_c) is given by equation 42. The power is based on the inlet (T_i) and outlet temperature (T_e) in °K of the air stream and the specific heat of air (C_p) which is assumed to be constant with a value of 1.0035 (kJ/kg °K). The exit flow velocity (in m/s) can be expressed in terms of air density (ρ_e) at the exit and the exit duct area (A_e).

$$P_i = C_p(T_e - T_i)\dot{M}_{air} + \frac{\dot{M}_{air}^3}{2(\rho_e A_e)^2} \quad [42]$$

Table 8 Compressor System Component Inlet and Outlet Temperatures and Pressures

Location	Temperature	Pressure	Density
Ambient Conditions	218 K	4445 Pa	0.071 kg/m ³
After Low Pressure Compressor, Before Intercooler	420 K	20892 Pa	0.173 kg/m ³
After Intercooler, Before High Pressure Compressor	261 K	20892 Pa	0.279 kg/m ³
After High Pressure Compressor, Before Aftercooler	518 K	101352 Pa	0.682 kg/m ³
Into Fuel Cell	321 K	101352 Pa	1.099 kg/m ³

From equations 41 and 42 it can be seen that the power needed to operate the compressors will depend on the total power required by the airship. This is due to the increase in airflow needed by the fuel cells with increasing power requirements. Determining the compressor power requires an iterative solution between air flow rate and the total airship power requirement. By using equations 41 and 42 and the values in table 8 the total power required can be expressed as a function of the airship power (P_a) which includes all propulsion (except for the air compressors), payload and operation power. This relationship for total power is given in equation 43 where the exit duct areas for the compressors are given by A_{le} for the low-pressure compressor and A_{he} for the high pressure compressor.

$$P_{tot} = 1.54P_a + (8.467E - 9)\left(\frac{P_{tot}^3}{A_{le}}\right) + (5.447E - 10)\left(\frac{P_{tot}^3}{A_{he}}\right) \quad [43]$$

If it is assumed that the exit flow velocity is sufficiently small that the second and third terms of equation 43 can be neglected then equation 43 states that the compressors will increase the total ship power requirement by 54%.

Electrolyzer

An electrolyzer is a device that will break apart water into its constituent elements, hydrogen and oxygen. It works on the same principle as the fuel cell described previously except in this case electricity is put in and hydrogen and oxygen are generated, which is the reverse of what a fuel cell does. The electrolyzer will be used to fill and maintain the hydrogen and oxygen storage tanks with a sufficient amount of reactants to maintain continuous operation of the airship.

The power to run the electrolyzer will come entirely from the solar array. Whenever the fuel cell is operating, the electrolyzer will not be operational. Because of the efficiency losses in the fuel cell and electrolyzer, operating the fuel cell to run the electrolyzer to produce hydrogen will result in a net decrease in hydrogen. The electrolyzer will be sized to operate at the maximum output power of the solar array. This is necessary in order to fully utilize the solar array and maintain the energy balance for the airship operation.

The electrolyzer will be operated by the control system and turned on or off depending upon the load demand from the airship and the power availability from the solar array.

The electrolyzer system consists of the electrolyzer unit, a heated water supply tank and hydrogen and oxygen connections to their respective storage tanks. A diagram of the electrolyzer system is shown in figure 45. Due to the cold ambient temperatures at the desired flight altitude, the water will need to be heated to ensure that it does not freeze. Since this is a power drain on the system, waste heat from the fuel cell or electrolyzer operation can be used as the heat source for keeping the water above freezing.

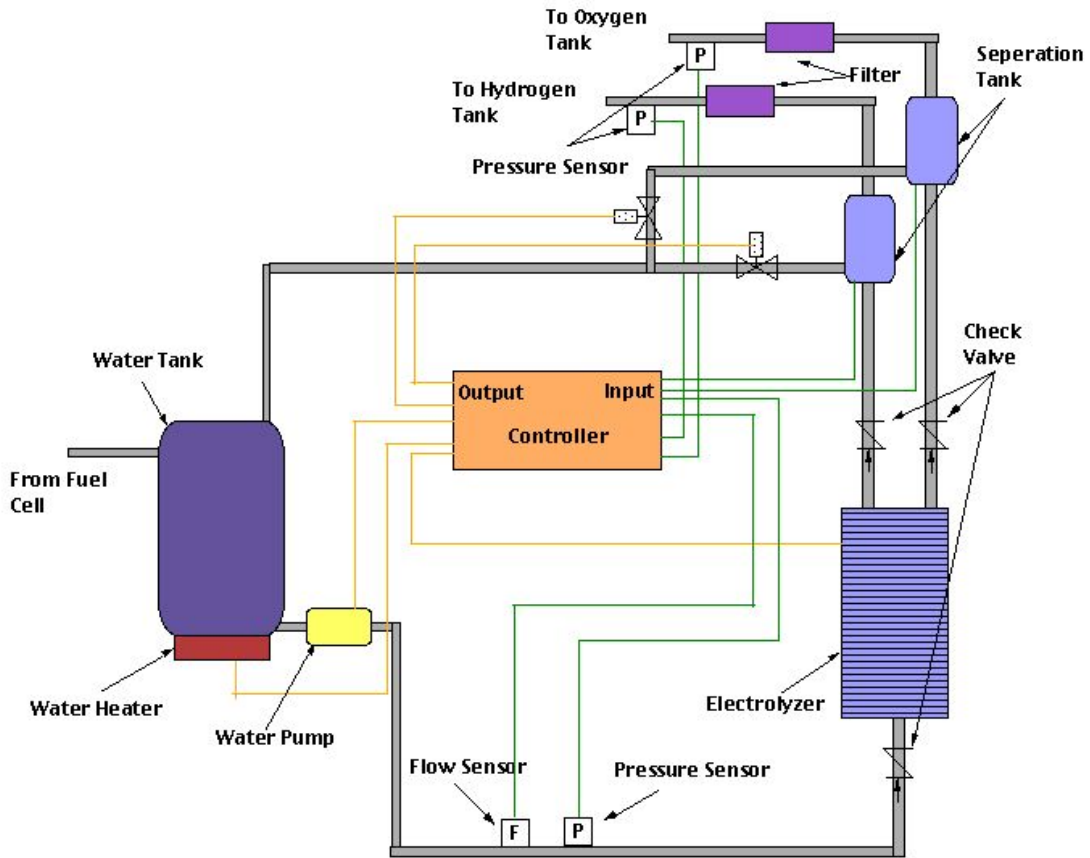


Figure 45 Electrolyzer System Layout

As with the fuel cell, scaling factors were devised to size the mass of the various components included in the electrolyzer system. A list of these components and their scaling factors are given in table 9.

Table 9 Electrolyzer System Component Scaling Factors

Component	Scaling Factor
Electrolyzer	1.00 kg/kw
Flow Control Valves	0.08 kg/kw
Filters	0.06 kg/kw
Separation Tanks	0.38 kg/kw
Controller	0.08 kg/kw
Check Valves	0.04 kg/kw
Flow Sensor	0.02 kg/kw
Pressure Sensors	0.02 kg/kw
Water Pump	0.27 kg/kw
Water Tanks and Heater	0.10 kg/kw
Lines and Fittings	0.26 kg/kw
Heat Exchanger	0.50 kg/kw

The scaling factor for the electrolyzer stack was equal to that of the fuel cell stack. Although they operate on the same principles, there has been significant effort placed into reducing the mass and volume of fuel cells. This is mainly due to their potential as an automotive power plant. However, the same development effort has not gone into the electrolyzer. It is reasonable to assume that with a similar development effort the electrolyzer specific mass can be reduced to that comparable to the fuel cell. Therefore a similar scaling value, to that of the fuel cell, was used for the electrolyzer stack. As with the fuel cell, the baseline for this analysis was to use off-the-shelf or near term technology for the various electrolyzer system components.

Electric Motor

An electric motor is used to drive the propellers that generate thrust. The efficiency and operational capabilities of the motor are major factors in the power consumption and overall capabilities of the airship. Since the solar array and the fuel cells put out DC power, the main power bus on the airship is DC. However, either of the two main types of electric motors, AC and DC, can be considered for the airship application. In addition to matching the bus current DC motors have another advantage when it comes to driving a propeller: Their torque-speed characteristics are easier to control than that of AC motors. Ironically most types of DC motors employ a mechanical switch (commutator) that turns the DC current into AC current within the motor armature [34].

Although the DC motor seems to be the logical choice for use in the airship, certain types of AC motors also offer advantages. For example an induction motor does not utilize a permanent magnet, instead it induces the magnetic field based on current flow. Because of this there is little resistance to rotation when the motor is shut off. This can be an advantage in a system in which multiple motors are used to drive a single shaft. If a motor fails or is not needed it can be shut off and poses little additional load on the remaining motors. Another advantage of an induction motor, as well as a brushless DC motor, is the elimination of the contact brushes used in a standard DC motor. These brushes can wear out and may be subject to arcing at the low density and pressure

environment within which the airship will be operating. If an induction motor is utilized, an inverter will be required to convert the DC bus current to AC. This presents an additional inefficiency and will add to the mass of the overall motor system.

The AC induction motor has been the choice for lightweight high output motors for high-speed electric automotive vehicle development. General Motors set an electric vehicle land speed record using an AC induction motor as the main drive motor for the vehicle [35]. And Lincoln Electric in conjunction with Bowling Green State University has developed a high speed electric vehicle (Electric Falcon) that utilizes a high power AC induction motor [36]. Because of the automotive industry development, this type of motor may be the most practical solution for a high output low mass motor for the airship application. Whatever motor is selected, development will most likely be needed to insure its operation within a rarefied high altitude environment.

For this analysis the motor was sized based on the output power requirement. The drive power and mass of a number of representative DC motors were used to generate a curve fit for motor mass (M_{em}) versus output power. This curve fit is given in equation 44 and is based on the maximum thrust and power level required by the motor (P_{max}) to overcome the 99th percentile wind speeds.

$$M_{em} = -0.2669 + 9.845E - 4P_{max} - 1.120E - 10P_{max}^2 \quad [44]$$

The motor efficiency will vary as a function of the motor power and its RPM. Certain types of motors will operate efficiently at or near their design RPM and will drop off in efficiency as they are operated off of this design point. If the motor needs to operate at or near a single RPM then a gearbox may be necessary in order to drive the propeller at the correct RPM. There is a tradeoff between running the motor “off-design” at reduced efficiency and carrying the extra weight of a gearbox. Gearbox efficiencies will tend to be in the 95%+ range and therefore will not have much of an effect on the drive system performance. The decision to utilize a gearbox will depend on the motor capabilities, it’s off design performance and the amount of time the motor will be operating off its design point. For this analysis a general relationship between motor efficiency (η_m) and power was used. This relationship, given in equation 45, is based on a standard 4-pole induction motor efficiency curve [34].

$$\eta_m = 75.844 + 8.6059 \log(P_m) \quad [45]$$

Propeller

The operation of the propeller is one of the more critical elements of the propulsion system. The efficiency and capabilities of the propeller directly affect the sizing of the power system as well as the other propulsion system components. The majority of the power produced and consumed by the airship is for the production of thrust. From the solar array to the energy storage system to the motors, the primary function of all these systems and their components is to drive the propellers. When considered from this

perspective one can see why propeller performance can have a great impact on the airship sizing and design. As discussed in the layout of the airship a dual propeller system will be used. The dual propeller system allows thrust to be generated efficiently over a wide range of operational conditions. It also adds some redundancy to the propulsion system.

The environmental conditions under which the propeller must operate will vary considerably. The airship will need to be controllable and therefore produce thrust from the surface up to its design altitude. At the design altitude the variation in wind speeds from the mean to 99th percentile winds can be considerable. The variation in wind velocity (V) at altitude, as well as the variation in atmospheric density (ρ) and viscosity (μ) as the airship ascends or descends, provides a wide aerodynamic operational range within which the propeller must be capable of operating. This large variation in operational conditions can pose a problem for the efficient operation of the propeller.

A propeller design is optimized for a single operating point. The design parameters such as revolutions per minute (RPM), diameter (d), chord length (c), airfoil and twist are all chosen to maximize the efficiency for a given amount of thrust at the design conditions. The design conditions, which are a combination of the environment and the operational and design parameters for the propeller, can be expressed by the design Reynolds number for the propeller. The Reynolds number (R_e) for the propeller is given in equation 46.

$$R_e = \frac{\rho c \sqrt{V^2 + \left(\frac{\pi d (RPM)}{60}\right)^2}}{\mu} \quad [46]$$

An example of the range of Reynolds numbers under which a single propeller would need to operate is show in figure 46. This figure shows the operational Reynolds number at the 0.7 radial station for a propeller with a diameter of 4.9 m, a chord length of 0.32 m and spinning at an RPM of 920. Reynolds number is plotted as a function of altitude from the surface up to 28 km. The propeller must be capable of operating throughout this range (from ~5 million to 100 thousand) in order to maintain control of the airship during ascent. Once at altitude the propeller must be capable of operating efficiently over the range of wind speeds (from 0 m/s to ~53.5 m/s) that can be encountered. It is because of this great variation in the flight environment as well as the large fluctuation in wind speeds at the operational altitude that a dual propeller system was selected.

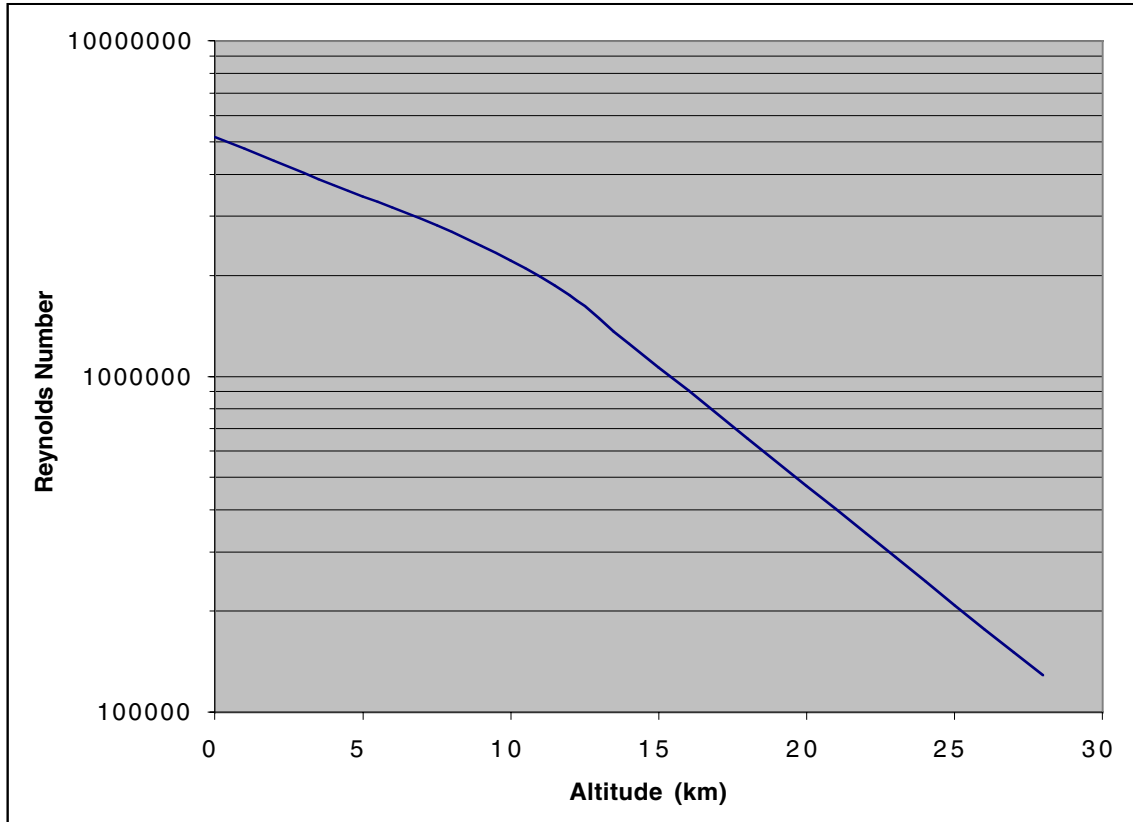


Figure 46 Propeller Reynolds Number as a Function of Airship Altitude

The dual propeller system provides a smaller propeller that can be used during station keeping under mean or low wind conditions and a larger propeller that can be used during high wind conditions and for producing increased thrust for maneuvering at high altitudes. The smaller propeller also provides a more efficient means of producing thrust and control at lower altitudes. During launch or descent to the surface the small propeller would be used for maneuvering and control of the airship.

The mean and 99th percentile wind speeds are used to size the propellers for the airship. The propellers must be capable of producing the thrust necessary to overcome the drag on the airship produced by the wind. The propellers are assumed to be operated independently, although in actual use they could be operated at the same time. For the analysis it was assumed that the small propellers would provide the mean thrust level and the larger propellers would provide the 99th percentile wind or maximum thrust level.

To size the propellers for a given airship configuration and operational location, a map of propeller performance for a characteristic propeller was needed. This map was generated using a vortex theory analysis code [37] for propeller configurations with 4, 5 and 6 blades. To generate this performance data a general propeller configuration was used. This propeller configuration was representative of a high altitude propeller design that would be consistent with the thrust levels required by the airship. Design parameters such as twist along the blade, chord length variation along the blade and airfoil selection were all chosen to be representative of the flight environment but were not altered to optimize the propeller for a specific airship design. Other parameters such as the number of blades,

propeller diameter and operational RPM were all adjustable to meet the needs of a specific airship configuration and flight environment.

The propeller geometry is given by the chord length (c) and twist (β) along the length of the blade from the hub to the propeller tip. The blade station (r) is a normalized distance along the blade given by 0 at the center of the hub and 1 at the tip. For the blade twist relationship, since a variable pitch propeller blade is assumed, the whole blade can be turned by the given pitch angle (ϕ). These are fixed relationships for all airship configurations and are given by equations 47 and 48. A plot of these functions is given in figure 47 for a propeller diameter of 4.9 m and zero pitch angle. Note that the increase in chord length below an r of 0.1 is due to the hub and is not representative of the propeller blade itself.

$$c = (0.084241 - 0.85789r + 4.7176r^2 - 9.6225r^3 + 8.5004r^4 - 2.7959r^5)d \quad [47]$$

$$\beta = \phi + 0.4387 + 0.3040r - 3.9616r^2 + 5.1180r^3 - 1.6284r^4 - 0.3244r^5 \quad [48]$$

The airfoil selected for the propeller is the SP-8000PT. It is a good all around propeller airfoil and has good low Reynolds number performance that is desirable for high altitude operation., The lift coefficient versus angle of attack, c_l vs α , curve is shown in figure 48, the lift coefficient (c_l) to drag coefficient (c_d) curve for the airfoil is shown in figure 49 and a cross-section of the airfoil is given in figure 50 [38].

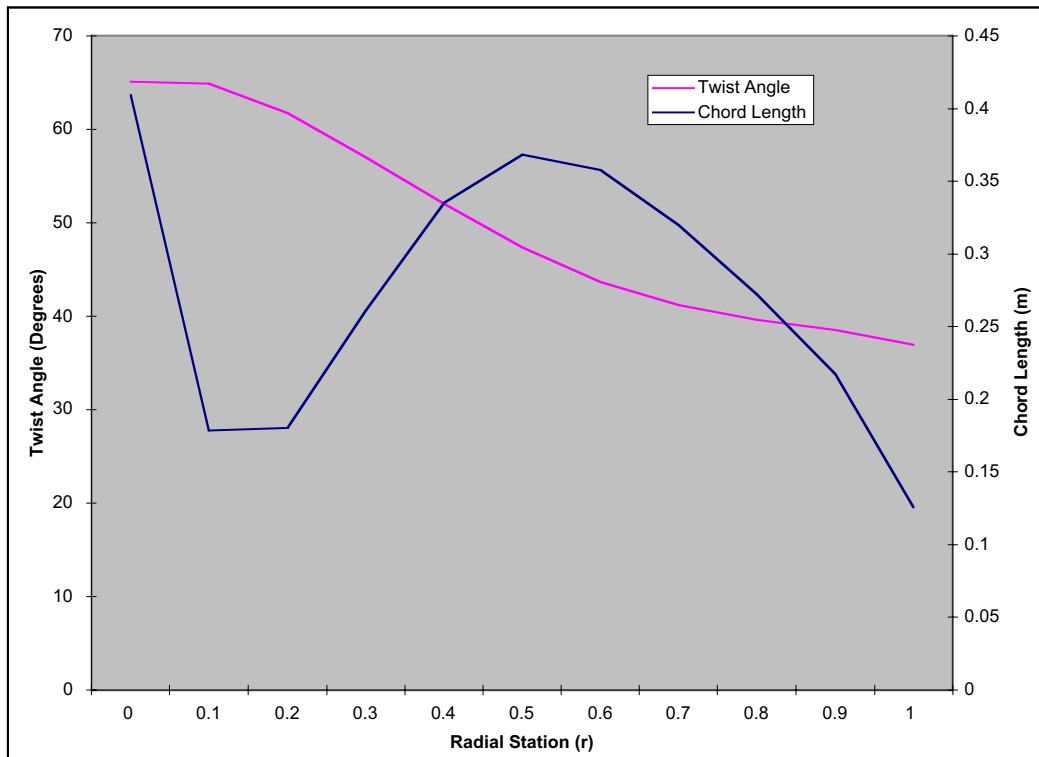


Figure 47 Blade Twist and Chord Length as a Function of Radial Station

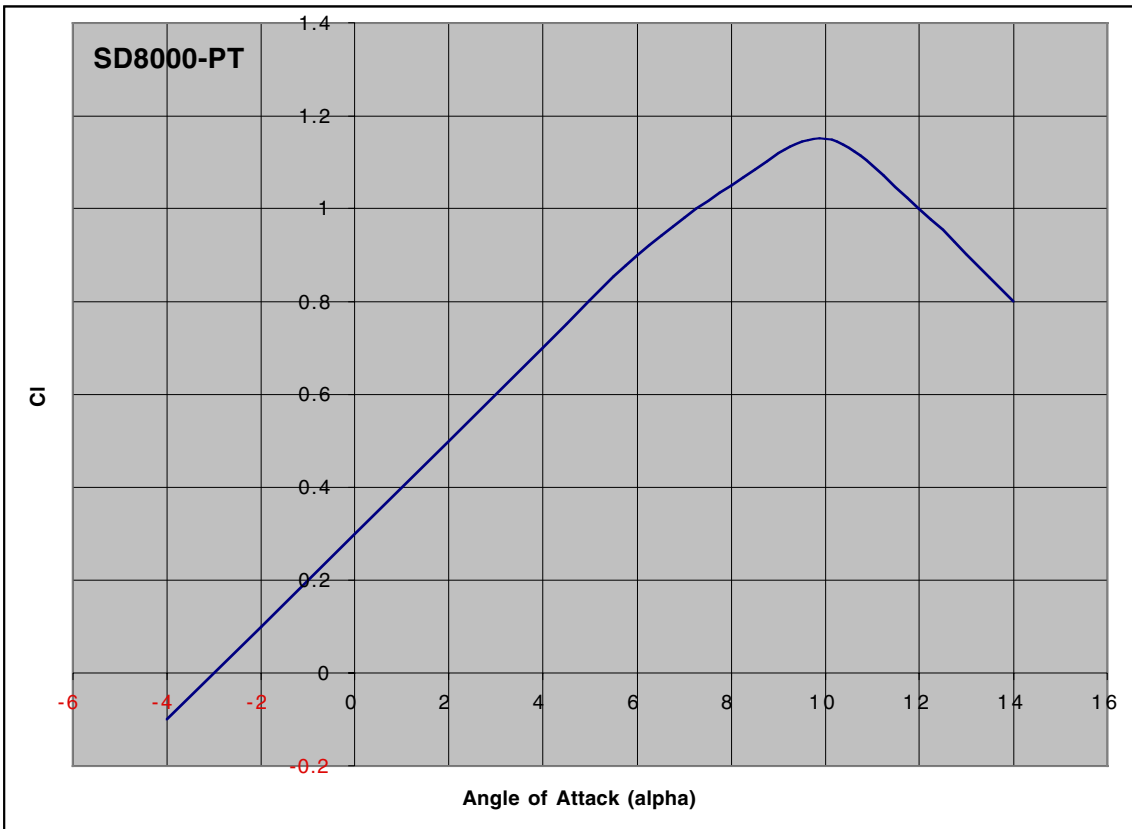


Figure 48 Lift Coefficient versus Angle of Attack for SD8000-PT airfoil at a Reynolds Number of 300,000 [38]

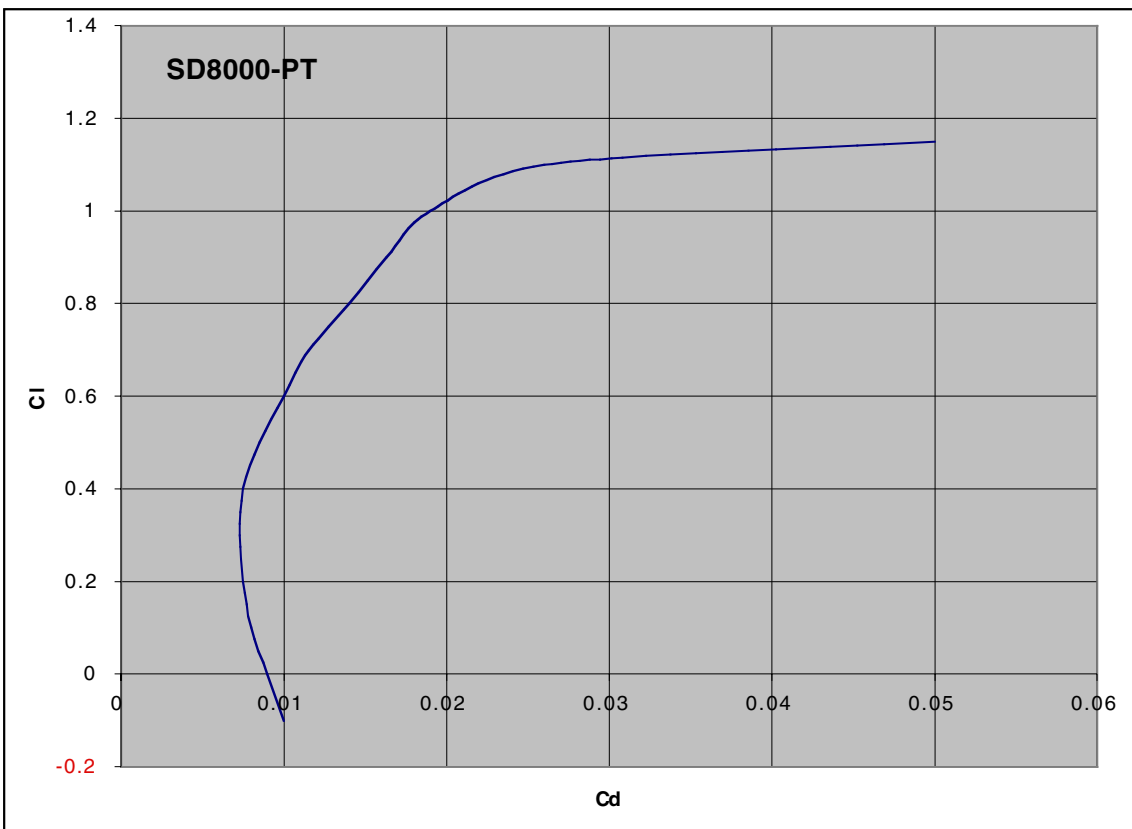


Figure 49 Lift Coefficient versus Drag Coefficient for SD8000-PT airfoil at a Reynolds Number of 300,000 [38]

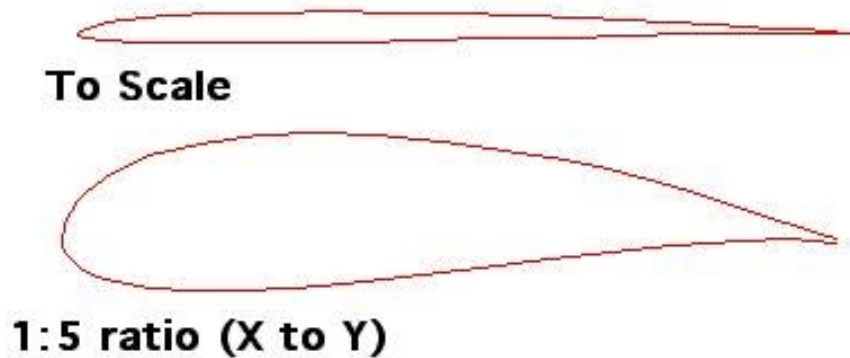


Figure 50 SD8000-PT Airfoil Cross Section: To Scale and with the Y axis Exaggerated by 5 times the X axis

The propeller operational thrust and power curves based on the SP-8000PT airfoil and the geometry relationships given by equations 47 and 48 are shown in figures 51 through 56.

The curves shown in figures 51 through 56 represent the operating capabilities for the propeller. The curves show thrust coefficient (c_t) and power coefficient (c_p) versus the advance ratio (J) for the propeller at various blade or pitch angles. The pitch angle of the propeller acts somewhat like a transmission system. The larger the pitch angle the more thrust is generated for a given RPM but the greater the torque needed to spin the propeller. The operational thrust of the propeller can be varied by changing either the pitch of the propeller and or its RPM. The pitch change is accomplished by rotating the propeller blade, thereby adjusting the angle of attack of the propeller airfoil to the incoming air stream. The pitch change in combination with varying the RPM can be used to produce varying levels of thrust over a range of operational conditions.

Using the drag of the airship that is generated either by the winds or the movement of the airship at a given speed, figures 51 through 56 are used to determine the diameter of the propeller, its operational RPM and the power required to generate the desired amount of thrust. The airship drag sets the thrust level the propeller must meet. It is assumed that each propeller will produce an equal amount of thrust. In other words if there are four propulsion modules on board each will need to produce thrust equal to one quarter of the drag.

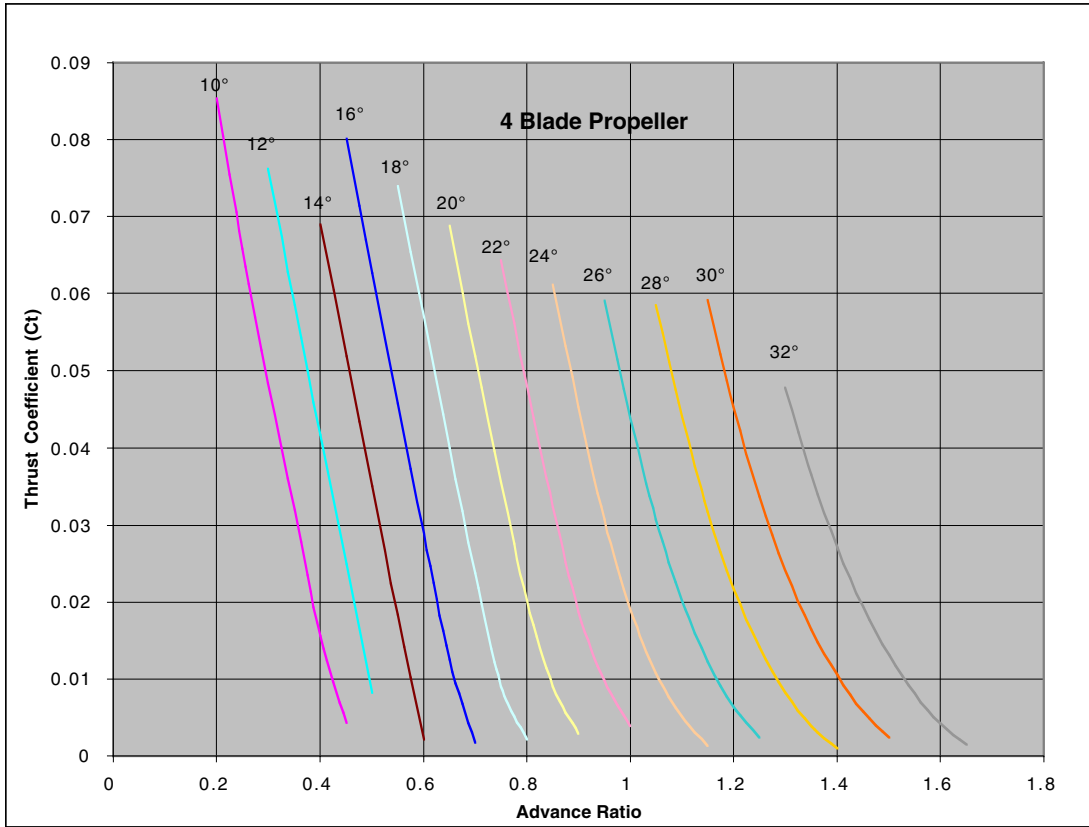


Figure 51 C_t vs J for a 4 Bladed Propeller at Various Pitch Angles

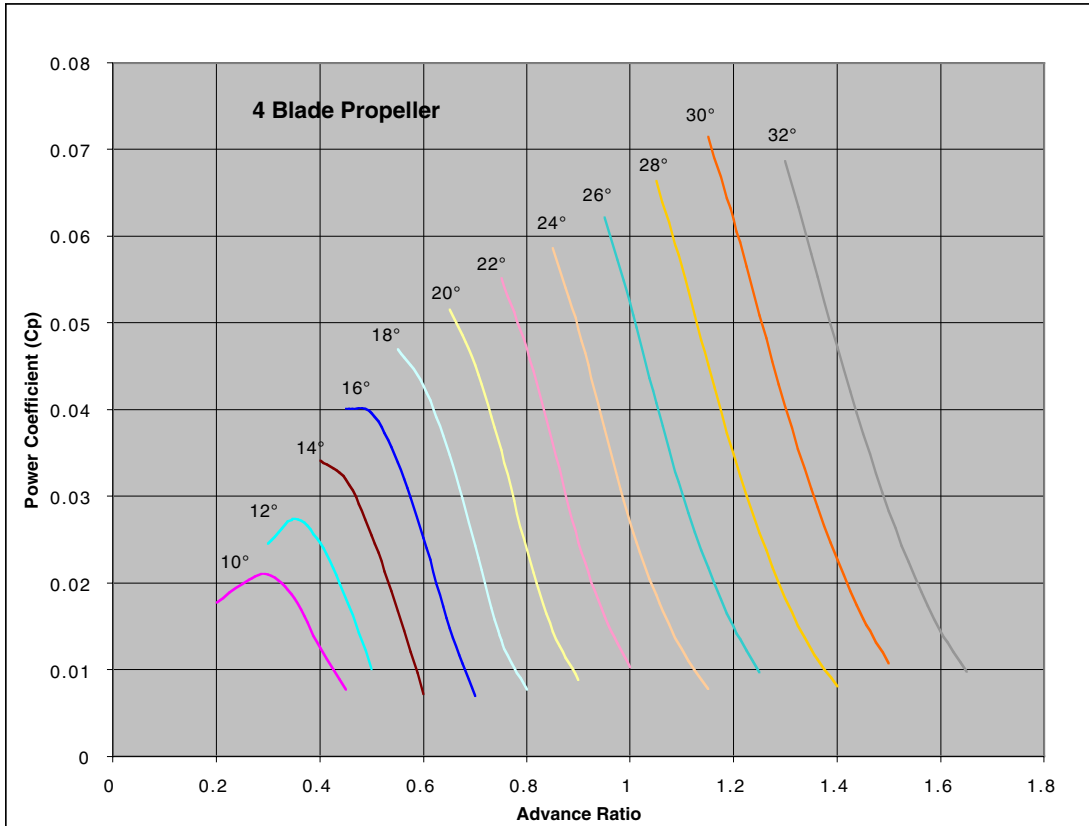


Figure 52 C_p vs J for a 4 Bladed Propeller at Various Pitch Angles

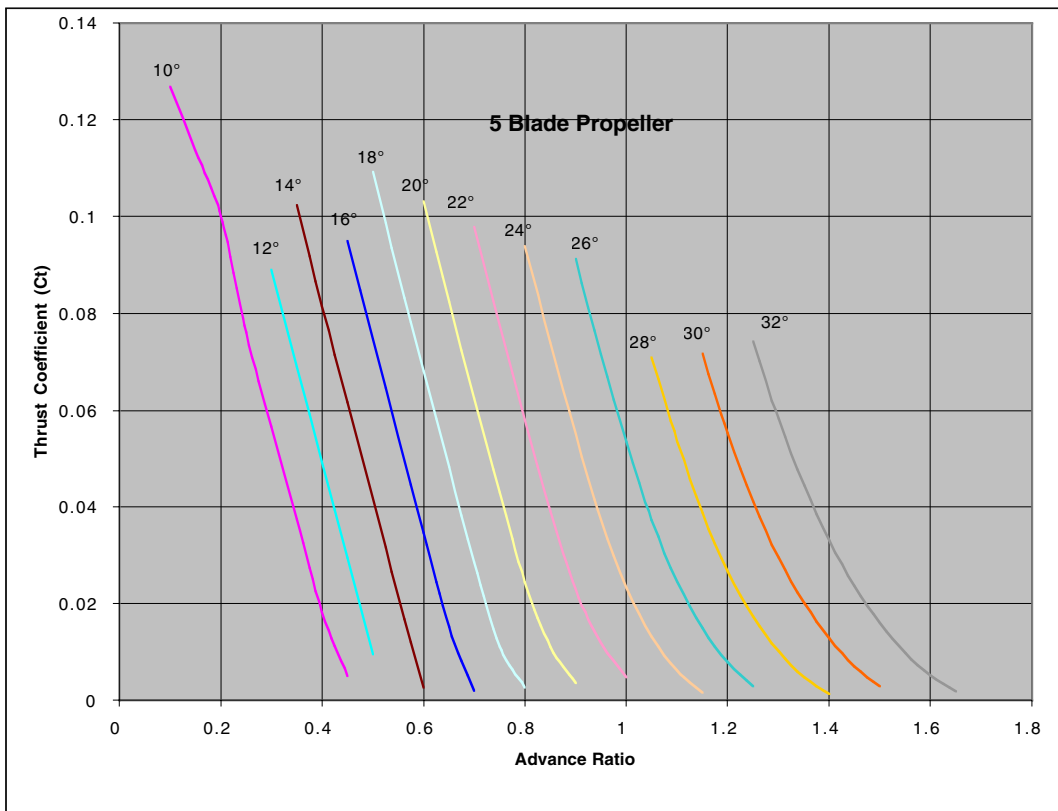


Figure 53 C_t vs J for a 5 Bladed Propeller at Various Pitch Angles

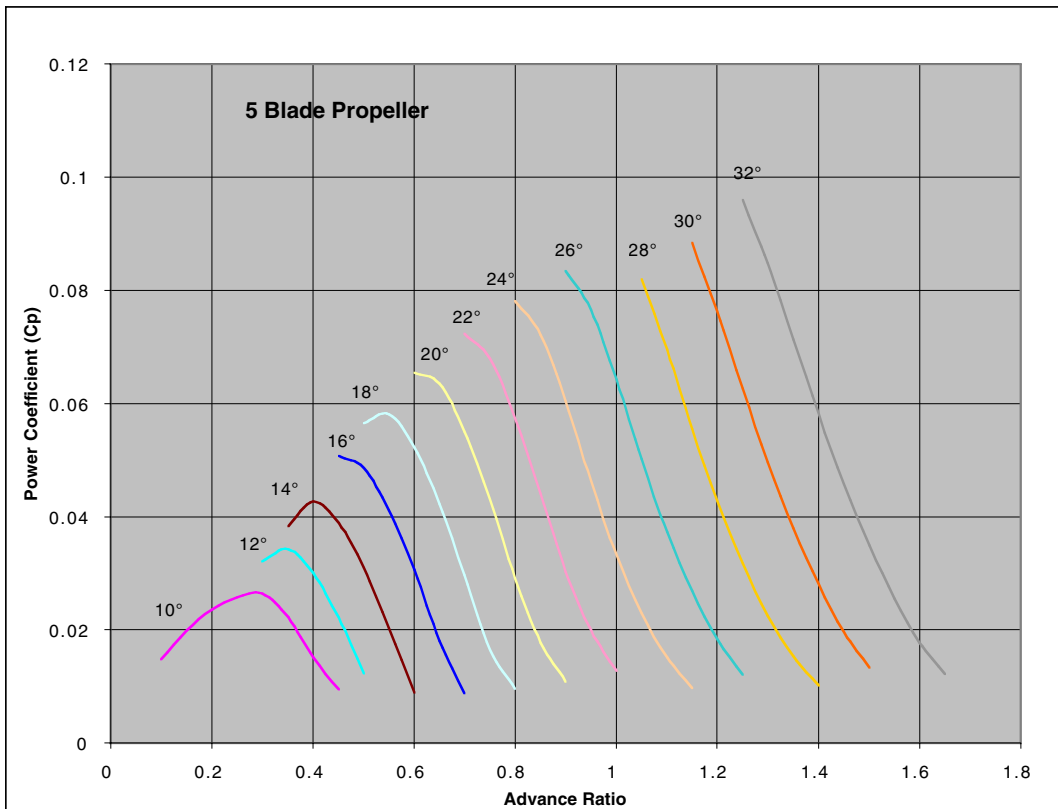


Figure 54 C_p vs J for a 5 Bladed Propeller at various Pitch Angles

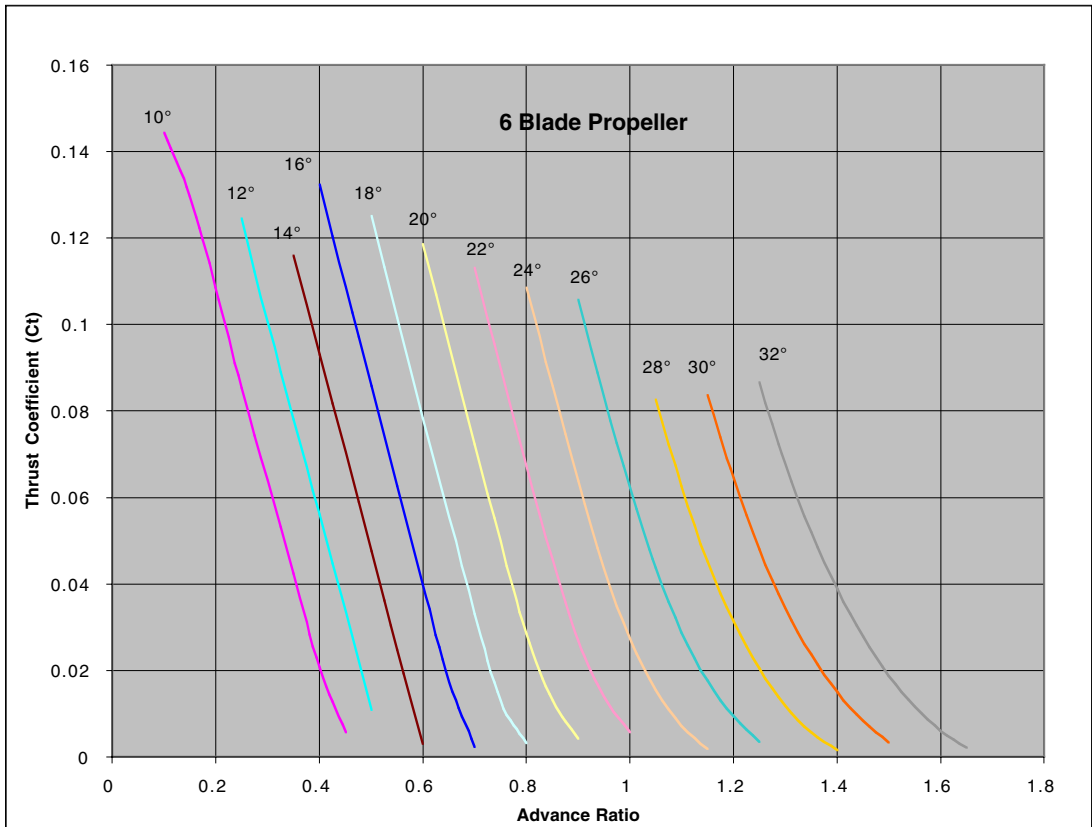


Figure 55 C_t vs J for a 6 Bladed Propeller at Various Pitch Angles

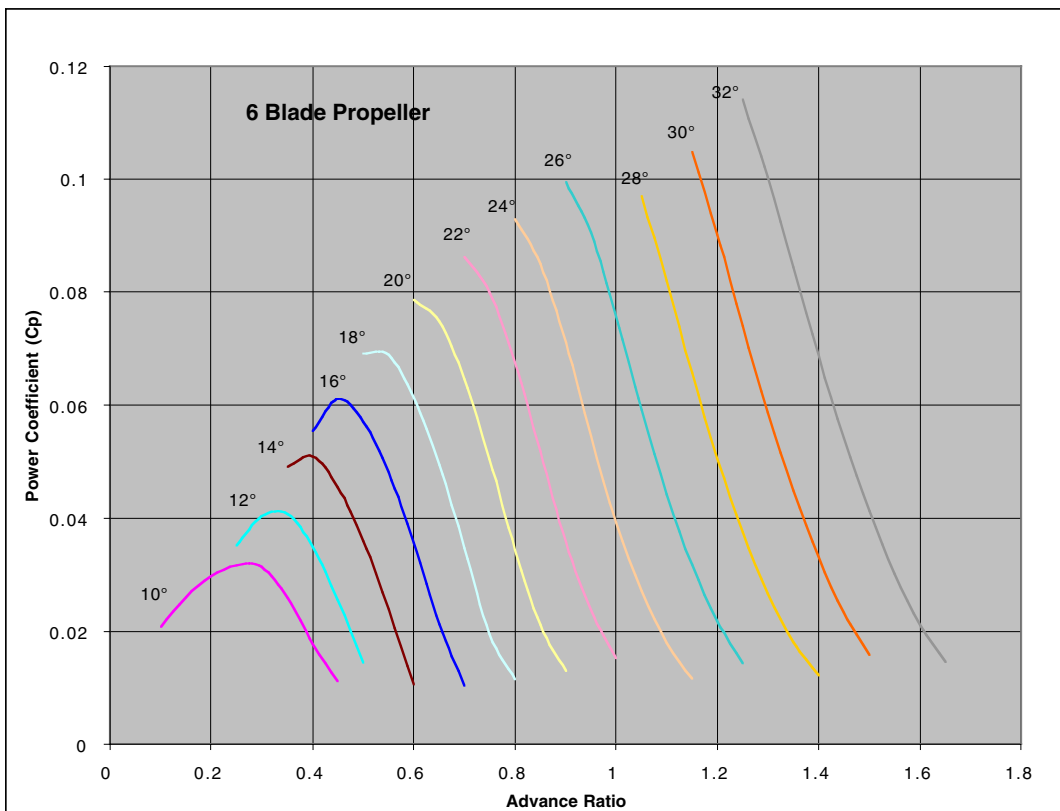


Figure 56 C_p vs J for a 6 Bladed Propeller at Various Pitch Angle

The propeller sizing was performed through an iterative process using the performance maps in the above figures and the following equations for thrust coefficient (c_t), advance ratio (J), propeller efficiency (η) and propeller RPM.

$$c_t = \frac{T_p}{\rho \left(\frac{RPM}{60}\right)^2 d^4} \quad [49]$$

$$J = \frac{V}{\left(\frac{RPM}{60}\right)d} \quad [50]$$

$$RPM = \frac{60}{\pi d} \sqrt{(MV_s)^2 - V^2} \quad [51]$$

Equation 49 represents the thrust coefficient as a function of the thrust (T_p) that is needed to overcome the drag on the airship. Thrust coefficient and advance ratio can be calculated for a given propeller diameter. Propeller RPM is based on the maximum tip speed allowable for a given propeller diameter. This tip speed is based on the speed of sound (V_s) and Mach number (M) of the propeller tip. The Mach number must be less than 1 to avoid the formation of shock waves. Maintaining a subsonic tip speed for the propeller is necessary for stability as well as the efficiency of the propeller. Shock waves can cause the propeller blade to flutter, potentially destroying the blade. They also produce a significant increase in drag on the blade greatly reducing its efficiency.

Using the calculated thrust coefficient and advance ratio for a given propeller diameter, and the c_t vs J chart corresponding to the number of blades on the propeller (figures 47, 49, or 51), a blade or pitch angle can be determined. With the pitch angle and advance ratio known, the power coefficient can be determined from figures 48, 50 or 52 (corresponding to the number of blades on the propeller). This power coefficient (c_p) can be used to determine the power consumed by the propeller at these conditions. Shaft power (P_p) required by the propeller is given in equation 52.

$$P_p = c_p \rho \left(\frac{RPM}{60}\right)^3 d^5 \quad [52]$$

The operational efficiency of the propeller (η) can be calculated by the thrust and power coefficients and advance ratio. This efficiency is given in equation 53.

$$\eta_p = \frac{c_t}{c_p} J \quad [53]$$

By iterating on the propeller diameter to maximize efficiency, equations 49 through 53 along with figures 51 through 56 can be used to determine the required diameter and subsequent operating conditions of the propeller.

Analysis

The evaluation of a high altitude airship is a complex process. There are a number of factors that come into play in determining the feasibility and capabilities of operating an airship at high altitudes for extended periods of time. Because of the desire for long duration flight the airship must collect its operating power from the environment by utilizing a solar array. This coupling of the airship's available power to the environment makes the capabilities of the airship dependent on where (latitude) and when (time of year) the airship is to be flown. The sizing and evaluation of the capabilities of a high altitude renewably powered airship is dependent on the mission requirements, environment and performance characteristics of the power, propulsion and airship components. All of these factors must be taken into account to determine what capabilities and limits there are on using a high altitude airship.

How the airship is to be used and where it needs to operate are critical factors in evaluating its feasibility. Some of these factors are illustrated in figure 57.

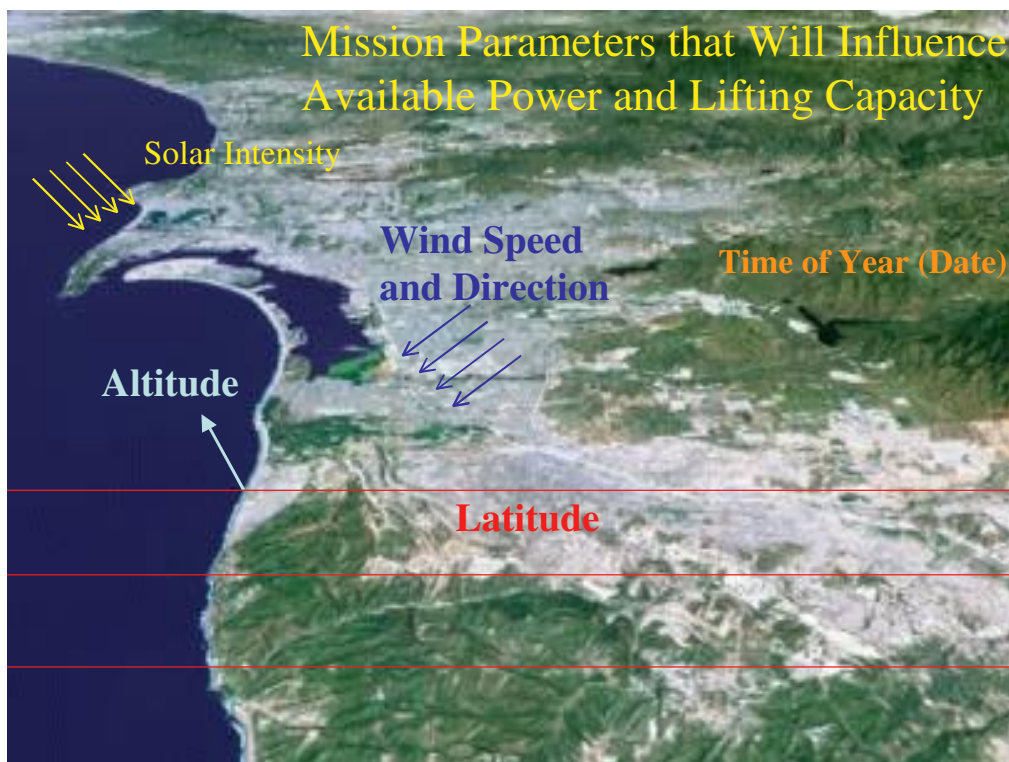


Figure 57 Mission and Environmental Factors that Influence the Airship Feasibility

To start the analysis some basic mission parameters are required. These are as follows:

- Flight Altitude
- Payload Requirements (Mass and Power)
- Flight Duration
- Flight Location (latitude)
- Operational Time of Year (if less than 1 year in duration)
- Mobility Requirement

Once the desired mission is established the analysis can be broken down into three main areas: power production, power consumption and lift generation. For the airship to be feasible and operate under the desired mission constraints, it must be capable of producing as much or more energy than it utilizes, and its size must be such that it can maintain its total mass at the desired altitude. Each of these three factors depends on various aspects of the environment, mission, component operational requirements and airship configuration. A diagram of the three main analysis components is shown in figure 58.

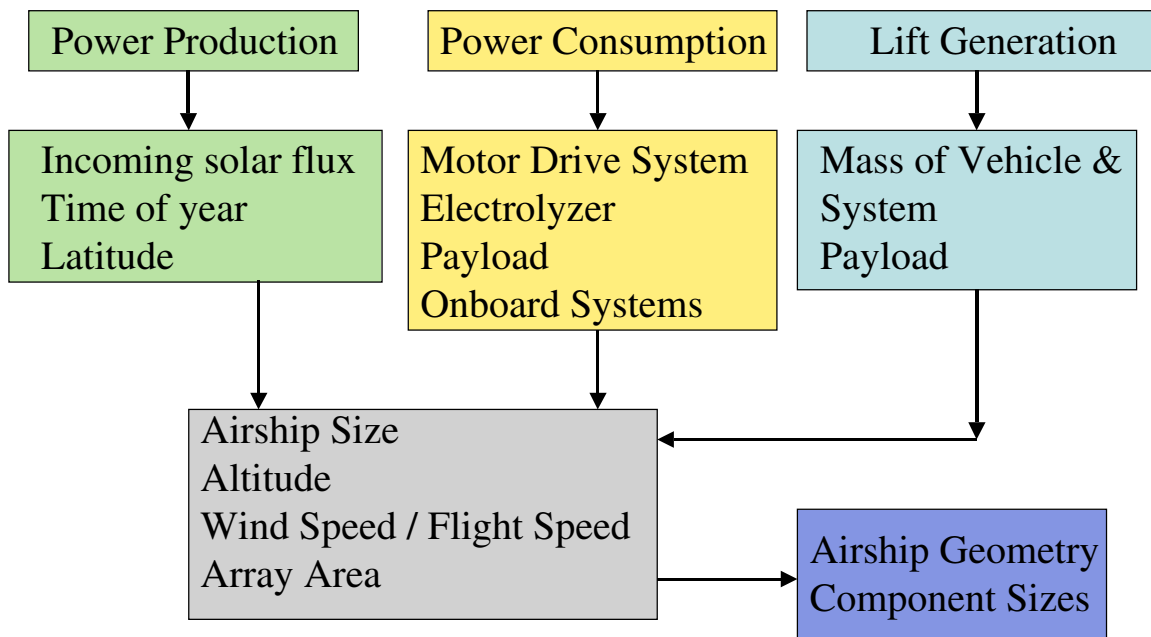


Figure 58 Main Components of the Analysis and Their Dependence

The power production capabilities are based solely on the output of the photovoltaic array. This output and how it is calculated is described in the photovoltaic (PV) array section of this report. Since this output is not constant throughout the day and since there is no photovoltaic power available during the nighttime, energy must be stored for use during the times when there is not sufficient solar power available to operate the airship. To determine the true operating power of the airship, an energy balance must be performed that establishes the continuous useable power for the airship in a given

24-hour period. The energy balance is performed through an iterative process between the energy produced by the solar array and the energy consumed by the airship over the 24-hour period. Integrating the array output power curve yields the total energy supplied by the array, which is the area under the array power curve (A). This is multiplied by the turn around efficiency of the energy storage system (η_{es}) and set equal to the energy consumed by the airship in the 24-hour period (B). By assuming that the operating power level is constant the energy consumed during the day is the area under the line marking the constant power level. The energy balance diagram, which graphically displays this process is shown in figure 59 for a simplified array output power curve. The energy balance relationship, equation 54, is based on the areas shown in figure 59.

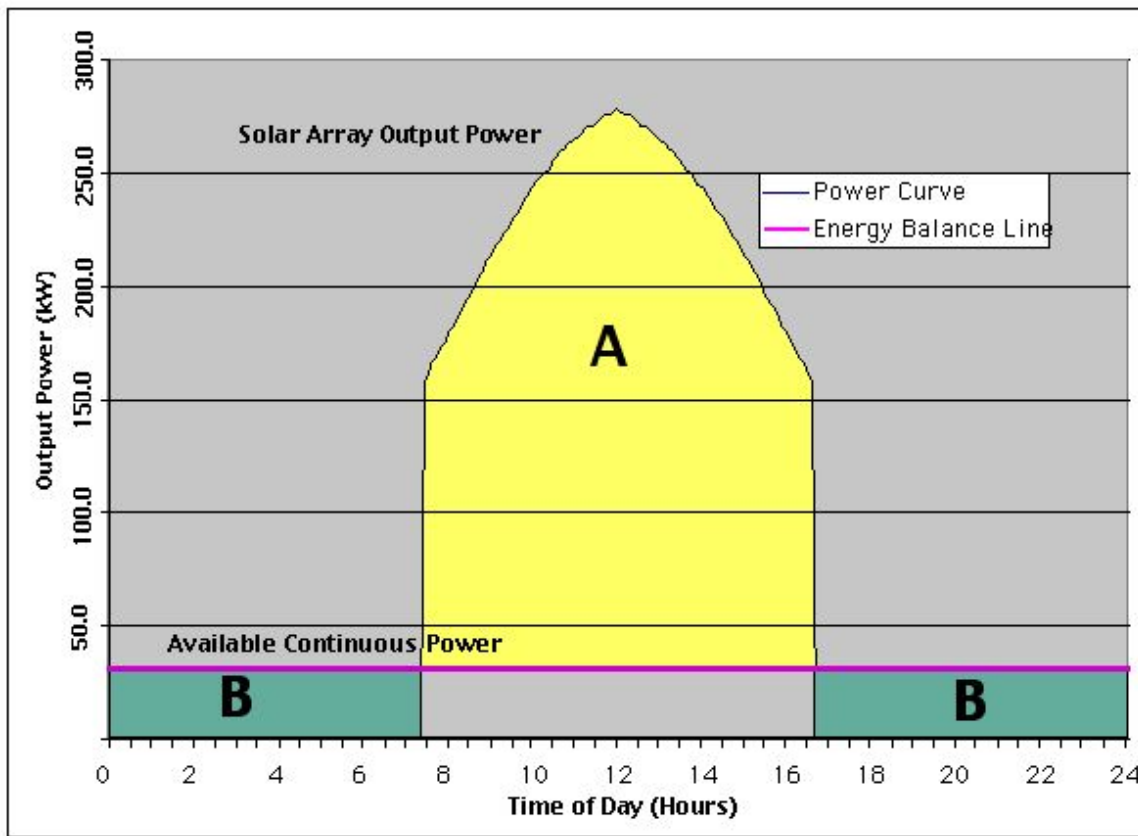


Figure 59 Energy Balance Diagram

$$A\eta_{es} = B \quad [54]$$

It should be noted that the energy balance for this analysis was performed for a given 24-hour period based on the day of operation. This means that the energy storage capabilities were for this specific day using the available solar energy and mean and 99th percentile wind speeds for the various component sizing. An energy balance could also be performed over larger periods of time, weeks or months. This would have the effect of moving energy from time periods where there are low winds or high solar availability to those where there are higher winds or lower solar availability. This increases the reactant storage requirements of the airship but would reduce the necessary

PV array area. The evaluation of extended energy balance periods was beyond the scope of this report that was directed toward an initial feasibility analysis and therefore was not considered. In addition to making an extended energy balance viable, detailed information on the daily estimated variation of wind speeds and direction would be needed. For the actual operation of an airship some amount of extended energy storage will be needed to compensate for times when there are excessive power demands, due mainly to periods of high wind speeds or mission maneuvering requirements.

The energy balance is the first step in determining the feasibility of the airship. With the energy balance completed, the available power is known for a given size airship and solar array at a specific location and time of year. The next step is determining if the size of the airship is sufficient to lift its mass and payload to the desired altitude, and subsequently if the calculated power level is sufficient to overcome the drag on the airship and maintain its position as well as provide power for the airship systems and payload.

The determination of required airship size and available power required is an iterative process. Increasing airship size provides increased lift. However the increased size now requires additional power to operate due to the greater drag profile. To provide the increased power the array area must increase along with all of the power system components. This in turn increases the mass of the airship and the cycle continues. Because of this connection between airship size, lifting capacity and power production, small changes in mass or power consumption can translate into large changes in airship size. This iterative process is illustrated in the diagram shown in figure 60.

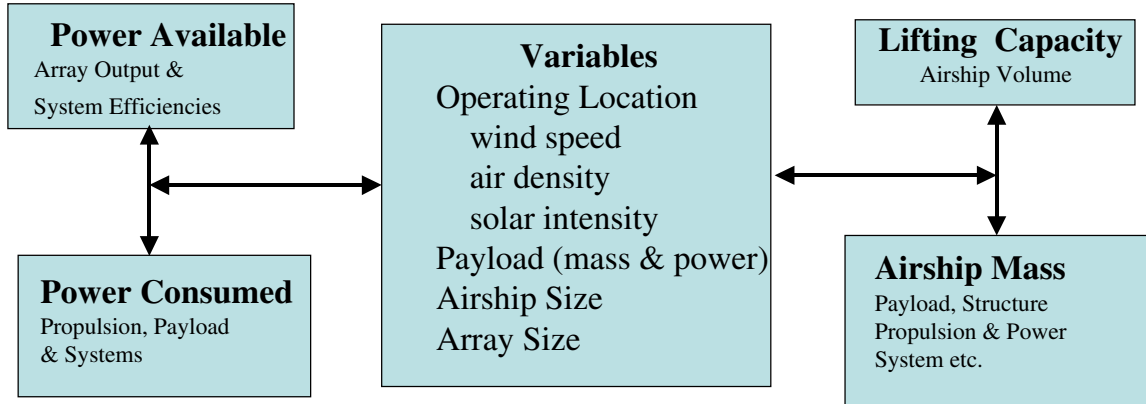


Figure 60 Airship Sizing Process

The power requirements for the airship are broken down into the following items.

- Payload Power
- Communications System Power
- System Operational Power
- Air Compressor Power (if utilized with the fuel cell system)
- Electrolyzer Power
- Propulsion System Power

Of these the first three, payload, communications and system power, are constants and do not vary with airship size. If compressed air is utilized as the oxidizer in the fuel cell system instead of stored oxygen then an air compressor system is needed. The power required by this air compressor system is given by equation 43. The electrolyzer requires power to operate. However since it is part of the energy storage system its power consumption is factored in during the energy balance process through the turn around efficiency of the energy storage system. For this analysis it was estimated that the electrolyzer operated at a 50% efficiency level.

The propulsion system power requirement is the main power draw for the airship. It is based on the efficiencies of the various components that make up the system and the thrust level that is needed to overcome the drag on the airship. From an energy standpoint, the power consumption based on mean wind speed is used to determine the energy requirement over the day period of the propulsion system. Alternatively when sizing the mass of the individual components of the propulsion and power system, maximum power levels are used to insure that the components can meet the maximum power demands. The airship drag (D), given in equation 55, is based on a volumetric drag coefficient (C_{dv}) and the airship volume (V_{as}). For this analysis it was assumed that the airship was to maintain position. Therefore the velocity (V) at which it is operating is the wind speed.

$$D = \frac{1}{2} \rho C_{dv} V^2 V_{as}^{2/3} \quad [55]$$

The drag coefficient is based on the fineness ratio of the airship. The fineness ratio (f) is the ratio of the length (l) of the airship to its diameter (d) or width as given by equation 56. The drag coefficient, given by equation 56, will decrease significantly as the shape moves from a sphere to an elongated cylinder and begins to level off at a fineness ratio of about 4. The equation representing the fineness ratio is valid for fineness ratios up to 10 for a cylindrical shape with hemispherical end [39].

$$f = \frac{l}{d} \quad [56]$$

$$C_{dv} = 0.23175 - 0.15757f + 0.04744f^2 - 7.0412E-3f^3 + 5.1534e-4f^4 - 1.4835e-5f^5 \quad [57]$$

The above equations along with the mean wind velocity are used to calculate the mean airship drag. This drag is what has to be overcome by the thrust from the propeller. The power required to produce this thrust is then calculated by the method outlined in the propeller section of this report.

Now that the power level of each of the power consuming components is known the total power requirement for the airship can be calculated by summing these values. This total mean operating power level is then compared to that calculated through the energy balance. If it is less than or equal to the energy balance power level then there is sufficient power for the airship to operate at the day and latitude for which the energy balance was calculated. The day of the year, in the northern hemisphere, that produces the lowest energy balance value is the winter solstice (December 21st). To determine whether year long operation is possible both the energy balance and wind speeds need to be considered. Sizing the airship for the day of the year that requires the highest energy balance power level will enable the airship to operate year long at that latitude as long as there is sufficient power available on the winter solstice for the airship's operation.

Providing sufficient power is only one part of the iterative process that is needed to determine if a given airship size and configuration is viable for the suggested mission. The other aspect is total vehicle mass and lifting capacity. The lifting capacity has to be sufficient for the airship to maintain the desired altitude. The lift generated by the airship is simply equal to the weight of air that it displaces. This simple principle of buoyancy is the basis of lift for all airships. The lifting force (F_L) generated by the airship is given by equation 58. Obviously the higher the operational altitude the lower the air density and therefore the lower the amount of lift generated for a given size vehicle. Therefore airships will tend to get very large the higher the operational altitude in order to lift the required mass.

$$F_L = \rho V_{ol} g \quad [58]$$

The larger the airship the greater the drag it has to overcome to maintain station over a particular location. This requires a larger power system, which in turn increases the airship size to lift the additional weight of the power system. As with the changes in required power, small changes in airship or payload mass can translate into large changes in airship size. With the lift generated by the airship known, the total airship mass must then be calculated to determine if the lift is sufficient to reach the desired altitude. The total mass of the airship can be broken down into the following items.

- Power System
- Propulsion System
- Lifting Gas
- Airship
 - o Envelope
 - o Fins
 - o Structure

The breakdown of the masses of the power and propulsion system components is detailed in the power and propulsion system section of this report. The masses for the components within these systems are listed, in most cases, as functions of power, and therefore can be scaled with the airship power and thrust requirements. Since there are variations in power requirements depending on the operational conditions, the various components of each of the airship systems will scale to different power levels depending on their operation. Also certain aspects of the component sizing will be based on a particular system power

level. Table 10 lists the different components and the power level that they scale to. The mean power level is based on operation during mean wind speed conditions, the peak power level is based on operation during 99th percentile wind speed conditions and the peak array output power is the maximum power the array puts out during the day.

Table 10 Power Levels to Which the Power/Propulsion System Components Scale

Mean Power Level	Peak Power Level	Peak Array Output Power
Storage Reactants and Storage Tanks	Electric Motor and Drive Train	Electrolyzer System
Small Diameter Propeller	Large Diameter Propeller	
Solar Array (Based On Energy Balance)	Fuel Cell System	

The mass of the lifting gas (M_{lg}) will depend on its molecular weight (MW_{lg}) and pressure. To minimize structural loading on the envelope material there will be little to no pressurization of the lifting gas. It is therefore assumed that the lifting gas will be at atmospheric pressure. The mass of the lifting gas, given in equation 59, can be calculated from the airship volume, the air density and molecular weight (MW_{air}).

$$M_{lg} = \rho \frac{MW_{lg}}{MW_{air}} V_{as} \quad [59]$$

For this analysis the airship mass was broken down into three items: the envelope, fins and remaining structure. The envelope mass is based on the dimensions of the airship, overall length (L_{as}) and radius (r_{as}), and the specific mass of the envelope material (ρ_e). For this application, with a design altitude of 21.5 km, the material specific mass used is 0.225 kg/m².

$$M_e = 2\pi r_{as} L_{as} \rho_e \quad [60]$$

The fin covering uses the same material as the envelope. To determine the mass of the fins the fin area must be known. The fin size is based on the volume of the airship. To determine a relationship between total fin area and airship volume a number of existing airships were used to establish a ratio of fin area to airship volume. The ratio of fin area (R_{fa}) to airship volume used for this analysis was 0.0121 m²/m³. A 20% increase in fin mass was assessed to account for the internal structure of the fins. Based on these assumptions the fin mass (M_f), given in equation 61, can be calculated.

$$M_f = R_{fa} V_{as} \rho_e 1.2 \quad [61]$$

The airship structure is highly dependent on the design and layout of the airship. The overall shape and interior structural design will greatly impact its structural mass. A detailed structural design of the airship was beyond the scope of this feasibility analysis. Therefore, internal structure masses were calculated for a number of existing airships. These were used to get an initial estimate of how to scale the structure of the airship. The internal structure was scaled based upon the total mass of the airship components (M_c) not including the lifting gas and payload. This component mass was a summation of the

power system mass, propulsion system mass, envelope mass and fin mass. It was estimated that the structural mass, given in equation 62, would be 25% of this total component mass.

$$M_s = 0.25M_c \quad [62]$$

Using both the energy balance and lifting capacity and the power required and mass calculations, an airship can be sized to carry out a particular mission. This sizing is an iterative process in which the main variables are airship length (for a specified fineness ratio) and array area. These variables can be adjusted until a configuration is achieved that meets the energy balance and lift requirements.

The objective of the analysis outlined above was to evaluate the feasibility of providing continuous surveillance along the East and West coasts of the United States. The latitude range that was considered was 28° N to 44° N along the East Coast and 35° N to 48° N along the West coast. There were two main approaches to the analysis. The first was to determine the payload capacity of various size airships over the total latitude range for the East and West coasts at different times of the year. The second was to select a baseline airship size and determine what its capabilities and flight range would be along each coast. The airship size selected was not to exceed the largest airships that have previously been constructed.

Results

The analysis method outlined in the previous section and the power, propulsion and airship models described previously were used to generate sizing results for various airship mission parameters and goals. An initial series of results were produced that provided payload capacity for various size airships at different times of the year along both the East and West coast. These results are used as a general means of determining the required size of an airship to carry a particular amount of payload at a given location and time of year. From these it can be determined whether a specific mission or capability is feasible and what size airship would be required to achieve the mission.

The lifting capacity results are given in figures 61 through 64 for the East coast and figures 65 through 68 for the West coast. The graphs are for different seasons, (Spring, Summer, Autumn and Winter). The results were generated seasonally since the available wind data was defined seasonally. The specific dates for each of the seasonal results were March 21st (vernal equinox) for spring, June 21st (summer solstice) for Summer, September 21st (autumnal equinox) for Autumn and December 21st (winter solstice) for winter. These dates represent the extremes in the solar cycle throughout the year. These results combine the effect of the seasonal winds and variation in solar intensity over the complete latitude range along the east and west coasts.

In addition to the lifting capacity, the flight duration and latitude range of a given size airship can also be determined from these figures. For example, along the East coast a 185 m long airship with a payload capacity of 4000 kg could not fly between 41° and 43° in the spring, could fly over the complete latitude range in the summer, could not fly

at latitudes greater than 40° in the autumn and could not fly in the winter months at any latitude.

For these results helium was used as the lifting gas and a continuous payload power consumption of 10 kw was assumed. The airship was assumed to be positioned in an East – West direction at an altitude of 21.5 km (70.5 kft). Airship lifting capacity up to 10,000 kg was examined. A fineness ratio of 4 was used for all airship lengths examined. The relationship between fineness ratio and the airship volume can be calculated by equation 63. This relation is graphed in figure 69 for a fineness ratio of 4.

$$V_{as} = \pi L^3 \left(\frac{1}{4f^2} + \frac{4}{24f^3} \right) \quad [63]$$

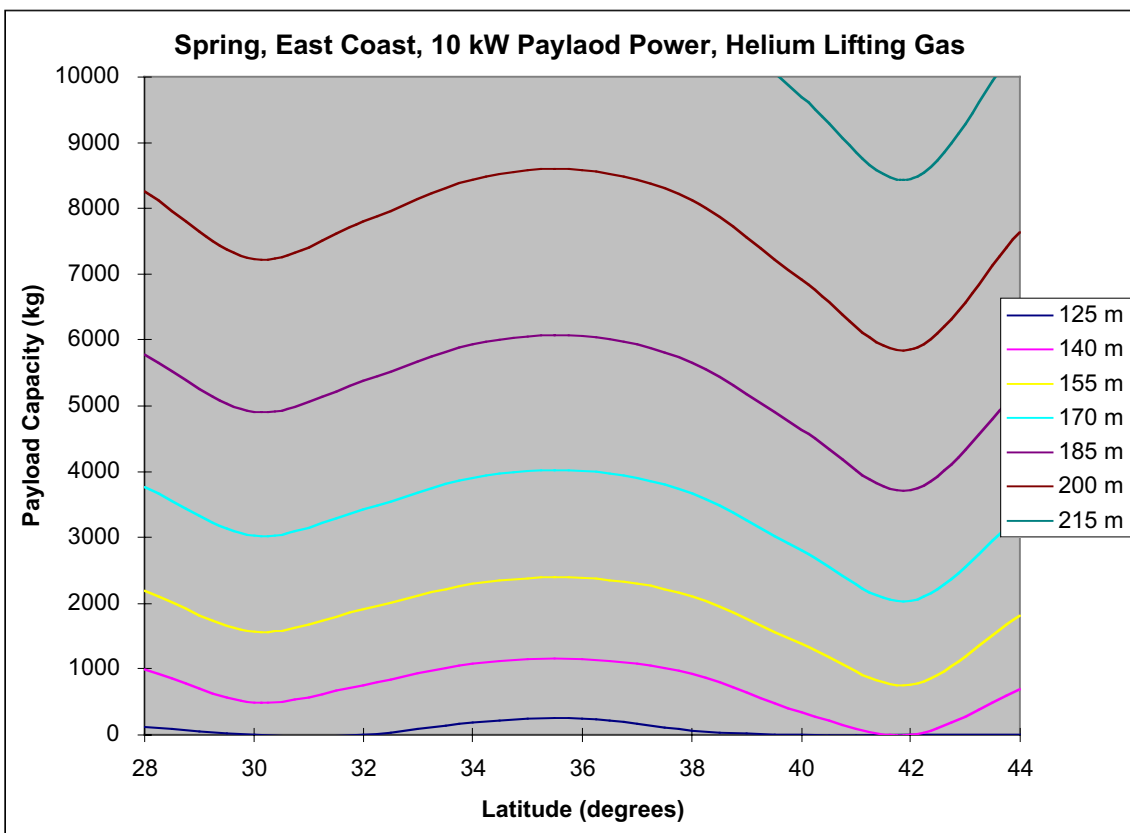


Figure 61 East Coast, Spring, Payload vs Latitude for Various Airship Lengths

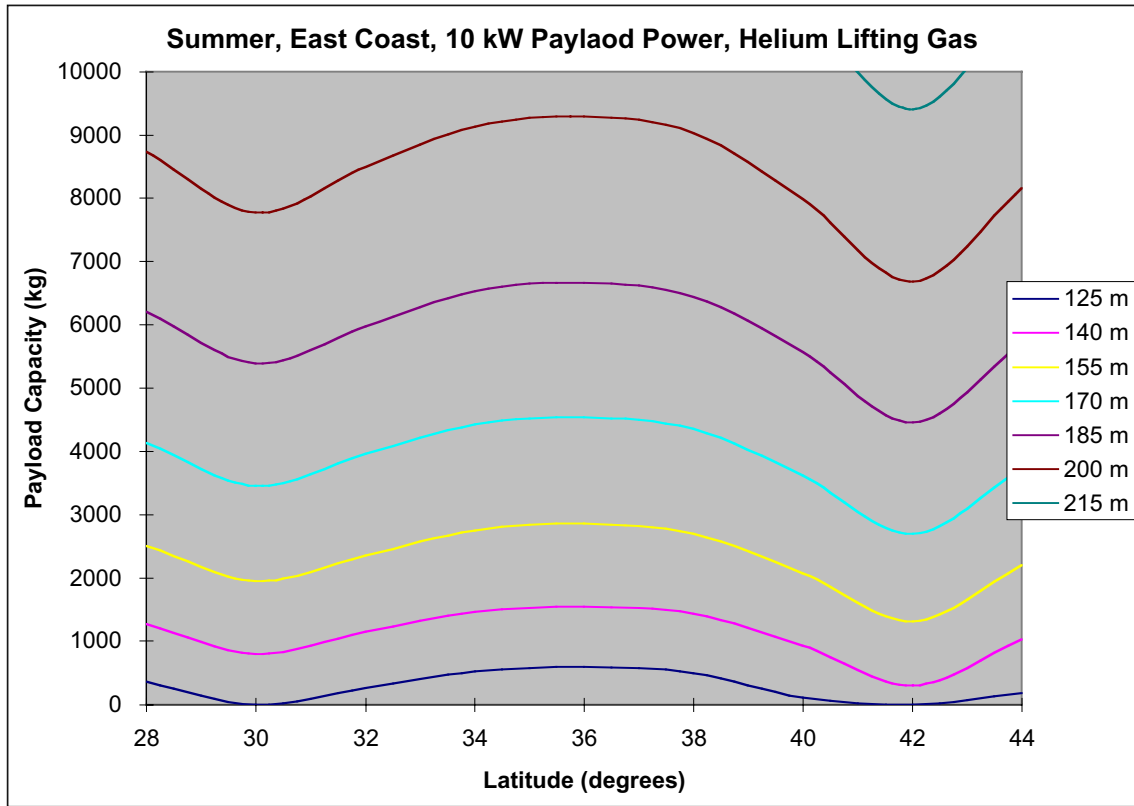


Figure 62 East Coast, Summer, Payload vs Latitude for Various Airship Lengths

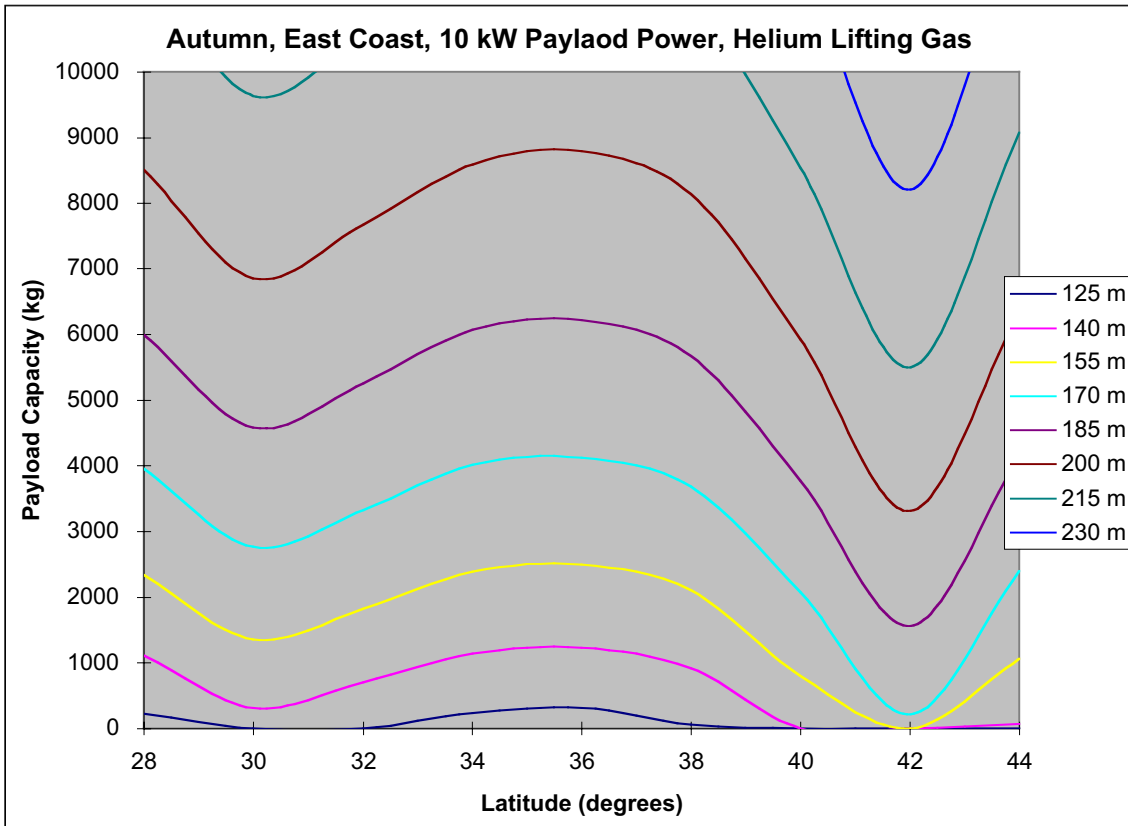


Figure 63 East Coast, Autumn, Payload vs Latitude for Various Airship Lengths

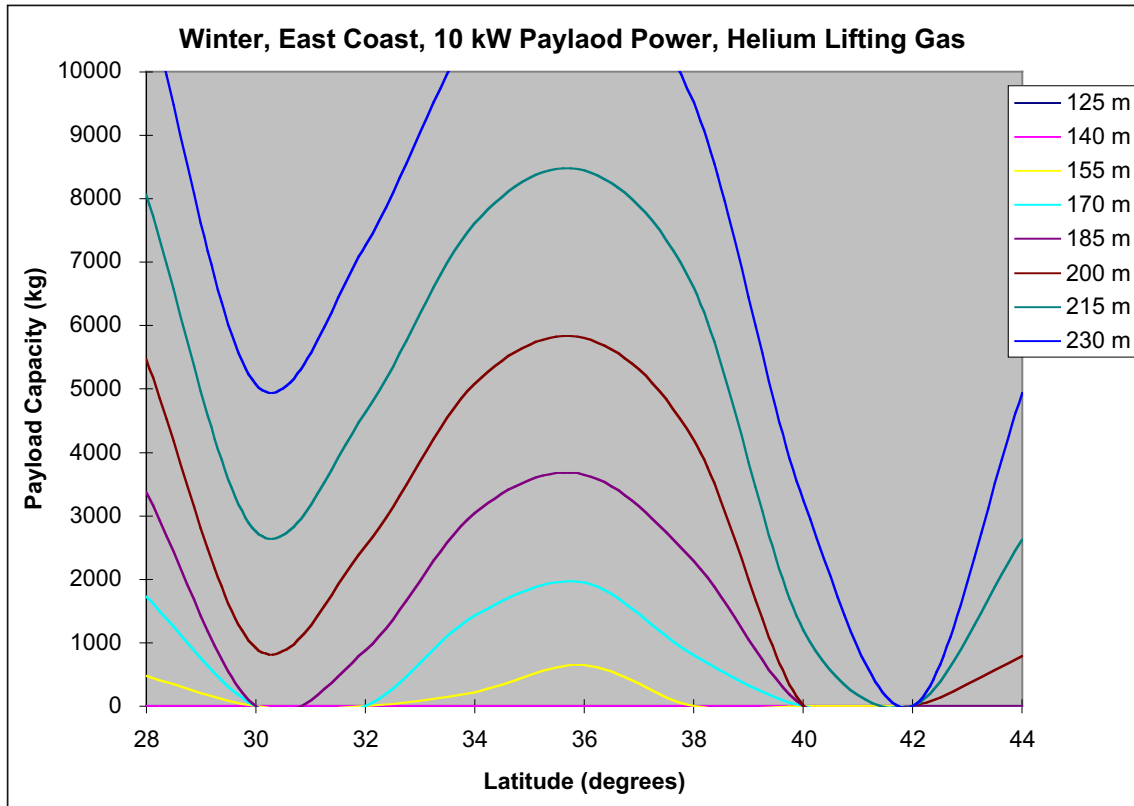


Figure 64 East Coast, Winter, Payload vs Latitude for Various Airship Lengths

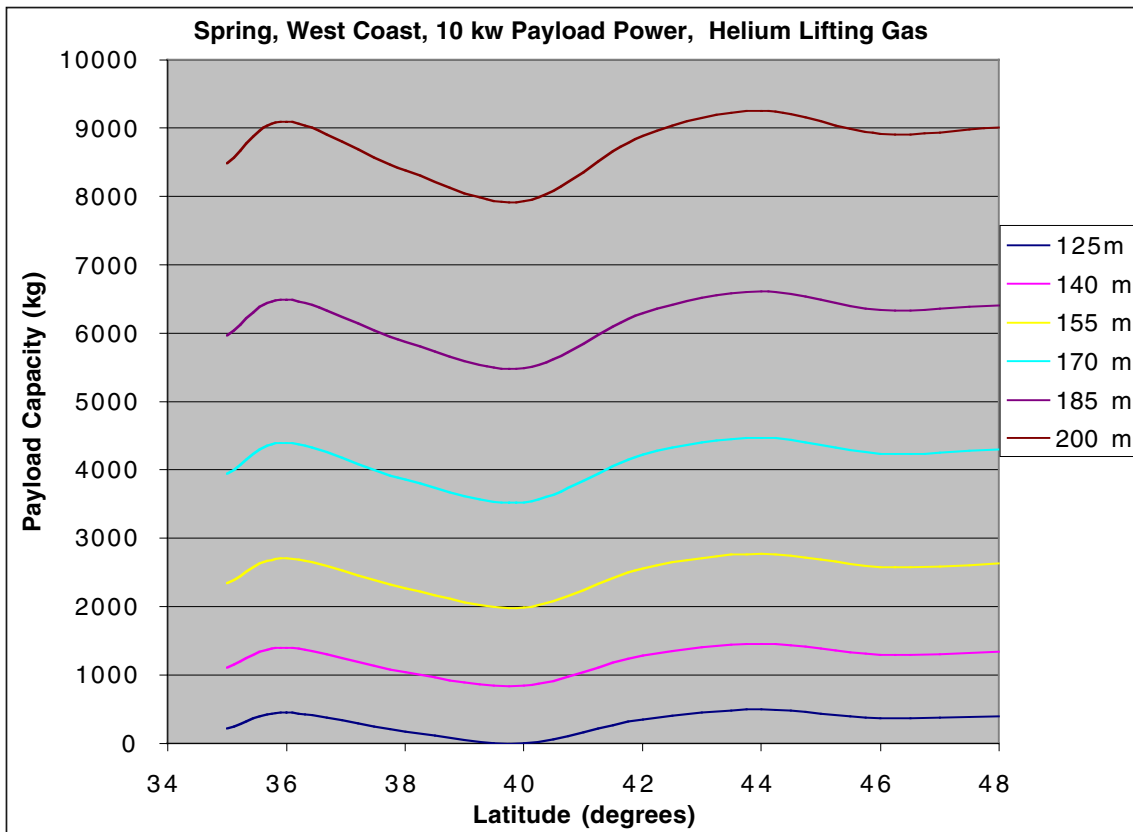


Figure 65 West Coast, Spring, Payload vs Latitude for Various Airship Lengths

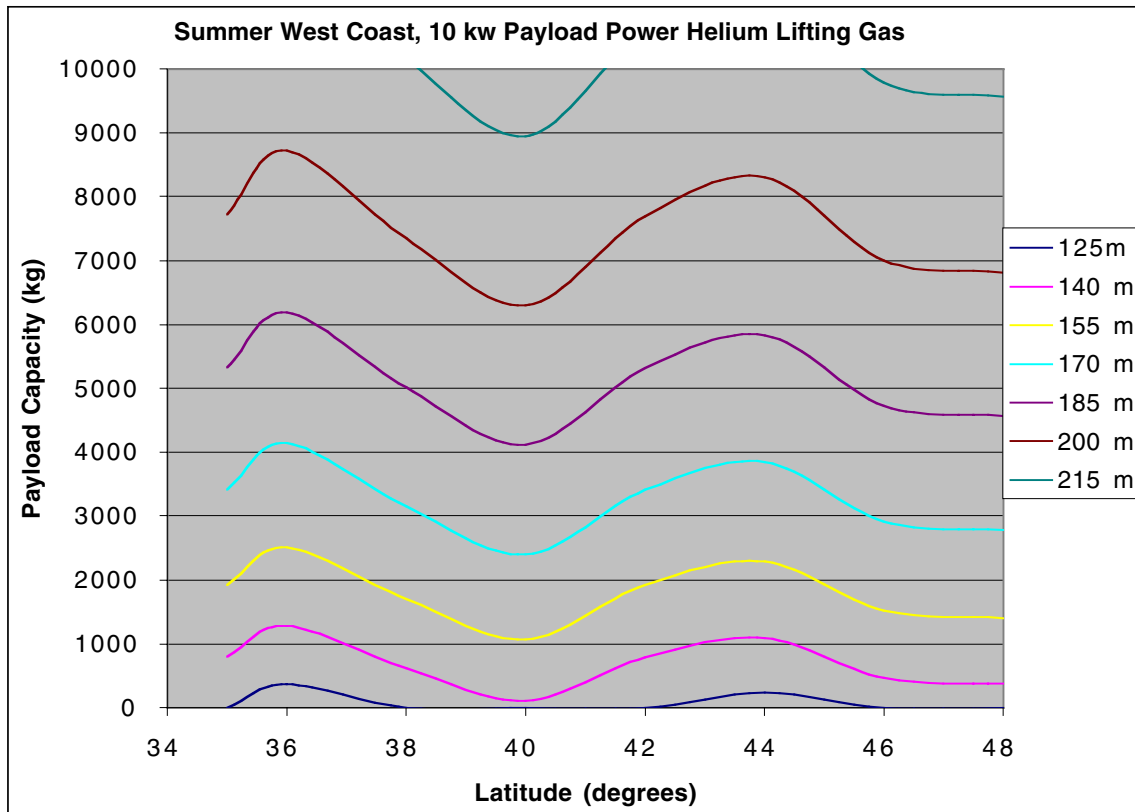


Figure 66 West Coast, Summer, Payload vs Latitude for Various Airship Lengths

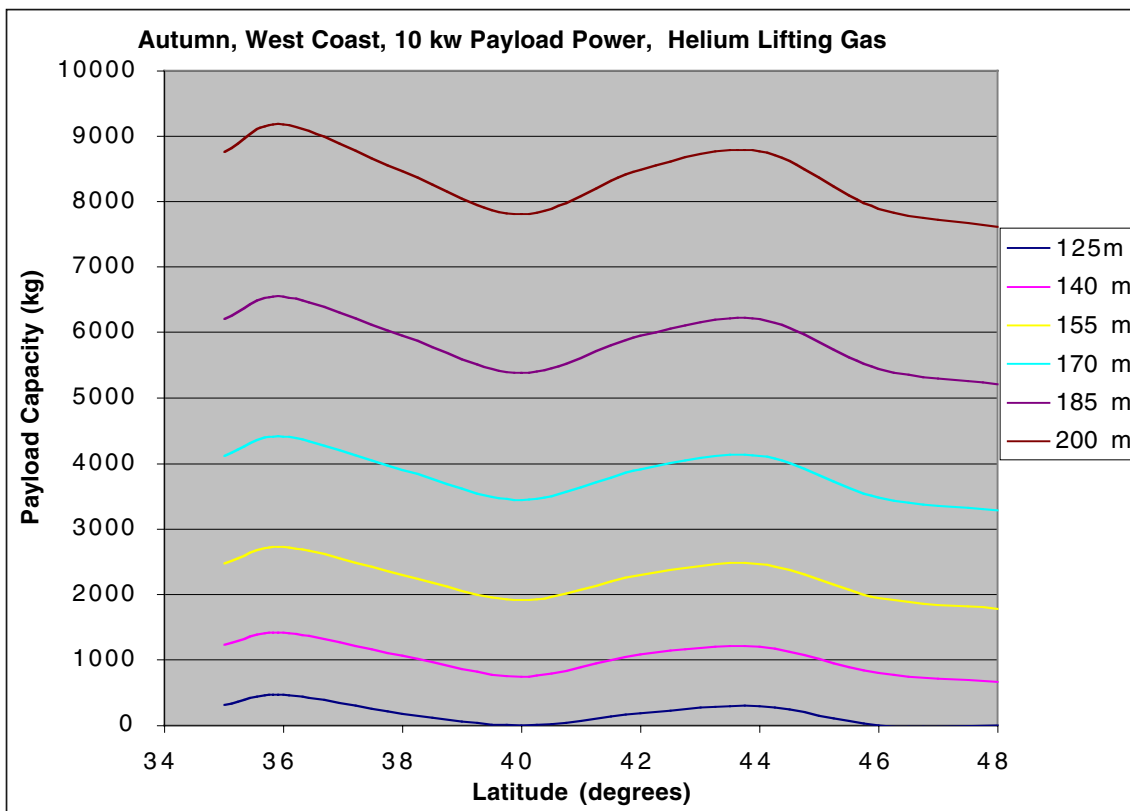


Figure 67 West Coast, Autumn, Payload vs Latitude for Various Airship Lengths

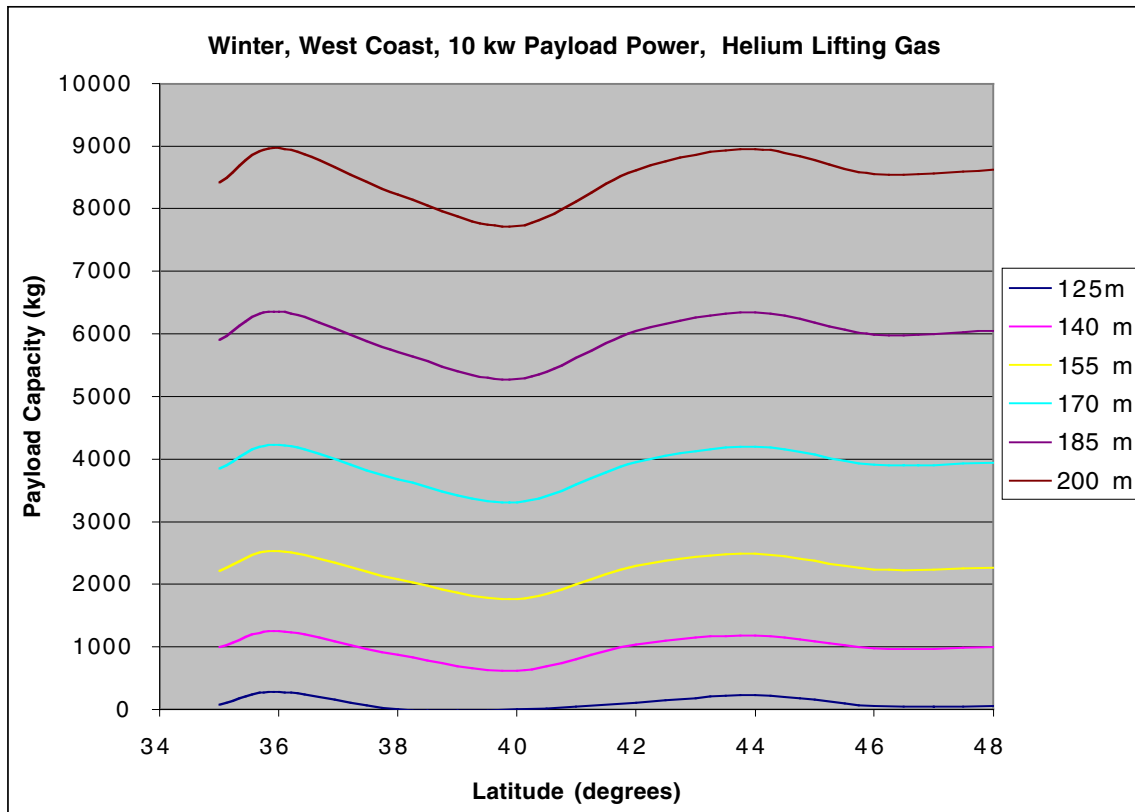


Figure 68 West Coast, Winter, Payload vs Latitude for Various Airship Lengths

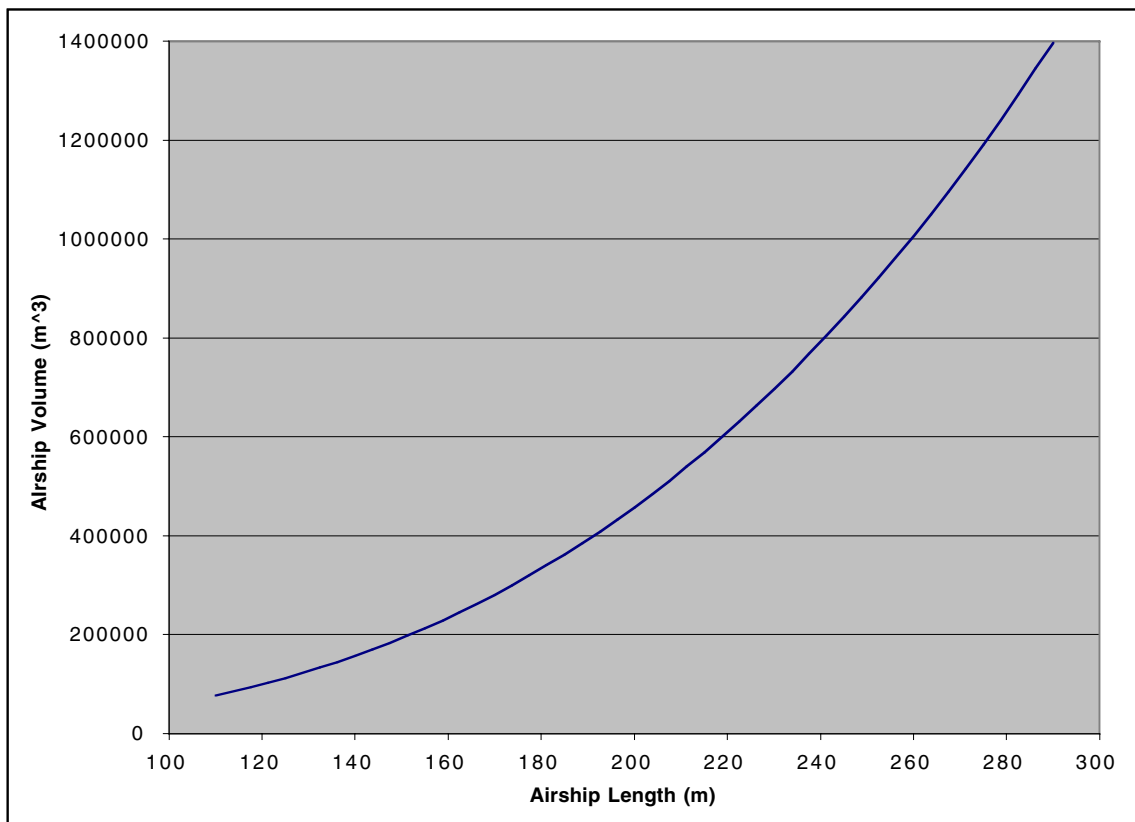


Figure 69 Airship Length vs Volume for a Fineness Ratio of 4

By comparing the payload capacity figures given above and the altitude wind speed plots, shown in figures 18 through 21, it can be seen that wind speed is a major factor influencing the airships capabilities. This is especially true along the East coast where the winter wind speeds are fairly high. At the 42° North latitude point, these high wind speeds in conjunction with the winter time low sun angles and short day lengths produce conditions in which none of the airship sizes examined would operate. Therefore, based upon the sizes of airships examined, it would not be possible to construct an airship for continuous operation at or near the 42° North latitude point along the East coast.

The West coast wind environment is much calmer then that of the East coast. For the most part, the payload capacity of the airship remains fairly constant throughout the year and over the latitude range examined. The summer period along the west coast has the highest wind speeds and produces the largest variation in lifting capacity with latitude. Because this time of high wind speeds occurs in the summer, its effect on the airship is somewhat compensated for by the high sun angles and long day times.

In addition to the lifting capacity, the mean and maximum power consumption for each size airship is also plotted. The mean power levels are plotted for the same latitude range as the payload capacity in figures 70 through 73 for the East coast and figures 74 through 77 for the west coast.

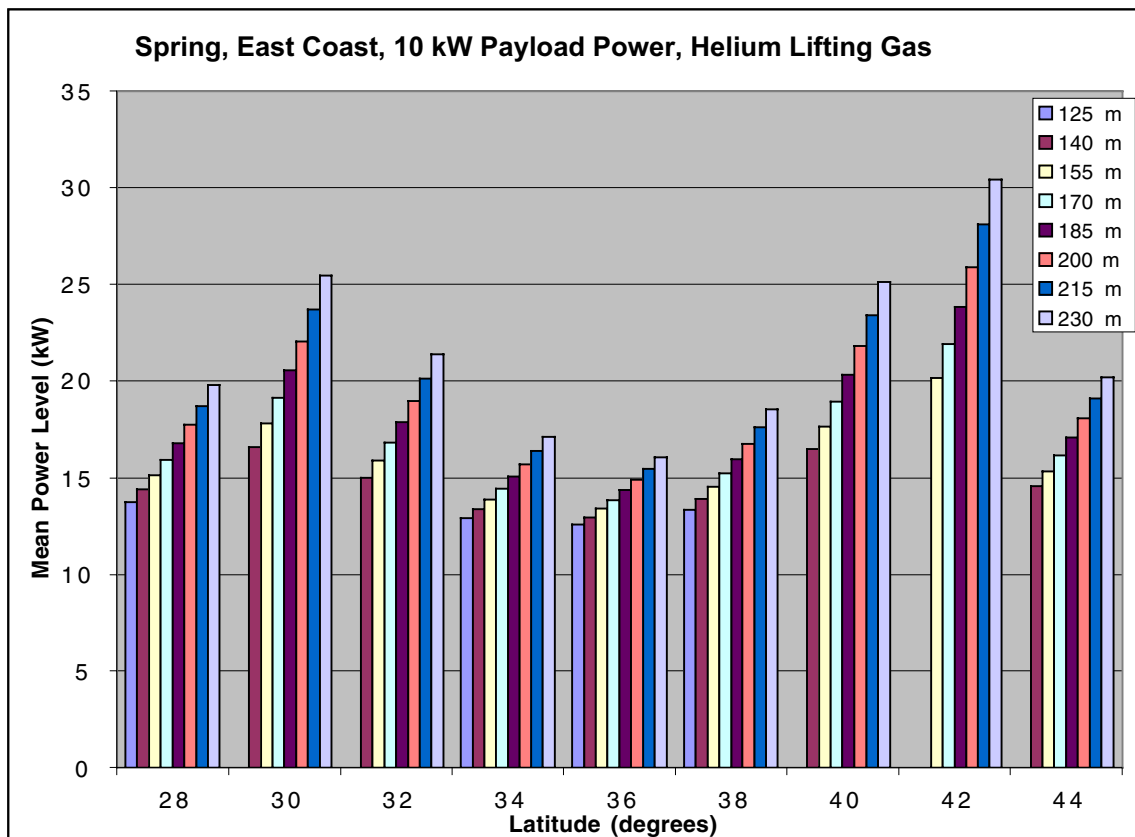


Figure 70 East Coast, Spring Mean Power Level for Various Airship Lengths

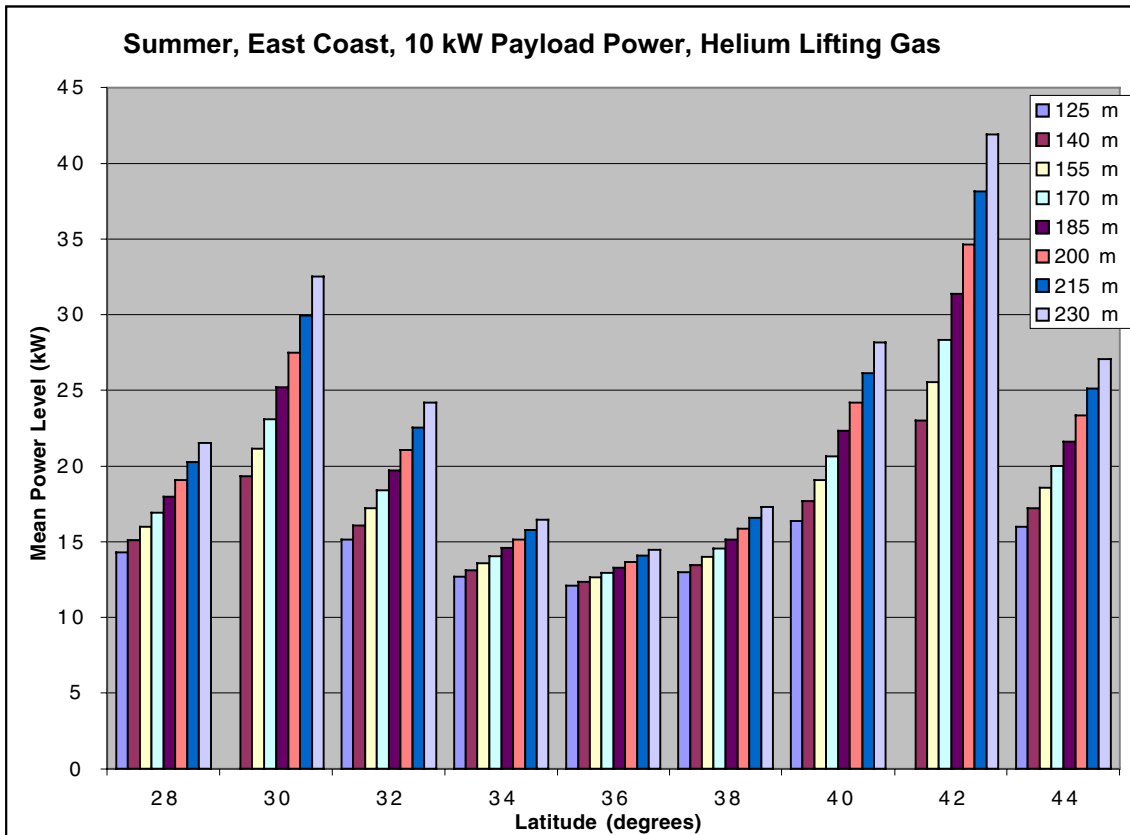


Figure 71 East Coast, Summer Mean Power Level for Various Airship Lengths

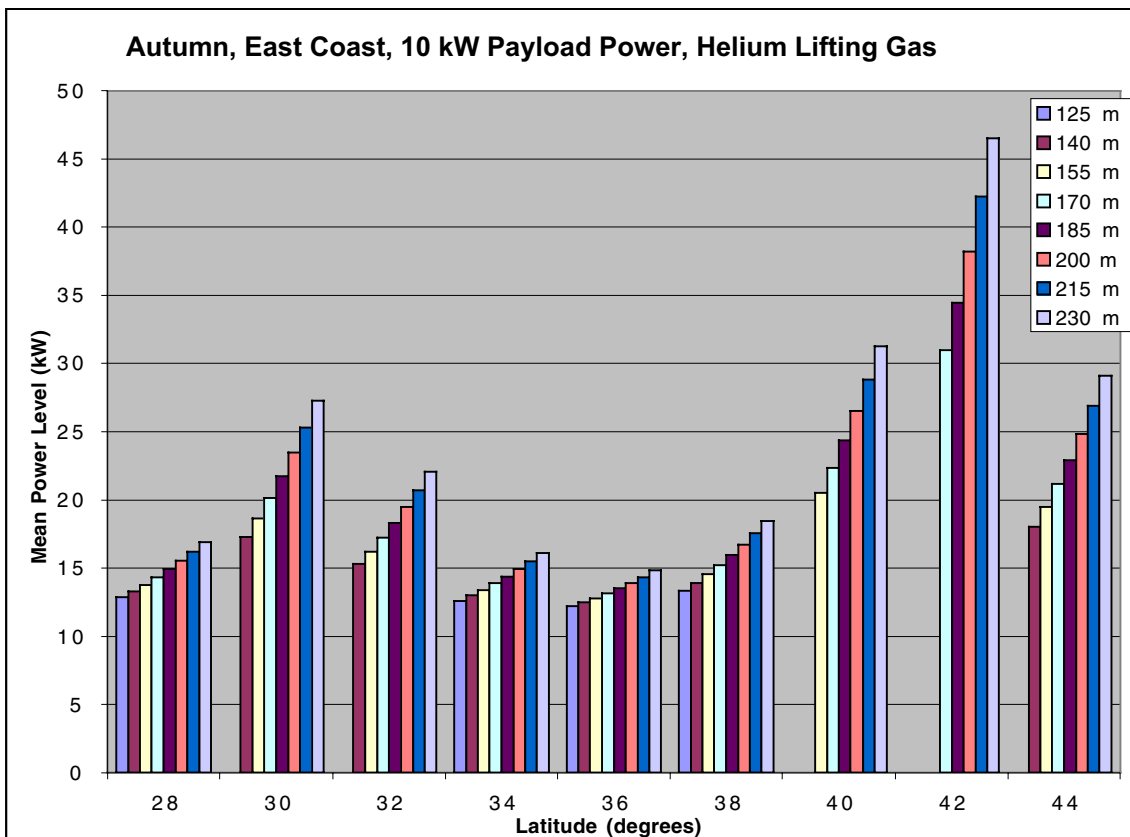


Figure 72 East Coast, Autumn Mean Power Level for Various Airship Lengths

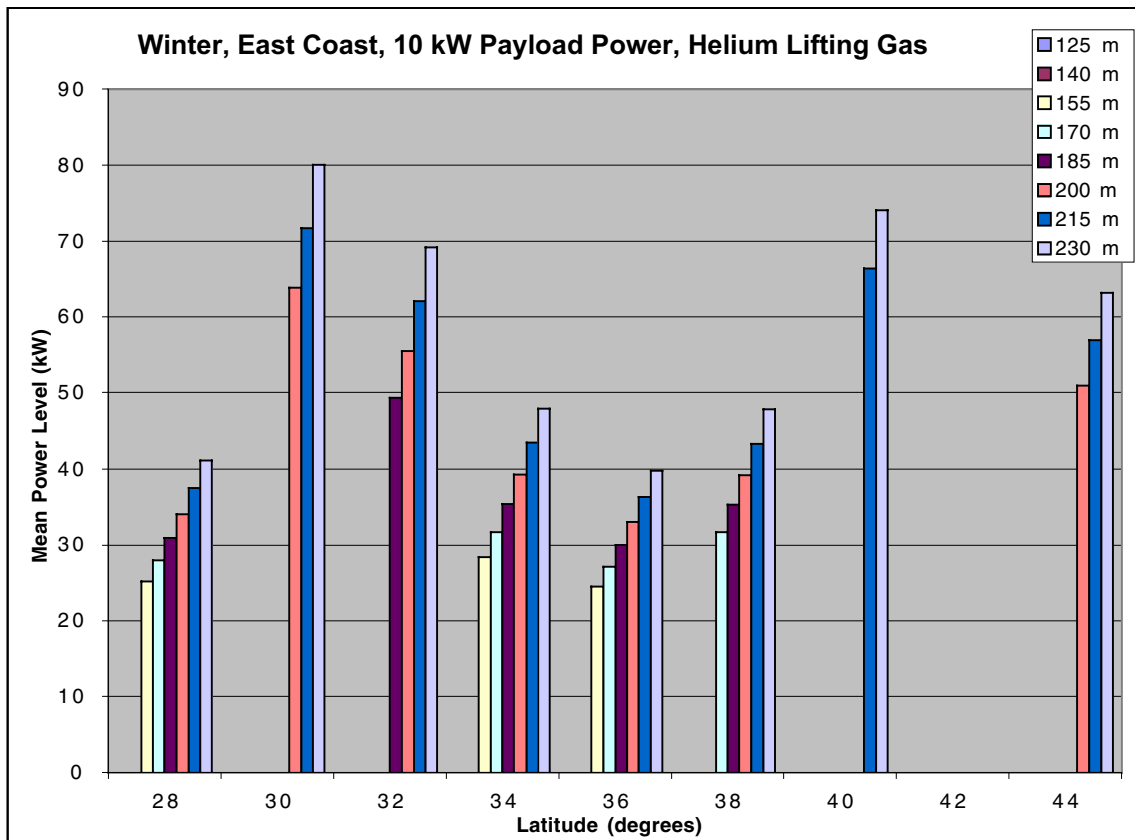


Figure 73 East Coast, Winter Mean Power Level for Various Airship Lengths

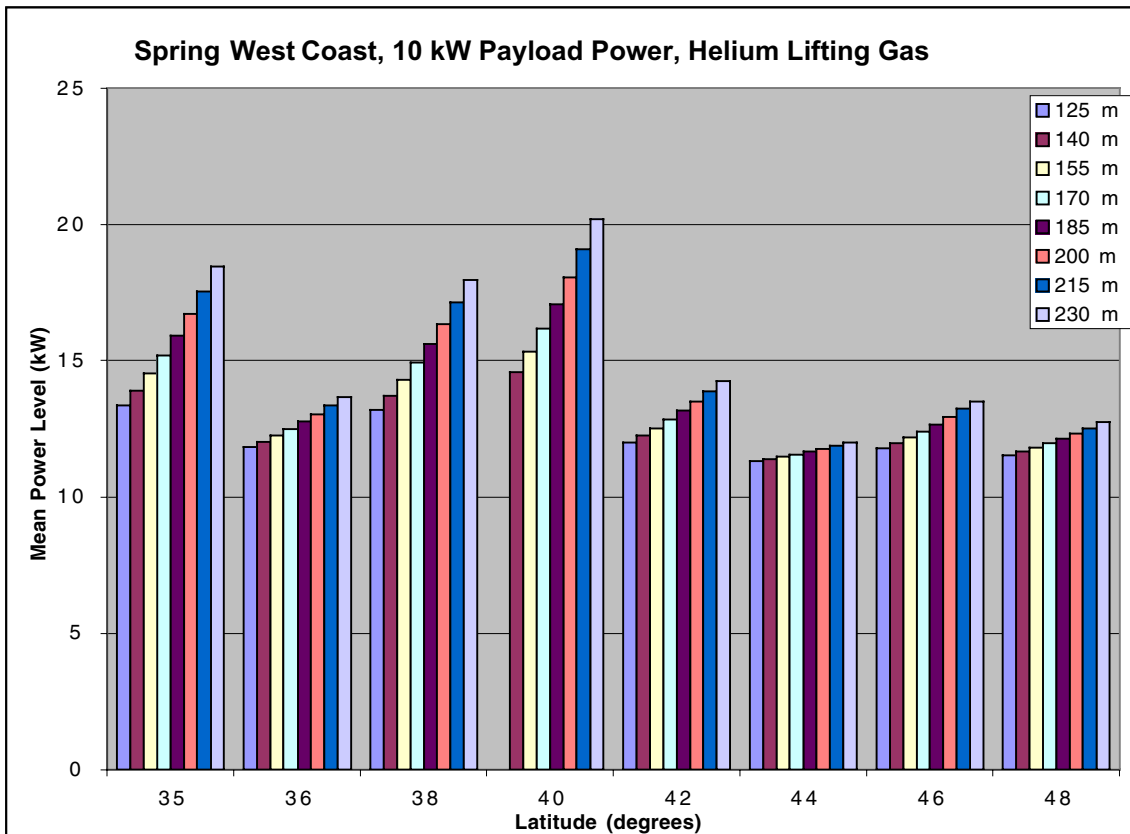


Figure 74 West Coast, Spring Mean Power Level for Various Airship Lengths

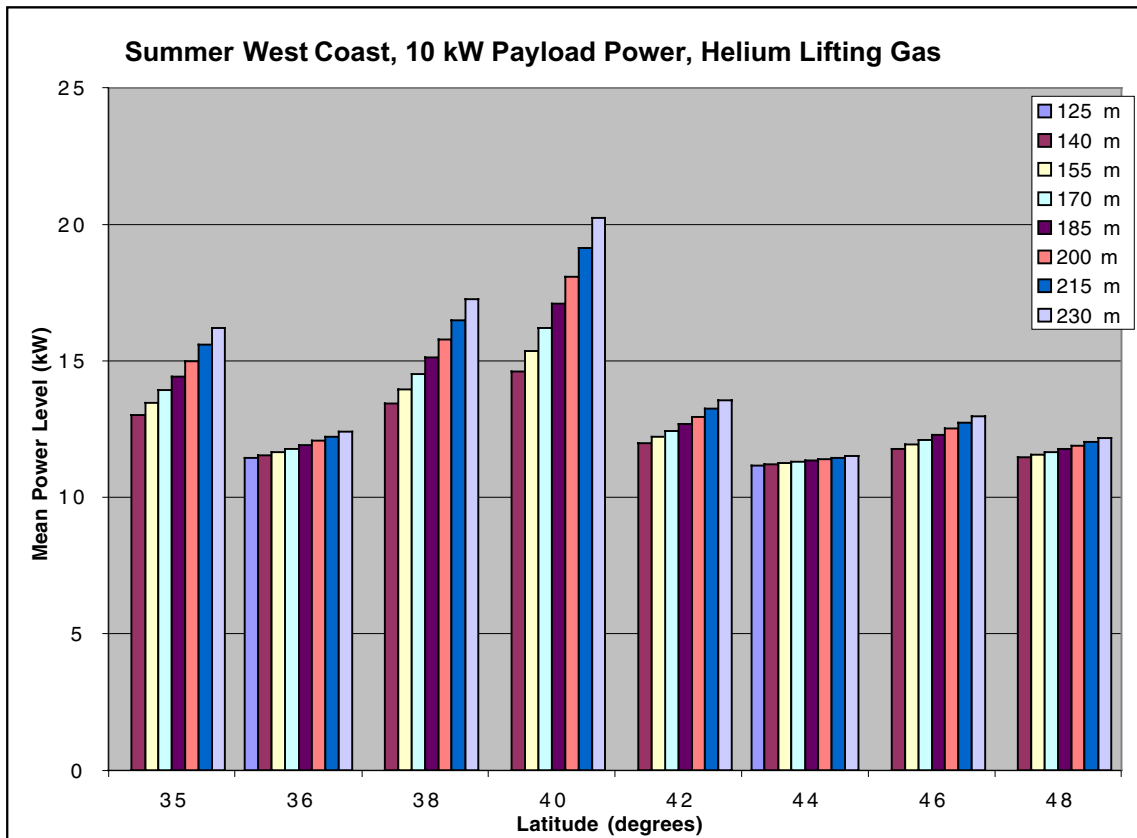


Figure 75 West Coast, Summer Mean Power Level for Various Airship Lengths

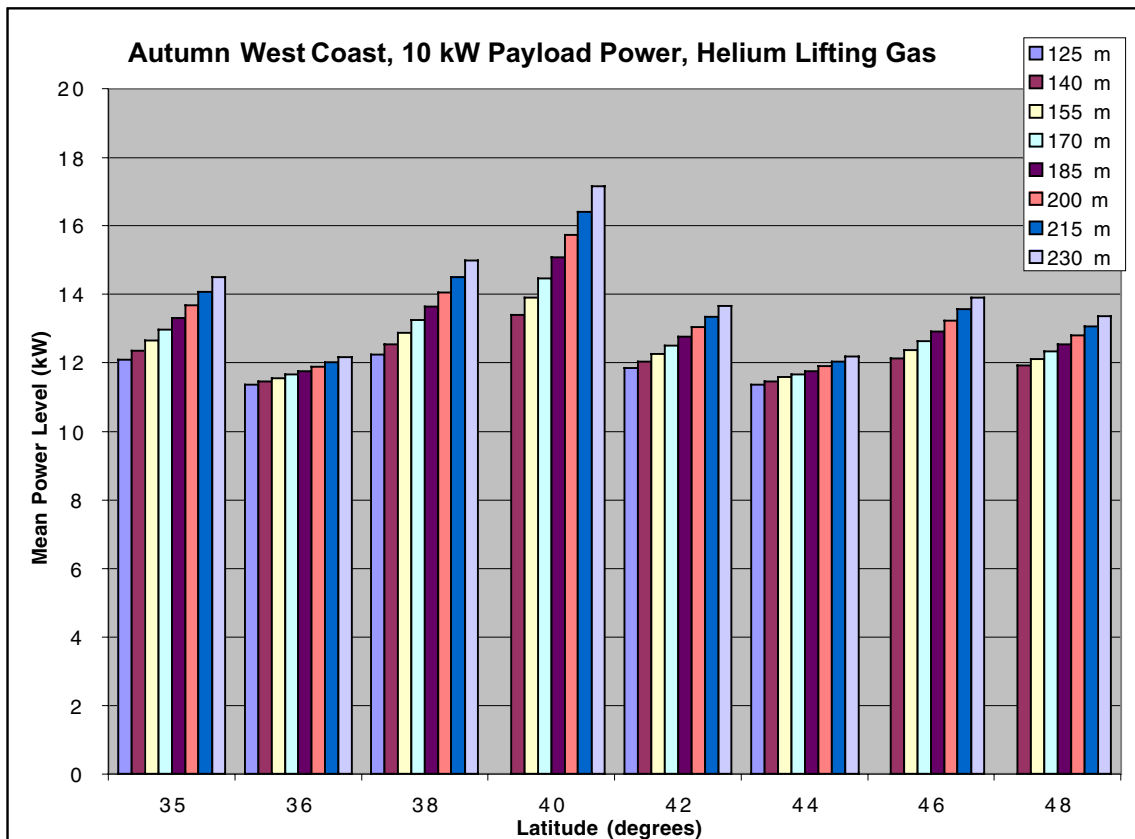


Figure 76 West Coast, Autumn Mean Power Level for Various Airship Lengths

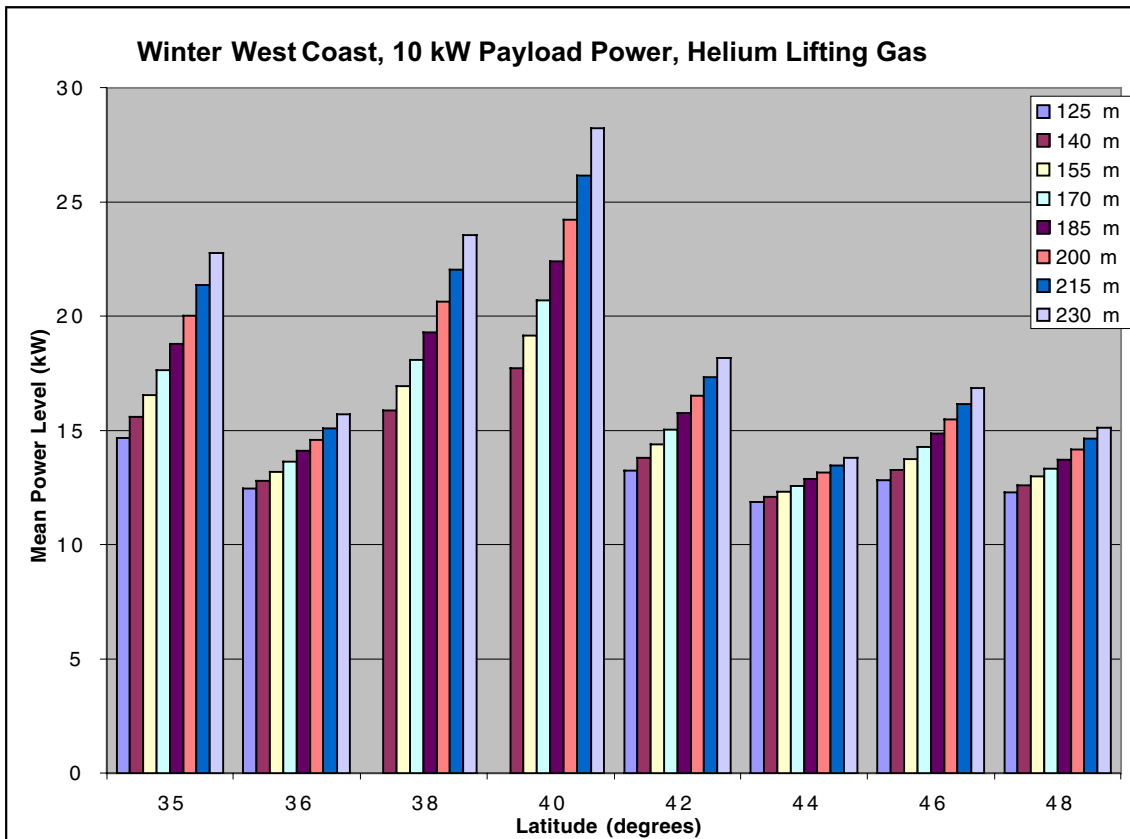


Figure 77 West Coast, Winter Mean Power Level for Various Airship Lengths

The mean power levels shown in the above figures are based on the total mean power requirement of the airship. This includes propulsion, payload and system power. These values will vary based on the airship drag which in turn is based on the mean wind speed at the given location and time of year. From these figures it can be seen that the mean power level for west coast operation, with a given size airship, is generally lower than that for east coast operation. This is due to the higher mean wind speeds which occur along the East coast. The highest mean power levels occur along the East coast during the winter. The highest West coast mean power levels also occur during the winter but these are significantly less than those for the East coast. The relatively low mean wind speeds along the West coast allow for reduced energy storage and collection requirements that translate into smaller airship sizes for a given payload.

The mean power levels are only half of the picture in terms of power for the airship. The maximum power levels are also very important. Whereas the mean power levels are used to size energy storage and collection requirements, the maximum power level is used to size the power producing and thrust generating components of the airship. The maximum power level for East coast operation is plotted in figures 78 through 81 for West coast operation in figures 82 through 85.

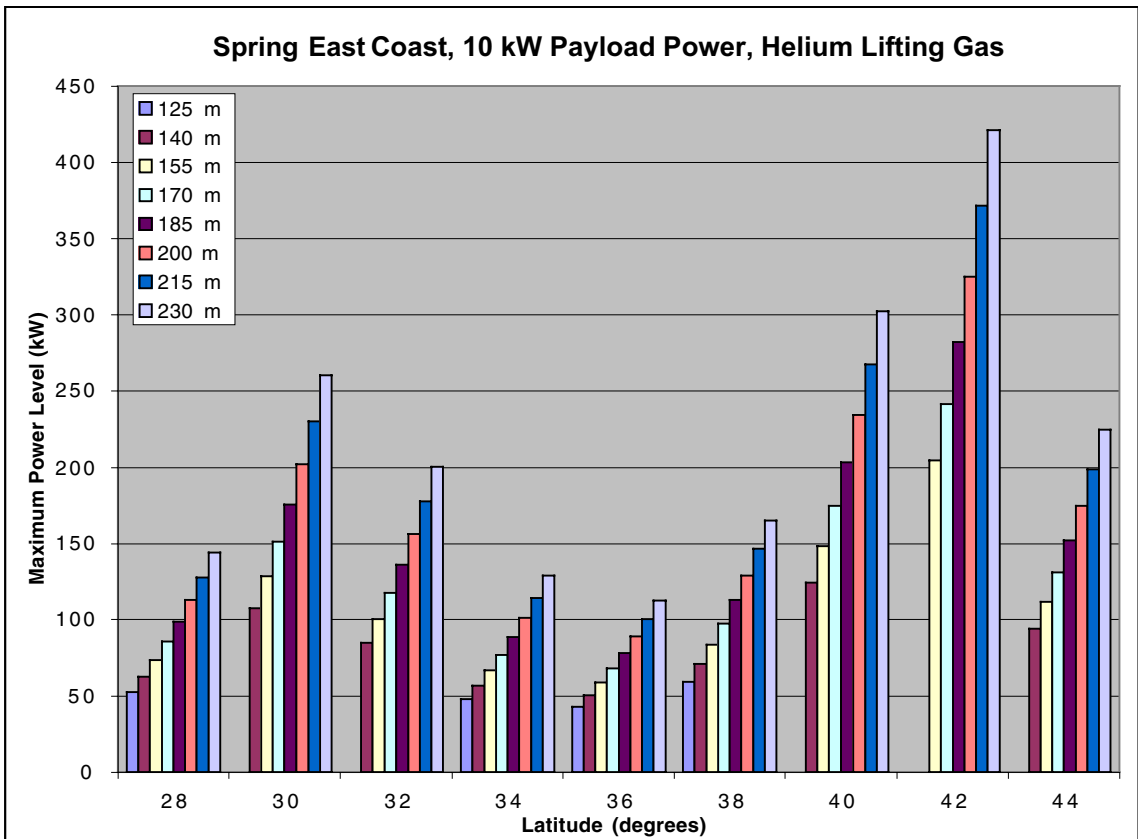


Figure 78 East Coast, Spring Maximum Power Level for Various Airship Lengths

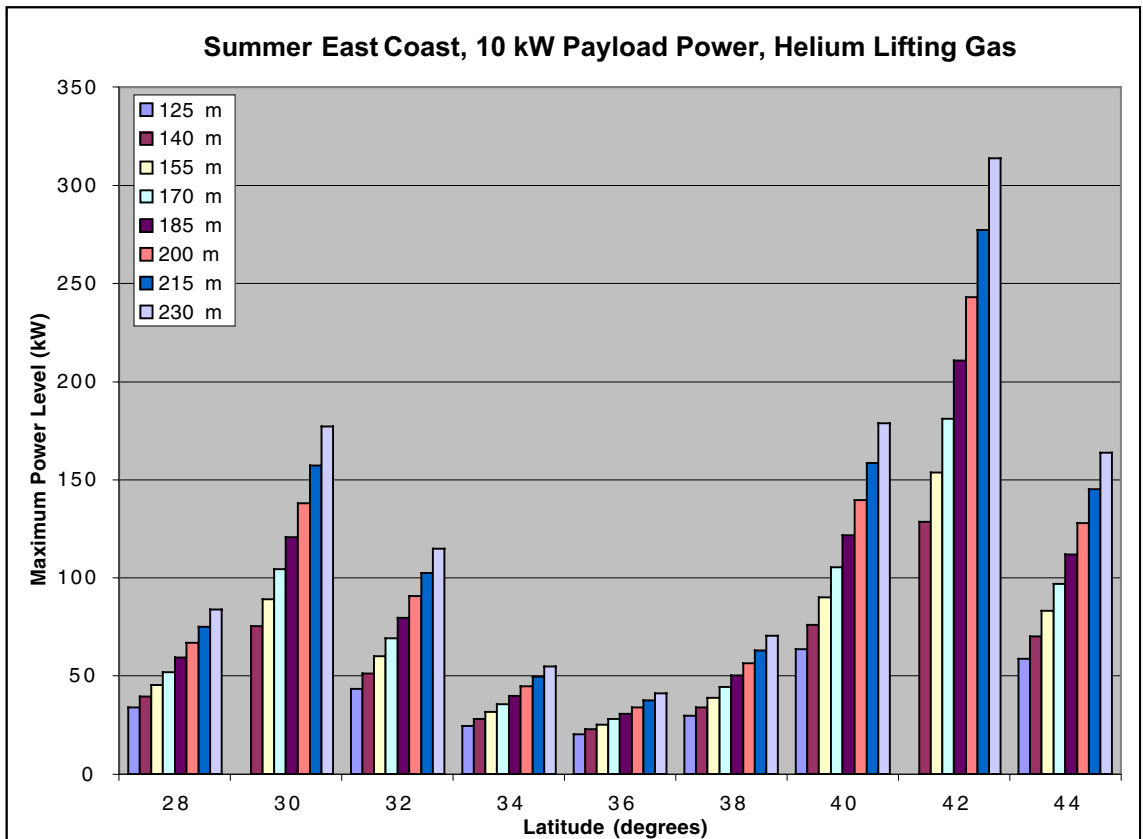


Figure 79 East Coast, Summer Maximum Power Level for Various Airship Lengths

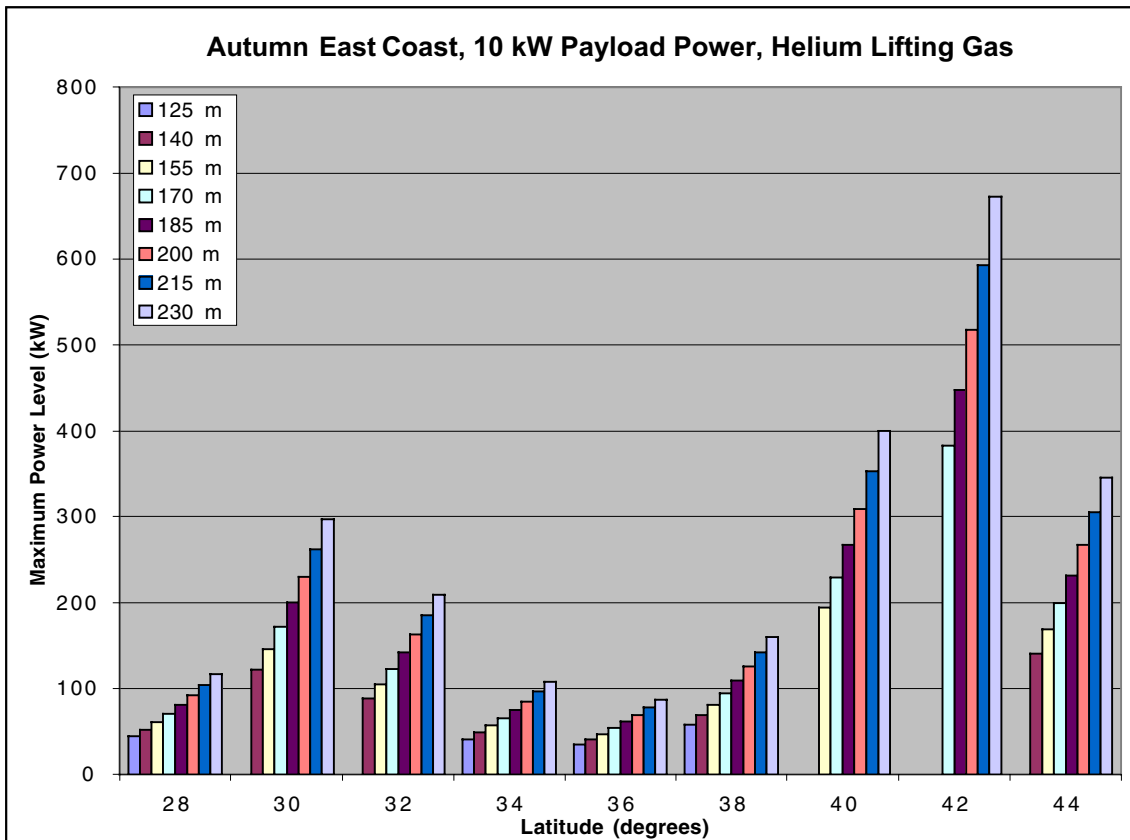


Figure 80 East Coast, Autumn Maximum Power Level for Various Airship Lengths

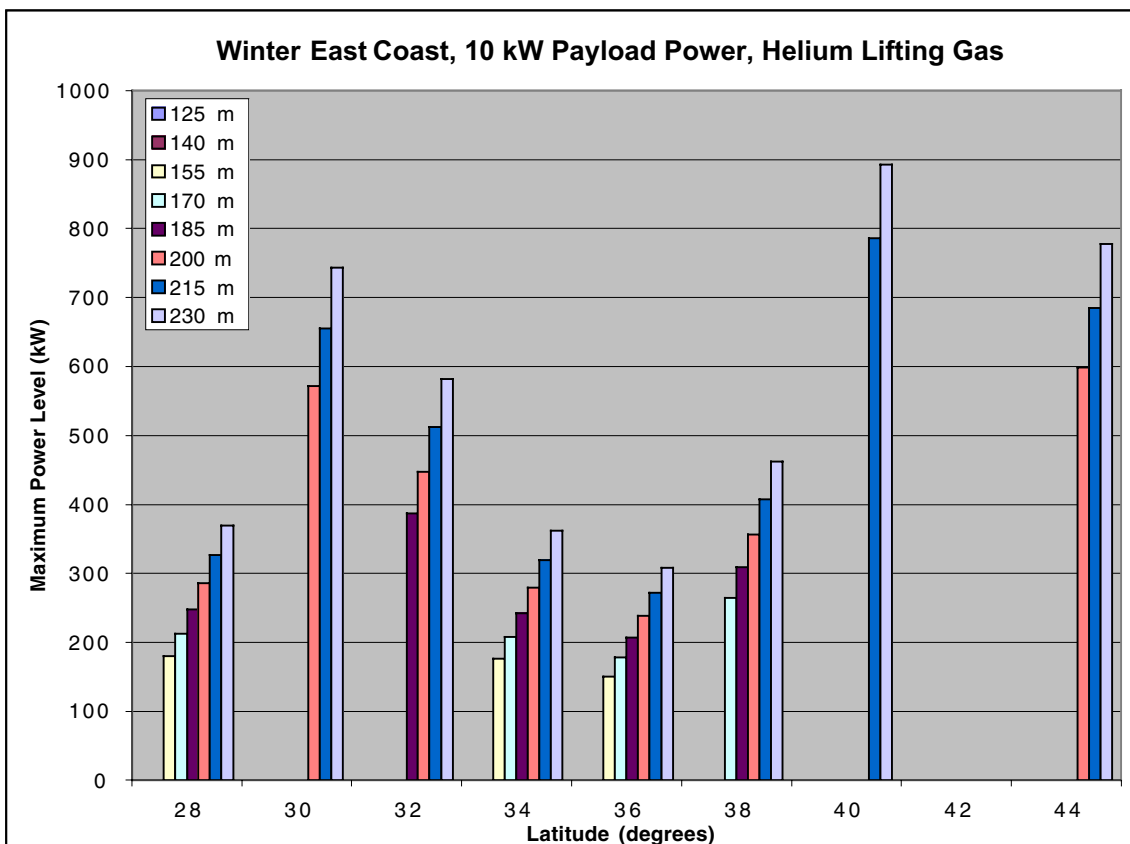


Figure 81 East Coast, Winter Maximum Power Level for Various Airship Lengths

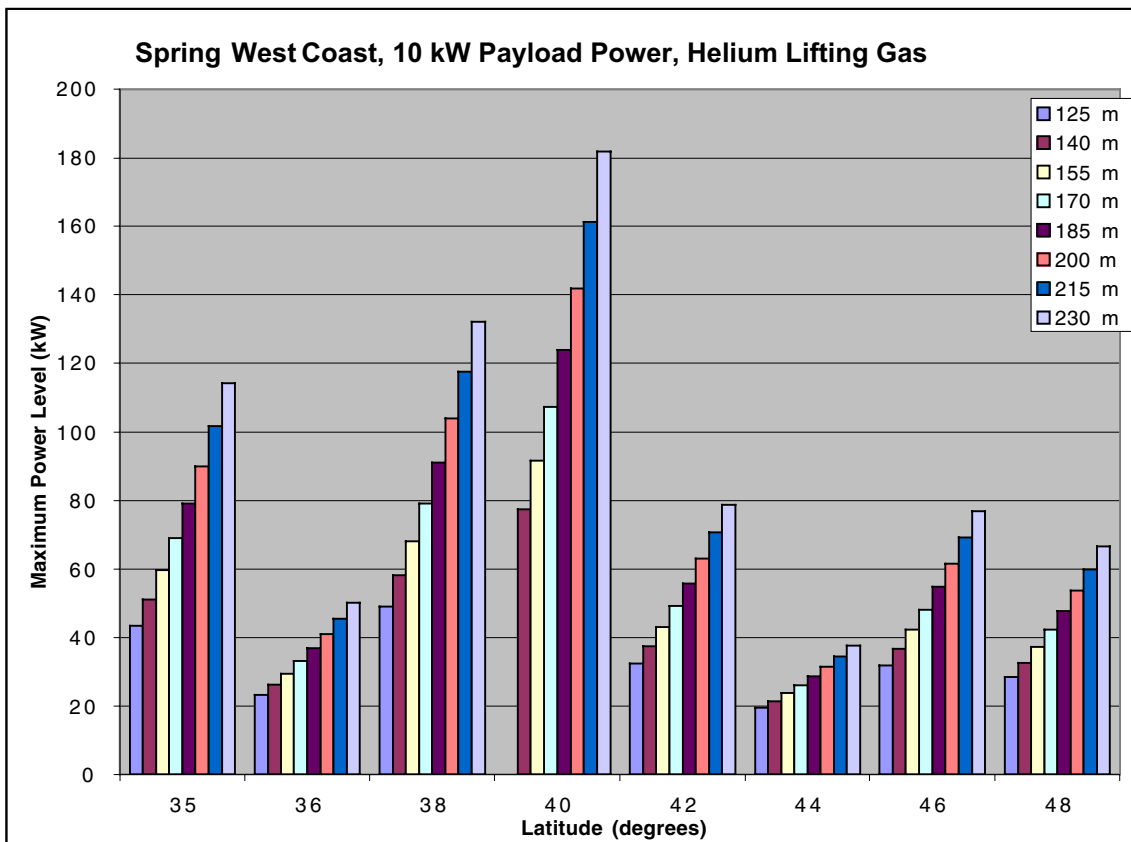


Figure 82 West Coast, Spring Maximum Power Level for Various Airship Lengths

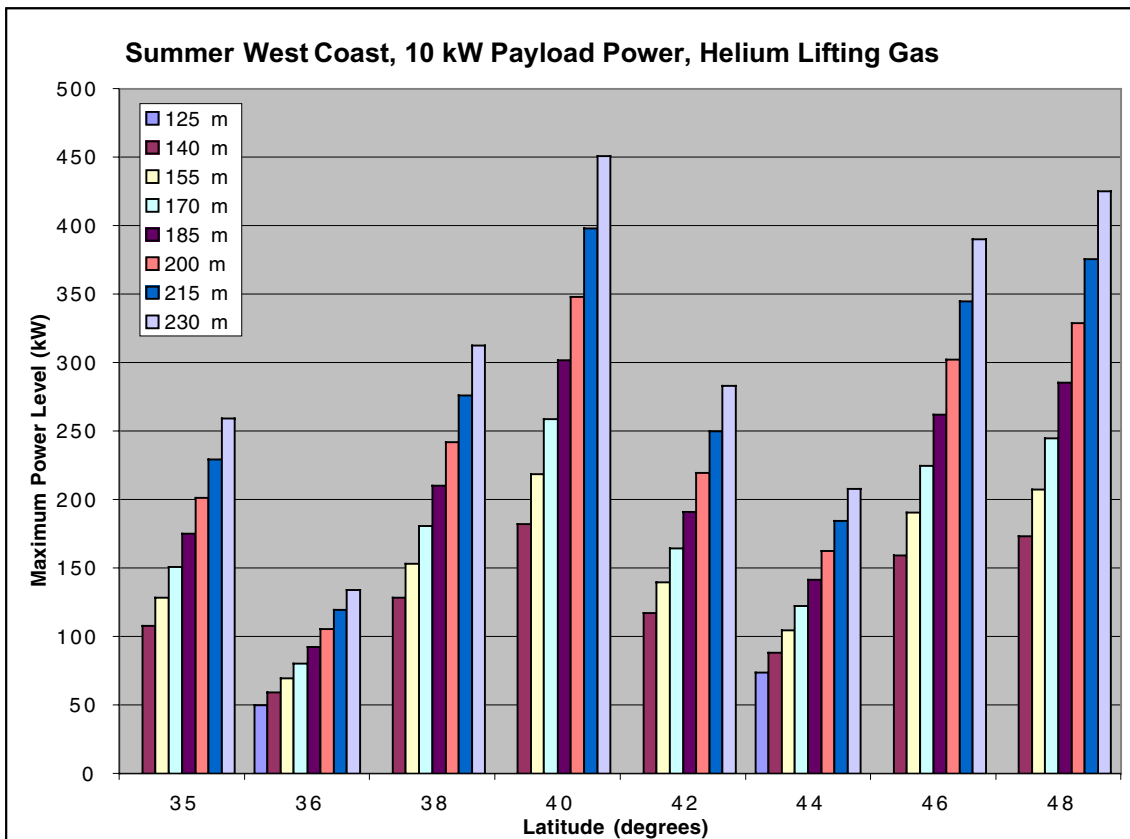


Figure 83 West Coast, Summer Maximum Power Level for Various Airship Lengths

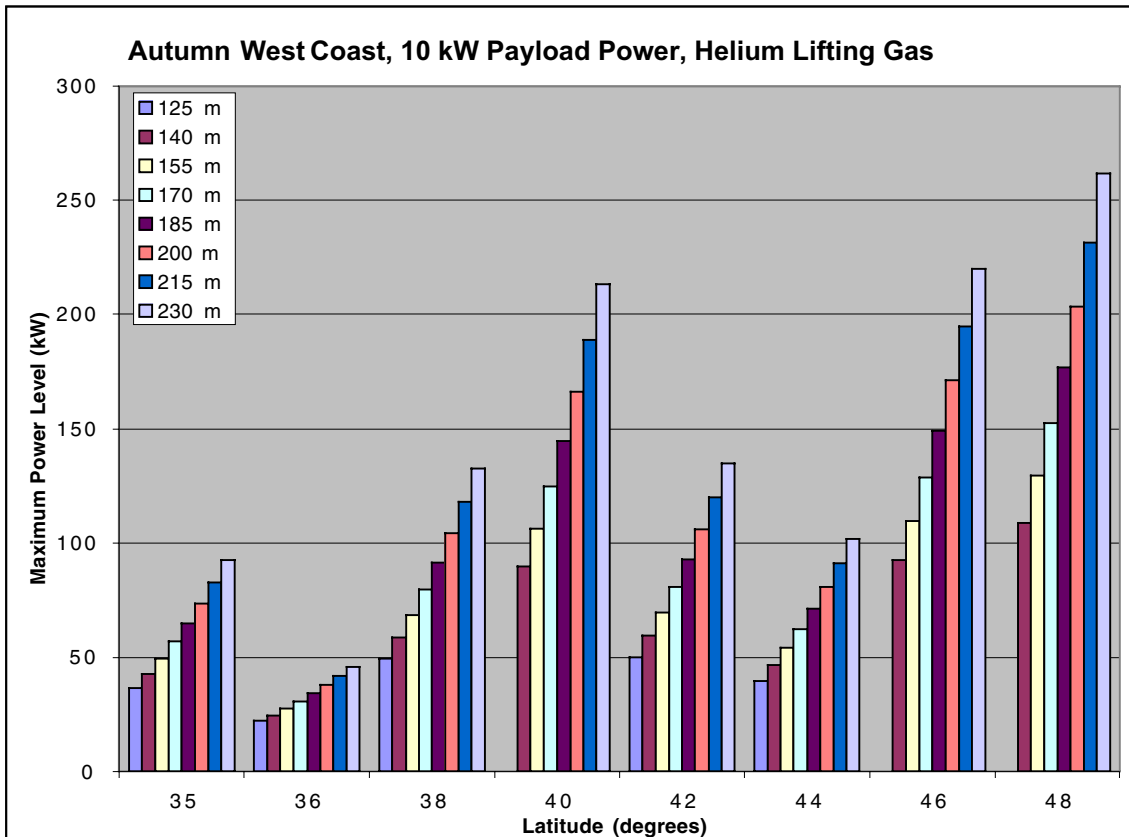


Figure 84 West Coast, Autumn Maximum Power Level for Various Airship Lengths

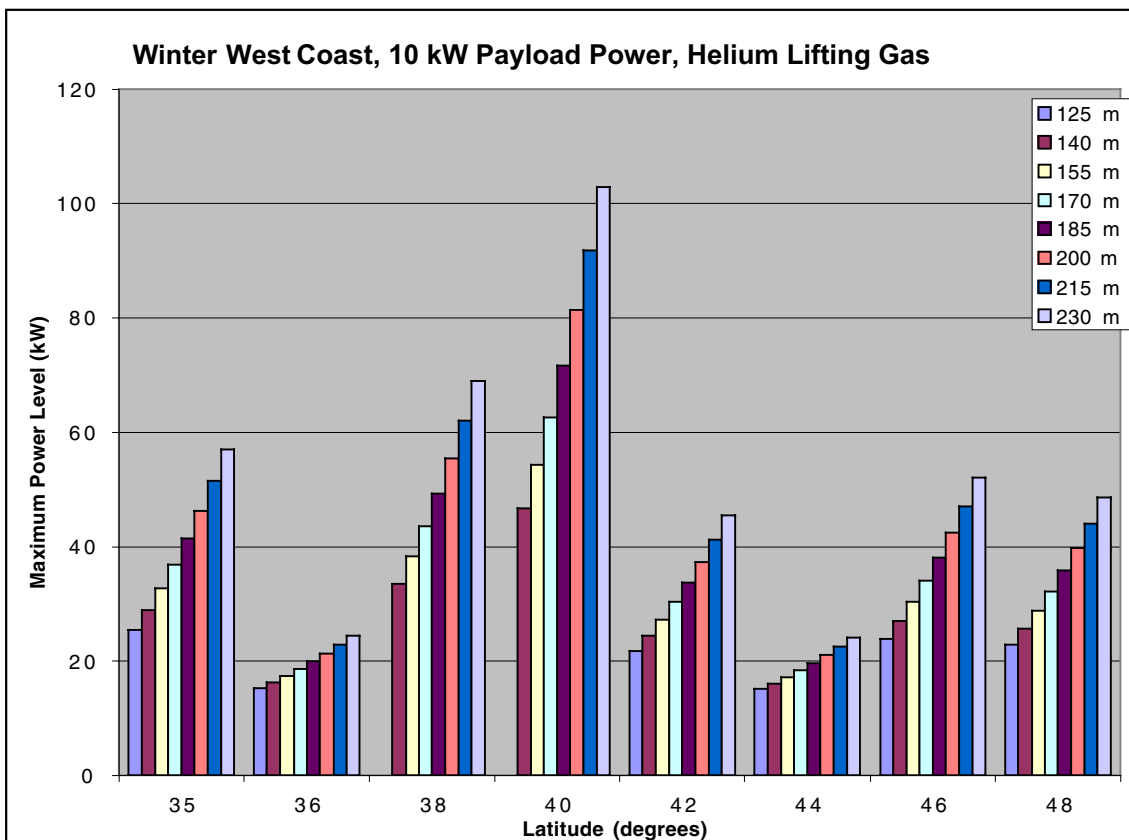


Figure 85 West Coast, Winter Maximum Power Level for Various Airship Lengths

As with the relationship between mean power level and mean wind speed, the maximum power level is highly dependent on the 99th percentile wind speeds the airship must overcome to maintain station. For the East coast the highest maximum power levels occur during the winter months whereas for the West coast they occur during the summer months. The maximum power level sizes the fuel cell and drive train so it is an integral part of scaling the airship.

The next step in the analysis was to evaluate a specific point airship design. The design selected was based on the largest size airship (185 m in length) that could be constructed using the present airship hangers available within the United States. The objective is to provide an airship that can operate continuously, year long, at any latitude along either the East or West coast. By looking at the figures 59 through 62, which represent the lifting capacity of various airship sizes along the East coast, it can be seen that continuous year-long coverage is not possible with the airship sizes examined. Therefore, as a starting point, the payload capacity of the airship along the East coast was selected to be 2000 kg with an airship length of 185 m. The details of this point design are given in table 11.

Table 11 Single Point Airship Design

<i>Airship Characteristic</i>	<i>East Coast</i>	<i>West Coast</i>
Lifting Gas	Helium	Helium
Shape	Cylindrical with Spherical Ends	Cylindrical with Spherical Ends
Length	185 m (607 ft)	185 m (607 ft)
Diameter	46 m (150 ft)	46 m (150 ft)
Volume	2.8E5 m ³ (9.9E6 ft ³)	2.8E5 m ³ (9.9E6 ft ³)
Fins	3	3
Payload Mass	2000 kg (4400 lbs)	4000 kg (8800 lbs)
Payload Power	10 kW	10 kW
System and Communications Power	1 kW	1 kW
Solar Array Efficiency & Specific Mass	8%, 0.12 kg/m ²	8%, 0.12 kg/m ²
Fuel Cell Efficiency	50%	50%
Electrolyzer Efficiency	50%	50%
Mean Power Level	35.3 kW	17.1 kW
Maximum Power Level	308.5 kW	301.6 kW
Operating Latitude Range (year long flight)	28° to 29° and 33° to 38°	35° to 48°

For East coast operation, this airship, outlined in table 10, would be capable of operating at latitudes below 29° and between latitudes of 33° and 38°. For latitudes outside of these ranges, the main problem occurs during the winter months. The high mean and 99th percentile winds provide a significant increase in drag and therefore power requirement. This coupled with the shorter daytime periods during the winter and the lower sun angles makes it impossible for the airship specified above to operate year long over the full latitude range of the East coast. However, spring, summer and autumn operation over

the complete latitude range of the East coast are all possible with the airship configuration shown in table 11.

For west coast operation the summer months provide the greatest challenge due to the higher 99th percentile wind speeds. However, because these higher wind speeds occur during the summer months they are somewhat offset by the longer day times and higher sun angles that occur during this season. The airship configuration listed in table 11 for West coast operation was capable of continuous year-long flight over the full latitude range. A breakdown of the mass distribution of the East and West coast airship is shown in figures 86 and 87

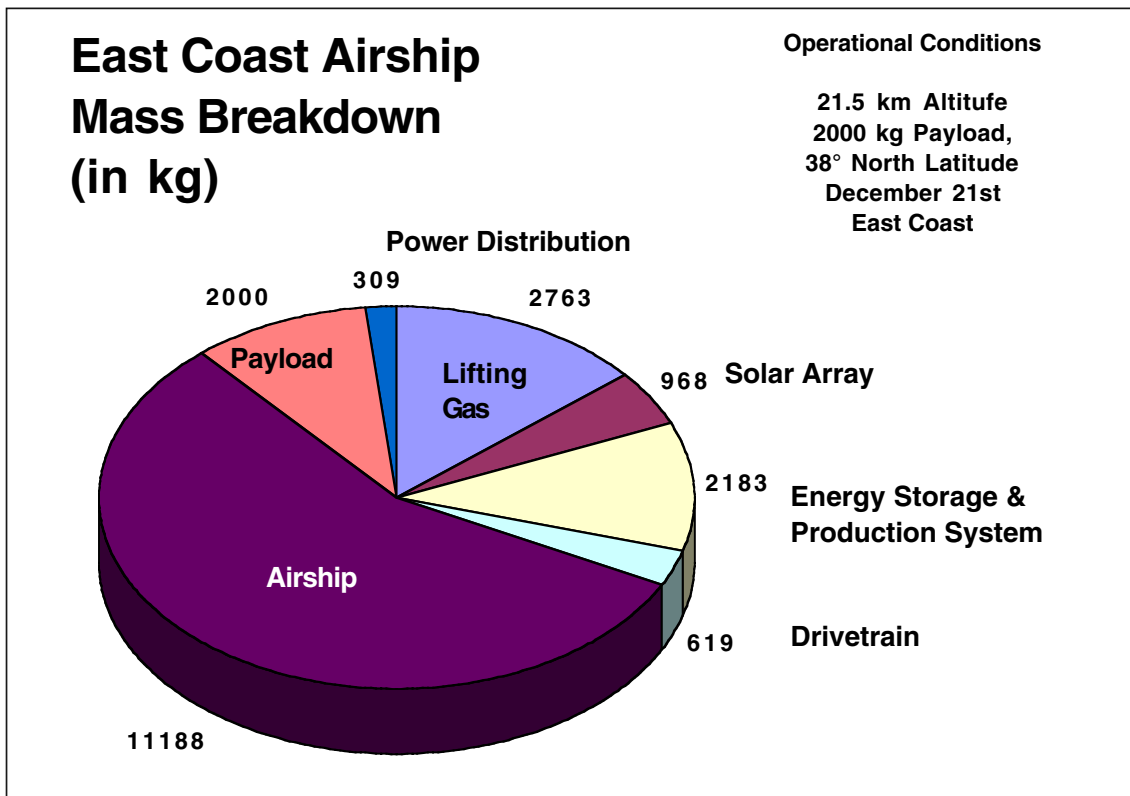


Figure 86 Mass Breakdown for East Coast Airship

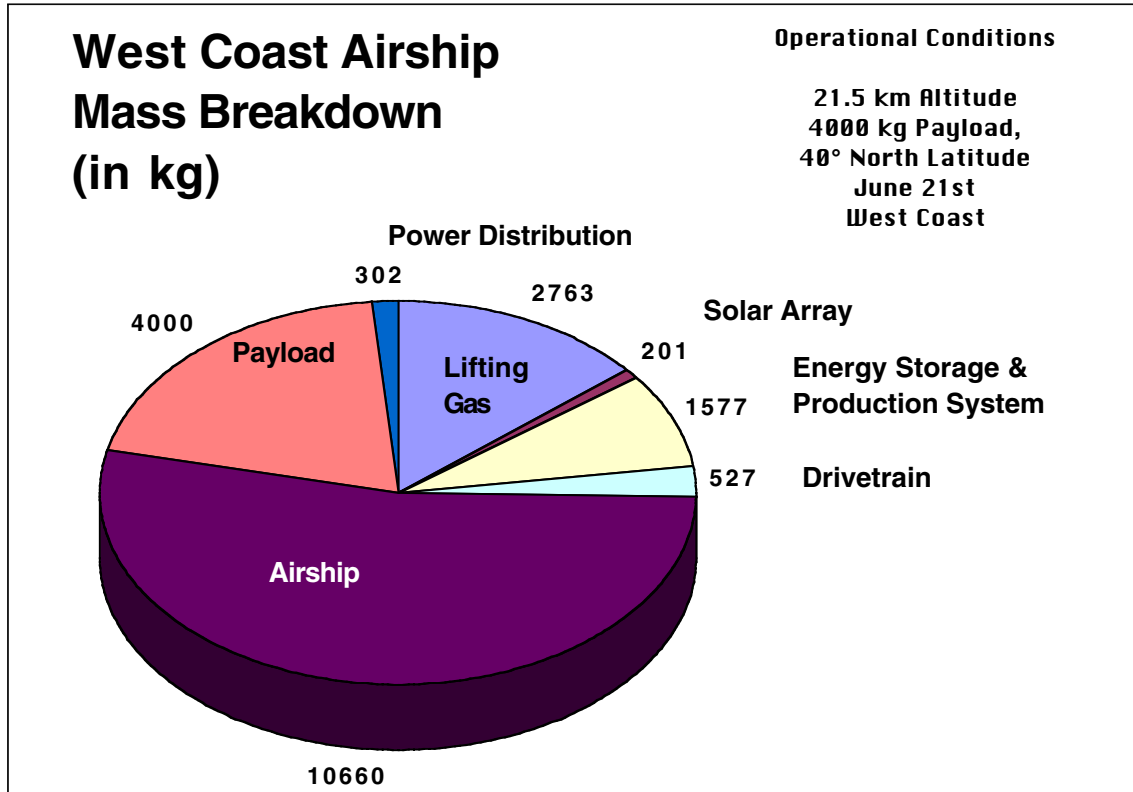


Figure 87 Mass Breakdown for West Coast Airship

The goal of the analysis was to provide continuous year-long coverage on both the East and West coasts, while carrying sufficient payload. With the assumptions made, this goal was met for West coast operation. For the East coast the goal was not met. To determine what it would take to produce an airship that could meet the continuous operation requirement along the East coast, a number of options were examined. First the constraint on the airship size of 185 m in length was removed. A sizing analysis was then performed to determine airship size required to carry 2000 kg at various latitudes along the East coast during the winter. These results are shown in figure 88. From this figure it can be seen that to meet the payload requirement the airship size becomes very large, approximately 270 m in length (volume of $8.75E5 \text{ m}^3$) and the maximum power level is around 1.8 MW. This brute force method requires the airship to be grossly oversized for all other latitudes of operation along the East coast. This large airship method of meeting the observation goal is illustrated in figure 89.

Looking at the airship operation there may be other means of providing coverage over the 42° latitude point without resorting to constructing such a large airship. From figure 88 it can be seen that the required airship size drops off significantly on either side of 42° . Based on figures 5 and 6 the distance to the horizon of an airship at 21.5 km altitude is about 500 km. Based on the Earth's diameter each degree of latitude represents a distance of approximately 111 km. If the airship was stationed at 38° it would still be able to observe the 42° latitude point. In addition, an airship stationed at up to 46° latitude would

also be able to observe the 42° latitude point. This option of observing into the areas where the airships cannot operate is shown in figure 90.

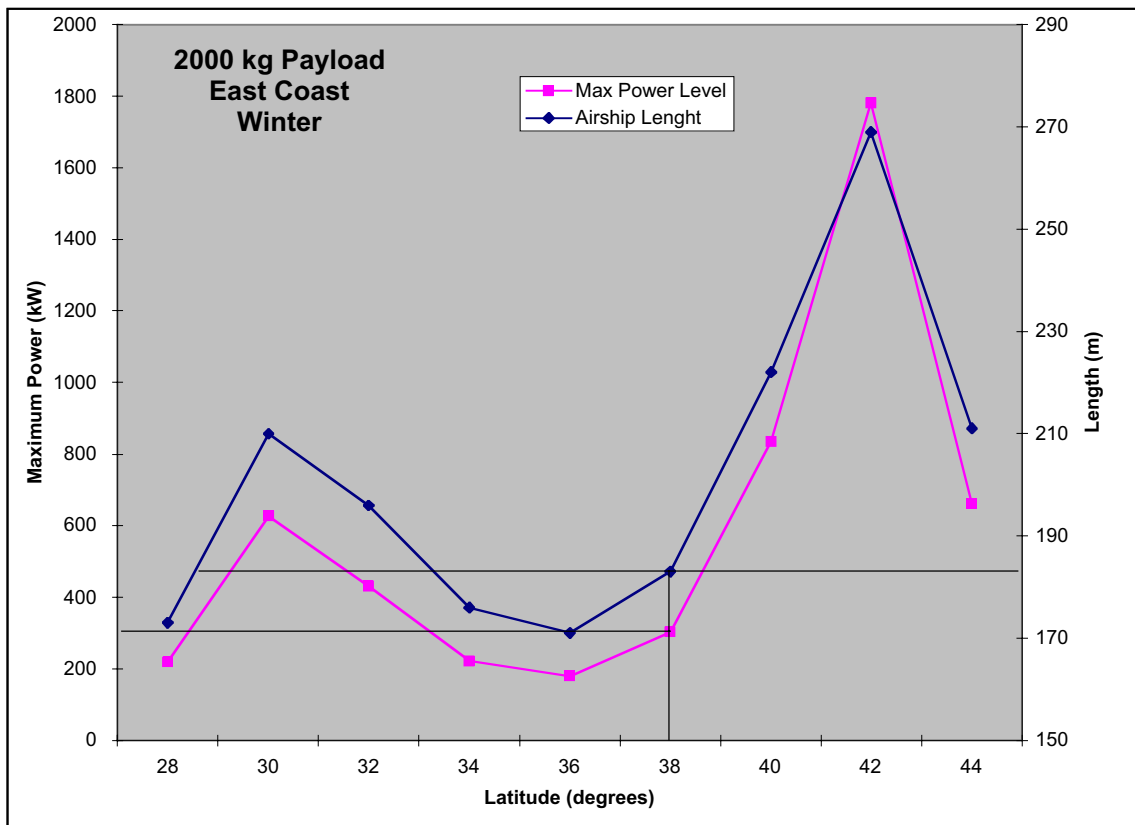


Figure 88 Airship Length and Maximum Power Needed for Continuous Operation Along the East Coast with a Payload of 2000 kg

In addition to observing from a distance to avoid placing the airship within the high wind environment, other options can also be considered. For example, multiple airships could be cycled through the high wind area. This would allow them to drift with the wind and still maintain continuous coverage. Once they were out of observational range they could move to a lower wind area and move back inland for another cycle. This concept is illustrated in figure 91. And finally there is the potential of changing altitude to avoid the high wind conditions. Since the high wind speeds are transient and do not occur simultaneously at all altitudes, changing altitude may be a way of remaining at station while avoiding the high wind conditions. This concept is illustrated in figure 92.

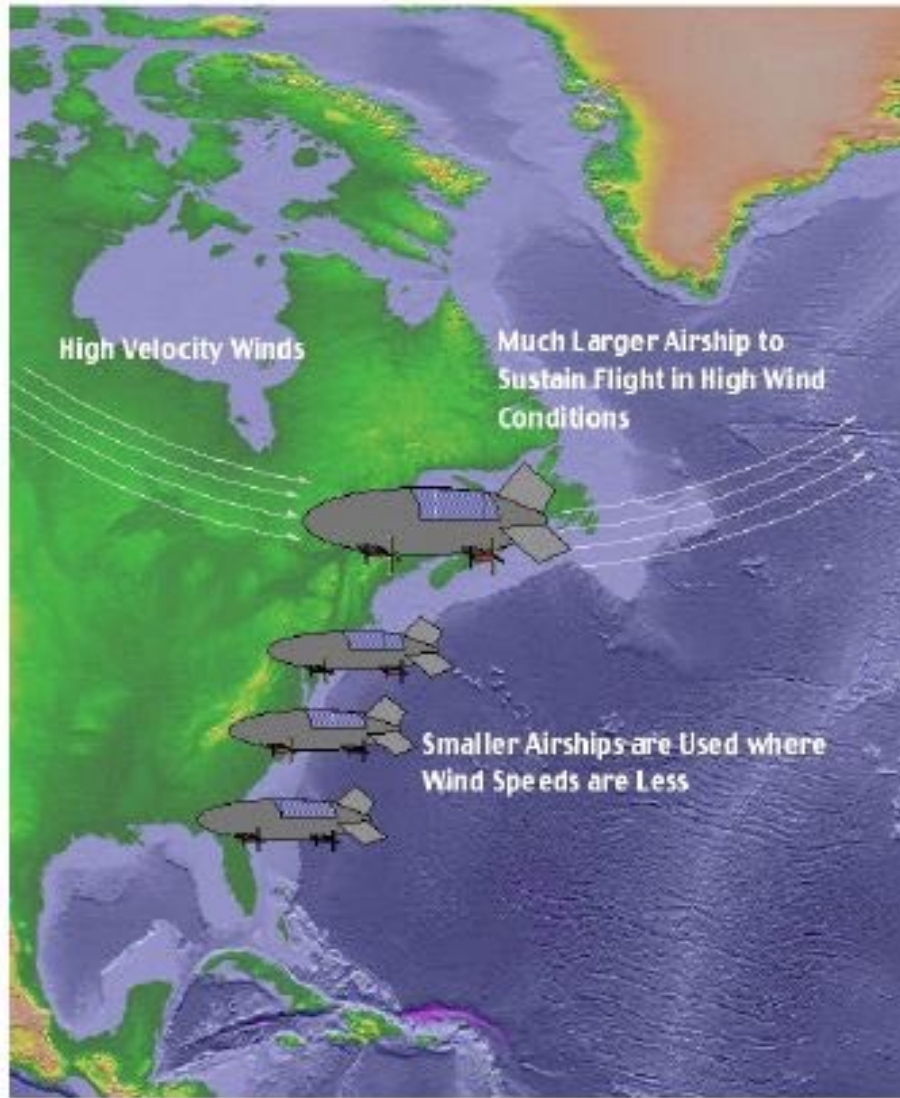


Figure 89 Large Airship Solution for Observing in High Wind Areas

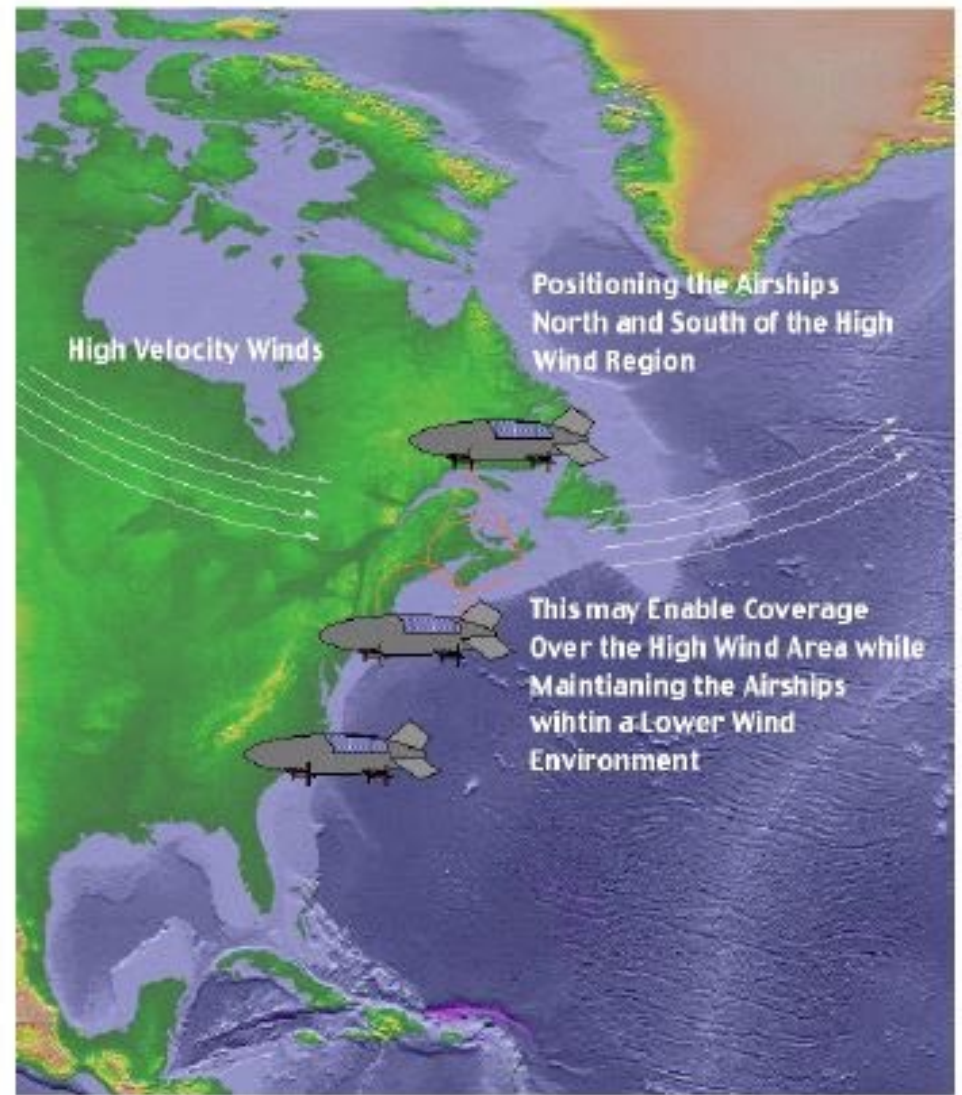


Figure 90 Observation Solution for Observing Within High Wind Areas



Figure 91 Rotate Airship Solution for Observing in High Wind Areas

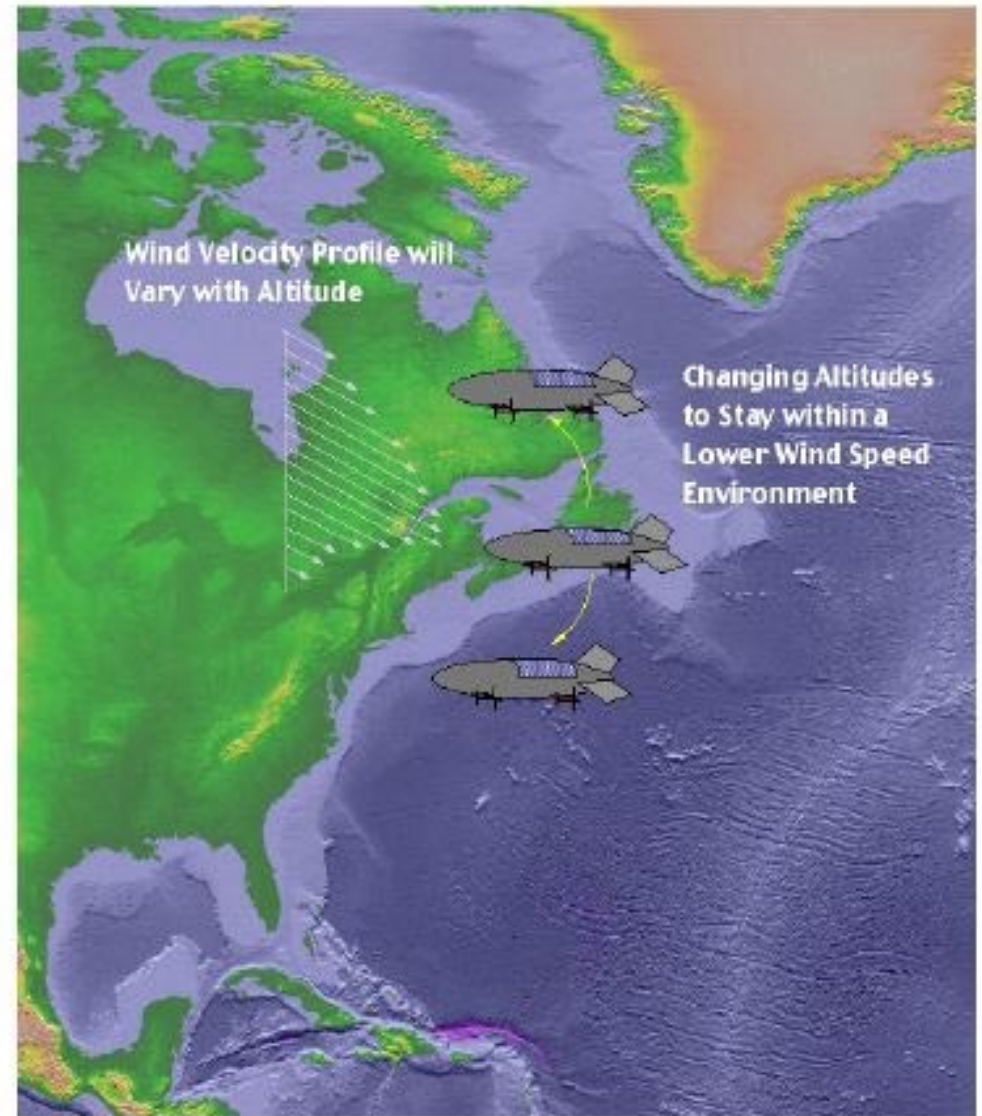


Figure 92 Altitude Change Solution for Observing in High Wind Areas

In addition to the operational solutions for providing continuous coverage along the East coast, advancements in the power and propulsion system can potentially provide the means of achieving complete year-long coverage. Variation in the power and propulsion system specifications from the baseline airship (described in table 10) were utilized to determine what type of technology developments would be necessary for this airship to achieve continuous year long coverage along the East coast. Efficiencies and specific masses of various power and propulsion system components were improved until the baseline airship was capable of operating at the 42° latitude location year long with a 2000 kg payload. The items changed from the baseline and the values required to achieve continuous operation are listed in table 12. It should be noted that this was not an optimization, and there may be multiple combinations of advancements that could be utilized to achieve the same result. Also since our main concern is with the propulsion and power system, no improvements to the airship structure or design (drag) were assumed. These results do however indicate the level of improvement needed to enable an airship, comparable in size to some of the largest airships previously constructed, to provide year-long operation within the high wind areas of the East coast.

Table 12 Advancements Needed for Baseline Airship to Operate at 42° N Latitude Year-Long

<i>Component</i>	<i>Baseline</i>	<i>Advanced</i>
Solar Cell Efficiency	8%	12% (50% increase)
Drive Train	2.39 kg/kw	1.79 kg/kw (25% reduction)
Power Distribution Specific Mass	1 kg/kw	0.5 kg/kw (50% reduction)
Fuel Cell / Electrolyzer Specific Energy	240 W-hr/kg	625 W-hr/kg (160% increase)
Fuel Cell Efficiency	50%	65% (30% increase)
Electrolyzer Efficiency	50%	65% (30% increase)
Lifting Gas	Helium	Hydrogen

In the overall analysis the only variation from the baseline system components was the use of a compressor system that would utilize the surrounding air instead of stored oxygen for reaction in the fuel cell. This system was shown in figure 40. However, since the analysis was based on a daily energy balance scheme, the mass of the oxygen tanks and oxygen reactant was not the driving factor in the airship power system mass. Whereas if a compressor system was utilized the added power needed to operate the compressor is significant, as seen by equation 43. As a result, the compressor system was not competitive with the stored oxygen operation of the baseline system. However, if the inclusion of more detailed wind distribution data requires a weekly or monthly energy balance to be utilized then the compressor system would need to be reconsidered.

This analysis was an initial look at the feasibility of operating a high altitude long endurance airship. The goal of the analysis was to establish the feasibility of the concept and point out any limitations or restrictions. The analysis used conservative “off-the-shelf” values for most of the components. With the environmental models used, the component scaling values and the assumptions made it was shown that continuous West coast operation is feasible using present day technology. East coast operation is also feasible for all but the winter months. The ability to operate in the winter months along the East coast could be achieved through operational or mission solutions or through technology development.

Since this was an initial feasibility study there are numerous areas that could benefit from more detailed modeling. These would include a more detailed airship design and a more refined wind data model providing statistical averages of monthly, weekly or even daily wind velocity and wind direction data that could be used to position the airship. The addition of some or all of these items could have an effect

on the results, and the size of the airship necessary to carry out the desired missions. However, since the results of this analysis are based on environmental data, and an energy balance that accounts for the airship shape, and daily and seasonal fluctuations in available solar energy, the general conclusion on the overall feasibility of the concept produced in this analysis should remain valid.

Reference

1. Jane's All the World Aircraft 1987–88, Jane's Publishing Co., 1987.
2. Jane's All the World Aircraft 1977–78, Jane's Publishing Co., 1977.
3. Hiller Aviation Museum, San Carlos, CA., Boeing Condor Exhibit, <http://www.hiller.org> , March 2003.
4. Aeronautical Systems Center, Wright-Patterson Air Force Base, US Air Force Fact Sheet: Global Hawk, <http://www.af.mil/news/factsheets/global.html>, December 2002.
5. NASA Dryden Flight Research Center, Helios Prototype, <http://www.dfrc.nasa.gov/Research/Erast/helios.html>, April 2002.
6. Air Force Research Laboratory, High Altitude Balloon Experiment Fact Sheet, <http://www.aftl.mil>, June 2002.
7. Tethered Aerostat Radar System Data Sheet, Air Combat Command Public Affairs Office, <http://gomwg.faa.gov/aerostat.htm>, March 1998.
8. Colozza, A.J., "High Altitude Towed Glider," NASA CR–198493, June 1996.
9. Colozza, A.J., "SEADYN Analysis of a Tow Line for a High Altitude Towed Glider," NASA CR–202308, December 1996.
10. Sprigg, C., The Airship, University Press of the Pacific, Honolulu, Hawaii, 2001.
11. Lockheed Martin, High Altitude Airship Data Sheet, <http://www.lockheedmartin.com/akron/protech/aeroweb/aerostat/haa.htm>, June 2003.
12. National Aerospace Laboratory of Japan, Stratospheric Platforms Project, <http://www.nal.go.jp/eng/research/spf/000.html>, June 2003.
13. Lindstrand Balloons Ltd., High Altitude Long Endurance Aerostatic Platforms Program, <http://www.lindstrand.co.uk/hale.htm>, February, 2003.
14. Advanced Technologies Group, World SkyCat Ltd., <http://www.airship.com/>, June 2003.
15. Sanswire Technologies, Stratellite, <http://www.stratellite.net/>, June 2003.
16. LTAS/CAMBOT LLC, Sub Orbital Solar Collector and Communications Station, <http://www.lvcm.com/walden/>, June 2003.
17. Abell, G.O., Exploration of the Universe, CBS College Publishing, 1982.
18. "On Line Journey Through Astronomy", Brooks/Cole Thompson Learning, <http://csep10.phys.utk.edu>, July 2002.
19. Wallace, J.M. and Hobbs, P.V., Atmospheric Science and Introductory Survey, Academic Press, 1977.
20. Handbook of Tables for Applied Engineering Science, 2nd Edition, CRC Press 1973.
21. Strganac, T.W., "Wind Study for High Altitude Platform Design," NASA Reference Publication 1044, December 1979.
22. Curtis, H., Internal Communication, NASA Glenn Research Center, June 2002.
23. "Mir Cooperative Solar Array (MCSA)", NASA Glenn Research Center, November 2002.
24. Hoffman, D.J., Kerslake, T.W., Hepp, A.F., Jacobs, M.K., and Ponnusamy, D., "Thin-Film Photovoltaic Solar Array Parametric Assessment," NASA/TM—2000-210342, July 2000.
25. Uni-Solar, United Solar Ovonic, Product Data Sheet, <http://www.uni-solar.com>, June 2002.
26. Scheiman, D.A., Personal Communication, NASA Glenn Research Center, December 1997.

27. Prokopius, K., Loyselle, P., Maloney, T., and Colozza, A. "Some Engineering Notes on Fuel Cells and Fuel Cell Systems," Presentation NASA Glenn Research Center, March 2000.
28. Colozza, A. and Maloney, T., "Initial Design and Construction of a Mobil Regenerative Fuel Cell System," Under Publication, August 2003.
29. Ballard, Transportation Fuel Cell Engines, Xcellsis HY-80 Product Brochure, <http://www.ballard.com>, June 2003.
30. United Technologies, UTC Fuel Cells, <http://www.utcfuelcells.com>, June 2003.
31. General Motors, Advanced Technology Vehicles, <http://www.gm.com/company/gmability>, June 2003.
32. Colozza, A.J., "Hydrogen Storage for Aircraft Applications Overview," NASA/CR—2002-211867, September 2002.
33. Bettner, J.L. and Blandford, C.S., "Propulsion System Assessment for Very High Altitude UAV Under ERAST," Final Report Draft 2, Allison Engine Company, April 1995.
34. Gottlieb, I.M., Electric Motors and Control Techniques, TAB Books, 1994.
35. ACDelco, Electric Vehicles, http://www.acdelco.com/html/ea_electric.htm, June 2003.
36. Lincoln Motors, Electric Falcon, <http://www.lincolnmotors.com/lincolnmotors/efalc.asp>, June 2003.
37. Colozza, A., "High Altitude Propeller Design and Analysis Overview," NASA/CR—1998-208520, October 1998.
38. Selig, M.S., Donovan, J.F., and Fraser, D.B., "Airfoils at Low Speeds," Soartech 8, H.A. Stokely Publisher, 1989.
39. McCormic, B.W., Aerodynamics, Aeronautics and Flight Mechanics, John Wiley and Sons, New York, 1979.

REPORT DOCUMENTATION PAGEForm Approved
OMB No. 0704-0188

Public reporting burden for this collection of information is estimated to average 1 hour per response, including the time for reviewing instructions, searching existing data sources, gathering and maintaining the data needed, and completing and reviewing the collection of information. Send comments regarding this burden estimate or any other aspect of this collection of information, including suggestions for reducing this burden, to Washington Headquarters Services, Directorate for Information Operations and Reports, 1215 Jefferson Davis Highway, Suite 1204, Arlington, VA 22202-4302, and to the Office of Management and Budget, Paperwork Reduction Project (0704-0188), Washington, DC 20503.

1. AGENCY USE ONLY (Leave blank)		2. REPORT DATE December 2003	3. REPORT TYPE AND DATES COVERED Final Contractor Report	
4. TITLE AND SUBTITLE Initial Feasibility Assessment of a High Altitude Long Endurance Airship			5. FUNDING NUMBERS WBS-22-719-30-02 NAS3-00145	
6. AUTHOR(S) Anthony Colozza				
7. PERFORMING ORGANIZATION NAME(S) AND ADDRESS(ES) Analex Corporation 3001 Aerospace Parkway Brook Park, Ohio 44142			8. PERFORMING ORGANIZATION REPORT NUMBER E-14248	
9. SPONSORING/MONITORING AGENCY NAME(S) AND ADDRESS(ES) National Aeronautics and Space Administration Washington, DC 20546-0001			10. SPONSORING/MONITORING AGENCY REPORT NUMBER NASA CR-2003-212724	
11. SUPPLEMENTARY NOTES Project Manager, James Dolce, Power and On-Board Propulsion Technology Division, NASA Glenn Research Center, organization code 5450, 216-433-8052.				
12a. DISTRIBUTION/AVAILABILITY STATEMENT Unclassified - Unlimited Subject Categories: 07 and 05 Available electronically at http://gltrs.grc.nasa.gov This publication is available from the NASA Center for AeroSpace Information, 301-621-0390.			12b. DISTRIBUTION CODE	
13. ABSTRACT (Maximum 200 words) A high altitude solar powered airship provides the ability to carry large payloads to high altitudes and remain on station for extended periods of time. This study examines the feasibility of this concept. Factors such as time of year, latitude, wind speeds and payload are considered in establishing the capabilities of a given size airship. East and West coast operation were evaluated. The key aspect to success of this type of airship is the design and operation of the propulsion and power system. A preliminary propulsion/power system design was produced based on a regenerative fuel cell energy storage system and solar photovoltaic array for energy production. A modular system design was chosen with four independent power/propulsion units utilized by the airship. Results on payload capacity and flight envelope (latitude and time of year) were produced for a range of airship sizes.				
14. SUBJECT TERMS Hydrogen oxygen fuel cells; Photovoltaic conversion; Airships			15. NUMBER OF PAGES 106	
			16. PRICE CODE	
17. SECURITY CLASSIFICATION OF REPORT Unclassified	18. SECURITY CLASSIFICATION OF THIS PAGE Unclassified	19. SECURITY CLASSIFICATION OF ABSTRACT Unclassified	20. LIMITATION OF ABSTRACT	